UNIVERSITY OF BELGRADE

SCHOOL OF ELECTRICAL ENGINEERING

Željko V. Janićijević

COMPOSITE RESERVOIRS WITH CROSSLINKED POLY(ACRYLIC ACID) HYDROGEL FOR CONTROLLED DRUG DELIVERY VIA NONSPECIFIC ELECTRICAL INTERACTIONS

Doctoral Dissertation

Belgrade, 2020

UNIVERZITET U BEOGRADU

ELEKTROTEHNIČKI FAKULTET

Željko V. Janićijević

KOMPOZITNI REZERVOARI SA UMREŽENIM HIDROGELOM POLI(AKRILNE KISELINE) ZA KONTROLISANU DOSTAVU LEKOVA PUTEM NESPECIFIČNIH ELEKTRIČNIH INTERAKCIJA

doktorska disertacija

Beograd, 2020

Mentor:

dr Miloš Vujisić, docent
Univerzitet u Beogradu, Elektrotehnički fakultet

Članovi komisije:

dr Olivera Ciraj-Bjelac, redovni profesor
Univerzitet u Beogradu, Elektrotehnički fakultet

dr Bojana Obradović, redovni profesor
Univerzitet u Beogradu, Tehnološko-metalurški fakultet

dr Magdalena Stevanović, naučni savetnik
Institut tehničkih nauka Srpske akademije nauka i umetnosti

dr Peđa Mihailović, vanredni profesor
Univerzitet u Beogradu, Elektrotehnički fakultet

Datum odbrane: __________________

Acknowledgments

Multidisciplinary research performed during my Ph.D. journey could not be completed without the support of many institutions and benevolent individuals.

I conducted the major part of experimental research related to this dissertation in the laboratories of the following institutions:

- Institute of Technical Sciences of the Serbian Academy of Sciences and Arts,
- School of Electrical Engineering, The Department of Microelectronics and Technical Physics, and
- Vinča Institute of Nuclear Sciences, Department of Radiation Chemistry and Physics.

Experiments mainly conducted by the coauthors were also performed at the Faculty of Technology and Metallurgy and at the Institute for Biological Research "Siniša Stanković".

The research was supported by the Ministry of Education, Science and Technological Development of the Republic of Serbia.

I would like to express my deep gratitude to Dr. Filip Radovanović for his patient and professional guidance, enthusiastic encouragement along the way, and countless hours of valuable discussions. His extensive experience in membrane technology was essential to the success of this research endeavor.

I would like to offer my special thanks to Prof. Dejan Raković for his generous help during the initial stages of my Ph.D. research and his continuous devotion to the sharing of knowledge. I want to express my appreciation to Asst. Prof. Miloš Vujisić for his guidance during my Ph.D. studies and valuable insights regarding the use of gamma irradiation in my research. I wish to thank Prof. Magdalena Stevanović for including me in different research activities related to biomaterials science and engineering, for the numerous helpful discussions, and for her continuous support throughout my Ph.D. studies. Prof. Olivera Ciraj-Bjelac provided constructive suggestions and advice about the experiments involving gamma irradiation. Discussions on the modeling of drug release with Prof. Bojana Obradović have been insightful and I appreciate her detailed feedback on the dissertation content.

I am particularly grateful for the valuable contributions of my coauthors: Prof. Milena Kataranovski, Asst. Prof. Đorđe Veljović, Dr. Marina Ninkov, and Dr. Ivica Vujčić. Working with you was a rewarding experience. I am also grateful to Dr. Nenad Filipović for his assistance with thermal analysis experiments, his constructive advice, and his practical suggestions. Special thanks to Assoc. Prof. Peđa Mihailović who kindly provided some of the equipment and resources required to conduct electrical characterization experiments. Iontophoresis experiments would not be possible without the Assoc. Prof. Filip Bihelović who skillfully made the side-by-side cell. Thanks should also go to Dr. Ana Stanković and Dr. Miodrag Lukić for their encouragement and assistance on numerous occasions.

I am deeply indebted to Petar Atanasijević for his relentless support during my Ph.D. years and the great effort he invested together with me in constructing the electronics required for different experiments. His contagious enthusiasm gave me additional energy along the way.

I thank my parents and my brother for their support throughout the many years of my academic endeavors.

Finally, I want to thank my wife Nataša Janićijević for her patience, continuous encouragement, and tremendous support throughout my numerous research efforts. She designed the illustrations in **Figures 1.1**, **2.1**-**2.4**, and **5.2**.

Doctoral dissertation title: Composite reservoirs with crosslinked poly(acrylic acid) hydrogel for controlled drug delivery via nonspecific electrical interactions

Abstract

Transdermal and subcutaneous drug delivery routes offer many advantages compared to the enteral route of drug administration including improved drug bioavailability, maintenance of optimal drug levels in the systemic circulation, reduction of toxicity, and better patient compliance. The overall aim of this dissertation was to synthesize and characterize composite hydrogels composed of the cross-linked poly(acrylic acid) hydrogel and the hydrophobic polymer base that are suitable for the storage and controlled delivery of cationic drugs mediated by non-specific electrical interactions. We successfully synthesized composite hydrogel membranes and implants by combining the ultraviolet or gamma irradiation-induced polymerization and liquid phase inversion. Physicochemical properties of the materials, such as chemical composition, microstructure, ion-exchange capacity, swelling behavior, and ionic conductivity, were analyzed. *In vitro* release from composite hydrogel reservoirs was investigated using methylene blue as the model drug. Examined composite hydrogel reservoirs showed mainly diffusion-controlled release kinetics. We developed a modeling approach based on the analytical solution for diffusion and the empirical Weber-Morris model that effectively describes the release kinetics using the concept of apparent diffusion coefficient. Rate-limiting barriers defined by the composite hydrogel microstructure and ion exchange governed the passive release kinetics. Iontophoretic excitation of composite membranes confirmed their electrical responsivity and induced an effective increase in the apparent diffusion coefficient. Obtained composite hydrogels hold promise for drug delivery, but also for applications in nanomaterial synthesis and iontronics.

Keywords: composite hydrogel, liquid phase inversion, drug reservoirs, cationic drugs, ion exchange, diffusion, iontophoresis, drug release

Scientific field: Biomaterials Engineering

Scientific subfield: Biomaterials for Drug Delivery

Naslov doktorske disertacije: Kompozitni rezervoari sa umreženim hidrogelom poli(akrilne kiseline) za kontrolisanu dostavu lekova putem nespecifičnih električnih interakcija

Sažetak

Transdermalni i subkutani načini dostave aktivnih supstanci nude brojne prednosti u poređenju sa enteralnim načinom jer se postiže veća bioraspoloživost leka, njegova optimalna koncentracija u sistemskoj cirkulaciji, smanjena toksičnost i veća komfornost pacijenata. Glavni cilj ove disertacije bila je sinteza i karakterizacija kompozitnih hidrogelova koji sadrže umreženi hidrogel poli(akrilne kiseline) i hidrofobnu polimernu bazu, a pogodni su za skladištenje i kontrolisanu dostavu katjonskih lekova putem nespecifičnih električnih interakcija. Kompozitni hidrogelovi, u formi membrana i implantata, su uspešno sintetisani kombinovanjem metoda polimerizacije indukovane ultraljubičastim ili gama zračenjem i metode mokre fazne inverzije. Analizirana su fizičko-hemijska svojstva materijala kao što su hemijski sastav, mikrostruktura, jonoizmenjivački kapacitet, karakteristike bubrenja i jonska provodljivost. Proces otpuštanja aktivne supstance iz kompozitnih rezervoara sa hidrogelom je ispitivan u *in vitro* uslovima korišćenjem metilenskog plavog kao model leka. Ispitani kompozitni rezervoari sa hidrogelom su pokazali uglavnom difuziono kontrolisanu kinetiku otpuštanja. Razvijen je pristup modelovanju zasnovan na analitičkom rešenju za difuziju i empirijskom Veber-Moris modelu koji efektivno opisuje kinetiku otpuštanja korišćenjem koncepta prividnog koeficijenta difuzije. Kinetika pasivnog otpuštanja je bila diktirana barijerama definisanim mikrostrukturom kompozitnog hidrogela i jonskom izmenom. Jontoforetska pobuda kompozitnih membrana potvrdila je njihovu elektroresponzivnost i indukovala efektivni porast prividnog koeficijenta difuzije. Očekuje se da dobijeni kompozitni hidrogelovi pronađu primenu u dostavi lekova, kao i u sintezi nanomaterijala i jontronici.

Ključne reči: kompozitni hidrogel, mokra fazna inverzija, rezervoari za lekove, katjonski lekovi, jonska izmena, difuzija, jontoforeza, otpuštanje leka

Naučna oblast: inženjerstvo biomaterijala

Uža naučna oblast: biomaterijali za dostavu lekova

Contents

List of Figures

List of Tables

Abbreviations

AA	acrylic acid
AAm	acrylamide
AD	analog-to-digital
ANOVA	analysis of variance
CA	citric acid monohydrate
CB	citrate buffer
CL	cross-linker
DIP	dual in-line package
DL-PLCL	poly(DL-lactide-*co*-ε-caprolactone)
DSC	Differential Scanning Calorimetry
ECB	ethanol-chlorobenzene solution
EIS	Electrical Impedance Spectroscopy
FESEM	field emission scanning electron microscope
FTIR-ATR	Fourier Transform Infrared Spectroscopy-Attenuated Total Reflectance
G-PLGA-PAA	composite PLGA/PAA implant synthesized using gamma irradiation
IEC	ion-exchange capacity
IMD	intramembrane diffusion
IV	intravenous
MB	methylene blue
MBAA	*N,N'*-Methylenebis(acrylamide)
MM	monomer
MSD	mass swelling degree
MV	mean value
n-MOSFET	n-channel metal-oxide-semiconductor field-effect transistor
NMP	N-methyl-2-pyrrolidone
PAA	poly(acrylic acid)

PAAm	polyacrylamide
PB	polymer base
PBS	phosphate-buffered saline
PDI	polydispersity index
PES	polyethersulfone
PI	photoinitiator Irgacure 819
p-JFET	p-channel junction gate field-effect transistor
PLGA	poly(DL-lactide-*co*-glycolide)
PVA	poly(vinyl alcohol)
PWM	pulse width modulation
RMS	root mean square
rpm	rotations per minute
RY	reaction yield
SD	standard deviation
SEM	Scanning Electron Microscopy
SPH	superporous hydrogel
SSE	sum of squared errors
TMPTA	trimethylolpropane ethoxylate triacrylate
USB	Universal Serial Bus
UV	ultraviolet
UV-PLGA-PAA	composite PLGA/PAA implant synthesized using UV irradiation
VISA	Virtual Instrument Software Architecture

Symbols and Variables

A	rate parameter ($\text{min}^{-0.5}$, $\text{h}^{-0.5}$)
A_C	contour distance between adjacent charged groups in the polymer chain (nm)
b	intercept describing the barrier to diffusion
B	intercept proportional to the boundary layer thickness
c	concentration of charged polymer segments (cm^{-3})
C	local MB concentration within the membrane hydrogel ($\text{g}\cdot\text{dm}^{-3}$)
C_0	initial MB concentration within the membrane ($\text{g}\cdot\text{dm}^{-3}$)
C_{cg}	concentration of carboxyl groups ($\text{mmol}\cdot\text{g}^{-1}$)
C_{MB}	initial concentration of MB in the loading solution ($\text{g}\cdot\text{dm}^{-3}$)
-COOH	carboxyl group
D	MB diffusion coefficient in the hydrogel phase ($\text{m}^2\cdot\text{s}^{-1}$)
D_a	apparent diffusion coefficient ($\text{m}^2\cdot\text{s}^{-1}$)
DC	duty cycle of the electric current pulse (%)
d_m	thickness of the clamped composite hydrogel membrane sample (µm)
EB_{MB}	fraction of electrostatically bound MB (%)
f	frequency of the electric current (kHz)
H	height of the cylinder (mm)
I	ionic strength (M)
i	amplitude of the electric current (mA)
I_L	electric current flowing through the load (mA)
J_0	Bessel function of the first kind and zero order
k	characteristic kinetic constant of the polymer/solute system ($\text{h}^{-\alpha}$)
K	scaling factor of the power law
K_H	Henry's constant ($\text{cm}^3\cdot\text{g}^{-1}$)
L	half of the cylinder height (mm)
l	half of the membrane thickness (µm)

L_{B}	bare persistence length (nm)
l_{B}	Bjerrum length (nm)
LE_{MB}	MB loading efficiency (%)
M_{∞}	cumulative amount of released drug after an infinite time period (mg)
MB^{+}	MB cation
m_{d}	dry sample weight (mg)
m_{dCH}	dry weight of the composite hydrogel (mg)
m_{LMB}	weight of MB in the loading solution (mg)
m_{MB}	weight of released MB normalized per dry weight of composite hydrogel ($\mathrm{g \cdot g^{-1}}$)
$\mathrm{M_n}$	number-average molecular weight (Da)
m_{PB}	weight of PB (mg)
m_{RMB}	weight of released MB (mg)
$\mathrm{MSD_e}$	MSD of DL-PLCL/PAA implants in equilibrium before drying (%)
M_{t}	cumulative amount of released drug after time t (mg)
$\mathrm{M_w}$	mass-average molecular weight (Da)
m_{w}	wet sample weight (mg)
M_{WMB}	molecular weight of MB ($\mathrm{g \cdot mol^{-1}}$)
M_{WMM}	molecular weight of MM ($\mathrm{g \cdot mol^{-1}}$)
N	number of replicates
n	dummy summation variable
$\mathrm{n(MB^{+})/n(\text{-}COOH)}$	molar ratio of MB cations to carboxyl groups
N_{A}	Avogadro constant ($\mathrm{mol^{-1}}$)
p	dummy summation variable
Q	local MB concentration in the release medium ($\mathrm{mg \cdot g^{-1}}$)
Q_{e}	cumulative MB concentration in equilibrium ($\mathrm{mg \cdot g^{-1}}$)
Q_{ie}	cumulative MB concentration at the end of iontophoretic release ($\mathrm{mg \cdot g^{-1}}$)
q_n	roots of J_0
Q_t	cumulative MB concentration in the release medium at time t ($\mathrm{mg \cdot g^{-1}}$)

R	radius of the cylinder (mm)
R^2	coefficient of determination
R_B	bulk resistance of the composite hydrogel membrane sample (Ω)
R_f	selectable feedback resistor (Ω)
R_JFET	voltage-controlled resistance of the individual p-JFET (Ω)
R_m	resistance of the composite hydrogel membrane ($\Omega\cdot\mathrm{cm}^2$)
s	slope coefficient of the Boltzmann sigmoid function (min)
S_e	surface area of stainless steel blocking electrodes (cm^2)
t	time (s, min, h, day)
$\mathrm{T_g}$	glass transition temperature (°C)
t_ip	inflection point of the Boltzmann sigmoid function (min)
t_lag	time lag parameter (h)
v	partial specific volume of the PAA gel in the composite hydrogel ($\mathrm{cm}^3\cdot\mathrm{g}^{-1}$)
V_b	mean volume of 0.01 M HCl used for blank probe solution titration (cm^3)
V_CH	composite hydrogel volume (cm^3)
$\mathrm{V_{GS}}$	gate-to-source voltage (V)
V_I	voltage measured between the pins JP_I1 and JP_I2 (V)
V_IN	voltage at the output of the voltage divider for pulse amplitude tuning (V)
V_l	volume of the MB loading solution (cm^3)
V_r	mean volume of 0.01 M HCl used for residual solution titration (cm^3)
$\mathrm{V_{SD}}$	source-to-drain voltage (V)
V_U	voltage measured between the pins JP_V1 and JP_V2 (V)
y_B	value of the Boltzmann sigmoid function (%)
y_f	final equilibrium value of the Boltzmann sigmoid function (%)
y_i	initial equilibrium value of the Boltzmann sigmoid function (%)
Z_x	unknown impedance under test (Ω)
a	diffusional exponent
β	power-law exponent

ε_p	membrane porosity given as the fractional volume of the hydrogel
ξ	gel correlation length (nm)
ϱ	membrane density ($\mathrm{g \cdot cm^{-3}}$)
ϱ_PB	density of PB ($\mathrm{g \cdot cm^{-3}}$)
σ_m	bulk ionic conductivity of the composite hydrogel membrane ($\mathrm{S \cdot m^{-1}}$)
τ	tortuosity factor
φ	PAA gel volume fraction

Chapter 1: Introduction

1.1 Fundamental concepts and state-of-the-art

1.1.1 Concept of controlled drug delivery and routes of drug administration

The primary goals of traditional pharmaceutical research are the discovery and development of potent drugs for therapeutic purposes. However, it became evident that positive therapeutic outcomes are more strongly linked to the formulation and delivery of the drug than to its potency [1]. With the emergence of personalized medicine, drug delivery becomes increasingly important as the therapy should be precisely tailored for the specific patient [2]. Hence, innovative drug delivery systems have attracted significant attention among pharmaceutical products [3]. Drug delivery systems for clinical use comprised a global market of above US$ 150 billion already in 2013 [4]. Estimates for the global market of advanced drug delivery indicate the expected growth from US$ 178.8 billion in 2015 to around $227.3 billion by 2020 [5].

The concept of controlled drug delivery encompasses the spatial and temporal control over the amount of drugs available to cells and tissues with the intention to achieve optimal therapeutic outcomes. Controlled drug delivery commonly requires the development of dedicated drug delivery systems which are becoming more important in clinical settings. Special systems for the improved control of drug delivery can offer many advantages including the maintenance of drug levels within adequate therapeutic boundaries, reduction of harmful side effects and toxicity, decrease in required drug dose, less invasive dosing, enhanced administration of pharmaceuticals with short half-lives *in vivo*, and improved patient compliance during treatment [6].

Drugs intended for systemic absorption in the body can be administered using mainly enteral (through the gastrointestinal tract) or parenteral (through the skin) routes [7]. The most common enteral approach is oral administration of the drug often involving repetitive intake and high dosages. Aggressive environment and unstable physiological state of the gastrointestinal tract, together with the first-pass metabolism effects limit the efficiency of oral administration. Oral administration is also not suitable for long term drug delivery due to short circulation times of only up to 12 h [8]. Parenteral routes of administration provide improved drug bioavailability and enable more accurate control of drug levels in the systemic circulation [7]. However, the administration of drugs through the skin also poses challenges in practical applications, especially if the aim is to avoid standard invasive procedures.

Skin is the largest organ in the human body taking up around 2 m^2 of surface area and approximately 7% of the total body weight of an average adult while also functioning as a blood reservoir which carries 8-10% of the total blood flow in the body at rest [9]. At the physiological pH of the body, skin exhibits a net negative charge [10]. The physiologically inactive top layer of the skin referred to as the *stratum corneum* is the main barrier to drug penetration and the most significant rate-limiting layer for drug transport through the skin [11].

Different approaches and systems for drug delivery have been developed to overcome the limitations imposed by skin properties. Here, we shall focus mainly on transdermal and subcutaneous drug delivery with particular emphasis on systems constructed using different polymeric biomaterials.

1.1.2 Transdermal drug delivery systems

The popular minimally invasive approach is transdermal drug delivery commonly coupled with various strategies for passive and active enhancement of drug permeation through the skin [12], [13]. In the passive transdermal drug delivery, transport of the drug proceeds mainly by diffusion through the skin. However, such transport leads to significant interpatient variability as it depends on multiple factors related to the physicochemical properties of the drug and the physiological state of the skin of the particular patient, as discussed in the review by Singh and Singh [14]. On the other hand, active enhancement methods rely on the application of external energy to overcome the barriers to drug transport [15]. A promising method for active physical enhancement of drug permeation is iontophoresis, which involves the use of electrical energy to improve and control drug transport through the skin. During iontophoresis, an electric current is applied through the skin between the active and indifferent electrode to force the migration of charged chemical species via electrostatic repulsion at the active electrode site [14]. Mechanisms of drug transport enhancement by iontophoresis are various, including electrophoresis, electroosmosis, and transient increase in skin permeability [16]. These mechanisms are discussed in the review by Dixit et al. [17]. The intensity of the applied electric current in iontophoresis should be sufficiently small and physiologically acceptable (up to 0.5 $mA\cdot cm^{-2}$) [18]. Continuous direct-current is commonly employed, but under certain conditions pulsed electric current may be more beneficial in terms of drug permeation [19] and retention of skin integrity [20]. Iontophoresis can provide controlled and programmable drug delivery by the adjustment of electric current parameters, and thereby reduce the effects of biological variability while also improving patient compliance [13], [17], [21]. Iontophoretic delivery is considered a safe procedure commonly not damaging the skin beyond mild erythema, although there is a risk of causing burns [22], [23]. It is important to mention that drug solution for iontophoresis must be sufficiently ionized to carry measurable electric current in biological systems (above 0.1 nA) [14].

Passive and iontophoretic systems for transdermal drug delivery include patch-like devices that are used to access the intended surface area of the skin [24]. In terms of their design, patches used for transdermal drug delivery can be mainly classified into matrix-type and reservoir-type patches (**Figure 1.1**) [25].

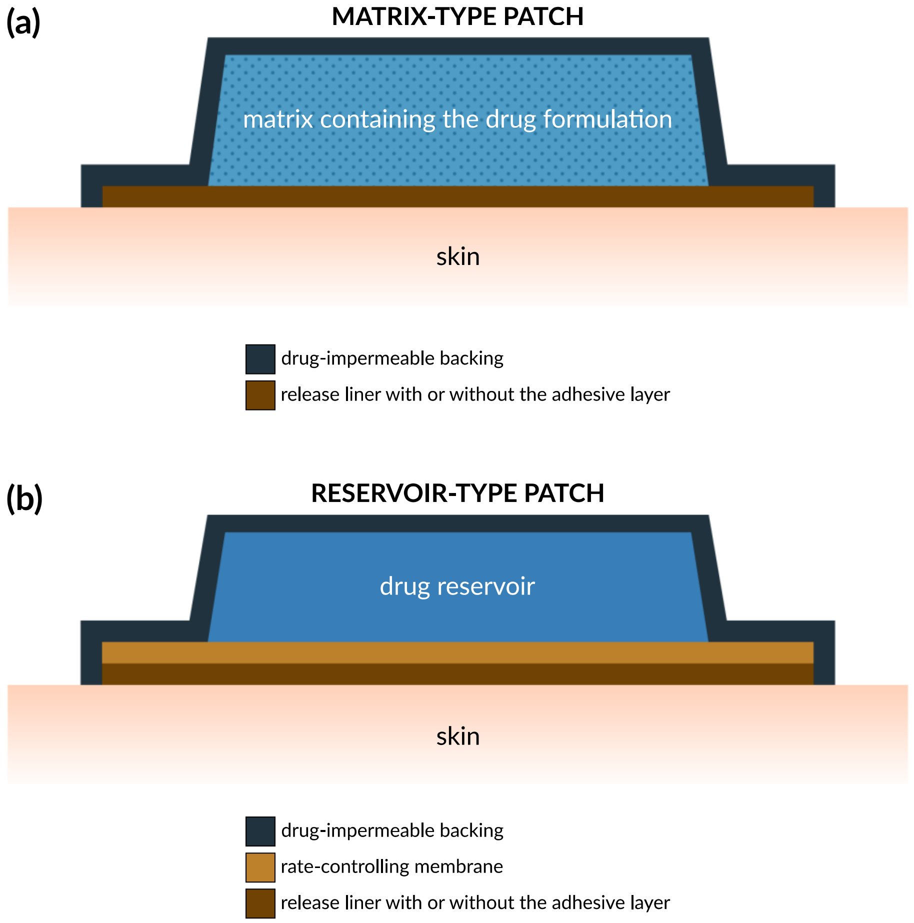

Figure 1.1. Schematic illustration of (a) the matrix-type patch and (b) the reservoir-type patch.

The passive drug delivery rate in matrix-type patches is governed by the skin permeability [26]. In reservoir-type patches, the passive drug delivery rate is controlled by the membrane [27]. In more complex patch designs, smart or active membranes can be used and the electronics can be integrated within the patch [24]. Patches for transdermal drug delivery via iontophoresis have a similar construction as the patches in passive systems with some distinctive features. Typical iontophoretic patches have the encapsulated drug formulation in the form of a highly conductive liquid or gel commonly bounded with an artificial membrane that provides a direct interface with the skin [28]. The selection of an appropriate patch depends on multiple factors including drug properties, required dose, and intended delivery rate to ensure optimal treatment [29].

As we can conclude from the overview of transdermal patches, membranes play an important role in the control of transdermal drug delivery. The release of drugs from polymer membranes can be modulated by tuning different parameters of the polymeric membrane materials including the material type, molecular weight, crystallinity, cross-linking degree, branching degree, swelling behavior, thickness, and porosity [28], [30]. Membranes interfacing the skin in iontophoretic patches should satisfy special requirements such as biocompatibility (to prevent skin irritation), minimal absorption of the drug, and low electrical resistance [28], [31]. The most relevant microporous and nanoporous polymer membranes used in transdermal drug delivery systems were reviewed by Mabrouk et al. [32].

1.1.3 Subcutaneous drug delivery systems

A more invasive approach to overcome the skin permeation barriers is the subcutaneous implantation of a drug delivery system. Subcutaneous tissue is a suitable region for implantation of drug reservoirs since it exhibits good properties for long-term drug delivery while minimizing the risks during and after the implantation procedure. Several beneficial properties are characteristic for subcutaneous tissue including reduced innervation, low risk of local inflammation, good hemoperfusion, and a high content of fat that promotes slower drug absorption [33]. The implanted reservoir should be cost-effective, biocompatible, sterile, and able to provide a controlled rate of drug release with adequate dosing, while also meeting practical requirements of environmental stability, easy fabrication, and facile handling during surgical procedures [34]–[36].

Polymeric implantable drug delivery systems are reviewed in detail by Santos et al. [37] and Stewart et al. [38]. Passive implants for drug delivery typically rely on diffusion-based phenomena to achieve drug release and the process can be partially adjusted by modifying physicochemical properties of the implant (such as microstructure, surface properties, and material type) [36]. Important parameters that also influence the rate of drug release are the drug solubility in the polymer, the drug diffusion coefficient in the polymer matrix, the drug loading degree in the reservoir, and the *in vivo* degradation rate of the polymer matrix [39].

Non-degradable implants can be divided into the matrix or monolithic type where the drug is uniformly dispersed throughout the implant volume [36] and the reservoir type where the drug diffuses from the implant core through the semi-permeable membrane of defined thickness which regulates the drug release rate [28].

Biodegradable implants should be designed to degrade in a controlled manner to provide sustained drug release. The release of drugs from biodegradable polymeric reservoirs is controlled either by diffusion or degradation, but it can also be regulated by the combination of these phenomena [40]. If the degradation of the polymer matrix proceeds via hydrolysis, the encapsulation of hydrophilic drugs and high drug concentrations may lead to accelerated release [41]. Therefore, the prediction of drug release from biodegradable polymer matrices may be a complex issue that requires dedicated modeling [42].

An important property for all implantable reservoirs for drug delivery is their biocompatibility. Many properties of the implant may affect biocompatibility including size and shape, chemical composition, surface charge, surface roughness, and surface wettability [36]. Immune response to the implant *in vivo* may be affected by its degradation which changes the implant surface properties and leads to the formation of degradation products [43].

Implantable drug reservoirs intended for subcutaneous use also require sterilization before they can be implanted *in vivo*. As medical devices evolved over time, many sterilization techniques have been investigated and utilized with a variable degree of efficiency [44]. Among these techniques, sterilization with gamma rays from the ^{60}Co source stands out as one of the most potent and widely used on polymeric materials. Sterilization dose for medical devices and pharmaceutical products according to typical recommendations is 25 kGy [45]. However, this dose can be quite high for radiation-sensitive polymers and the actually required sterilization dose also depends on the initial level of bioburden. The use of lower sterilization doses is always beneficial when the initial bioburden of the polymer is low, and different methods exist for validation of the sterilization effectiveness [46]. In the case of radiation-sensitive polymeric drug carriers, a combination of aseptic preparation with a low dose of radiation at high energies can prevent the deterioration of important material properties [47].

1.1.4 Types of polymeric materials used in drug delivery systems

Polymeric biomaterials have played a very important role in advancing many types of drug delivery systems [48]. They are widely used in the transdermal and subcutaneous systems for controlled drug delivery. As materials used in the controlled release of drugs, polymers must fulfill multiple requirements such as biocompatibility, processability, adequate mechanical strength, suitable permeability to relevant molecules, and a proper degree of degradability [49].

As reviewed by Santos et al., transdermal patches can be composed of natural and synthetic polymers (biodegradable or non-biodegradable) or even different types of their blends [24]. Subcutaneous implants were successfully constructed from several types of synthetic non-degradable polymers, but the use of biodegradable polymers is commonly preferred in order to avoid surgical removal and associated risks [36]. The use of biodegradable polymers in implantable drug delivery systems offers a significant advantage as such polymers can be metabolized within the body and broken down to non-toxic products which can be safely absorbed or excreted [50]–[52]. Biodegradable polymers are commonly classified into several categories including poly(esters), poly(ortho esters), poly(anhydrides), poly(amides), poly(ester amides), poly(phosphoesters), and naturally occurring biodegradable polymers [53]. Among these polymers, poly(esters) such as poly(lactic acid), poly(lactic-*co*-glycolic acid), poly(caprolactone), and their copolymers have been the most widely explored and used materials with well-documented biocompatibility and safety of degradation products [36].

Except according to their degradability, polymeric biomaterials are also commonly classified according to their typical behaviors and other properties relevant to biomedical applications. Here, we shall provide a brief overview of stimuli-responsive polymers, polymeric ion-exchange materials, and hydrogels. Polymeric biomaterials can also be engineered to exhibit a suitable combination of properties and behaviors tailored for a specific application, and this is often achieved by fabricating polymer composites.

1.1.5 Stimuli-responsive polymers

Polymeric biomaterials can be designed to respond to different types of physical, chemical, and biological stimuli that act as triggers [54]. Among such materials, pH-sensitive and electrically responsive polymers are of special interest in controlled drug delivery. pH-sensitive polymers commonly contain functional groups that can change their ionization state depending on pH thereby changing the overall behavior of the polymer [55]. Materials comprising pH-sensitive polymers can respond differently to pH variations through swelling and shrinking, but also degradation and dissociation [56]. Electrically responsive polymers enable the control of biomaterial properties or behavior by applying electric fields. These polymers have been used for various biomedical applications including notable interactions with cells [57] and controlled drug delivery [58], [59]. According to their structure, such polymers are commonly highly conjugated aromatic systems [60], [61]. However, polyelectrolytes (polymers containing a significant amount of ionizable or ionic groups, or a combination of both [62]) exhibit ionic conductivity and can also respond to electric fields which may enable controlled transport of charged chemical formulations [63]. In addition, polyelectrolytes commonly exhibit pH-sensitivity resulting from the presence of numerous ionizable functional groups [64].

1.1.6 Polymeric ion-exchange materials

Polymers containing fixed ionizable groups are of special interest for the delivery of charged drugs since they can behave as ion exchangers (solid materials that carry exchangeable cations or anions). Ion exchangers offer many advantages in drug delivery applications such as high drug loading capacity, facile drug loading, good retainment of the drug, improved drug stability, and better uniformity of drug release [65]–[67].

Ion exchange is the process where the counter ions exiting the ion exchanger are replaced with the stoichiometrically equivalent amount of other counter ions from the electrolyte solution acting as the surrounding medium [68]. The behavior of fixed ionizable groups present in the ion exchanger dictates how the ion exchange occurs under given conditions. The concentration of ionizable groups defines the capacity for ion exchange, while the chemical properties of these groups determine the ion exchange equilibrium [68], [69]. The stoichiometric nature of the ion exchange process stems from the electroneutrality requirement, while from the standpoint of kinetics it can be considered approximately as a diffusion phenomenon [68].

Common ionizable functional groups in ion exchangers used for delivery of cationic drugs include the carboxyl group which can be weakly ionized and sulfonic group that can be strongly ionized [70]. Depending on its properties, the drug can be bound to ion-exchange groups by electrostatic interactions which enable the release of mobile ions or adsorbed by non-electrostatic interactions (involving hydrogen bonding and hydrophobic forces) [67]–[69], [71], [72]. Appropriate selection of multiple parameters related to the external release medium, physicochemical properties of the drug, and physicochemical properties of the ion-exchange material can provide tunable permeation and release kinetics of the drug as summarized in the review by Hirvonen [67]. Distribution of the drug between the ion exchanger and the release medium in equilibrium is defined by electrostatic interactions (quantified by the electrical partition coefficient) and hydrophobic interactions (quantified by the chemical partition coefficient) as discussed in more detail by Hirvonen [67]. Due to the presence of abundant ionized groups, ion-exchange materials are typically electrically conductive and can be combined with iontophoresis to enable an additional degree of external control. Iontophoresis has been successfully combined with different forms of ion-exchange materials including gels, resins, membranes, and fibers [73]–[80]. It is easy to deduce from their beneficial properties, that ion-exchange materials can be a useful tool for the improvement of passive as well as iontophoretic drug delivery.

1.1.7 Hydrogels

Among different polymeric biomaterials, hydrogels have attracted a lot of attention in the last several decades starting from the pioneering work in the 1960s [81] and leading to numerous patents and commercial products for various biomedical applications [82]. Hydrogels are hydrophilic three-dimensional cross-linked polymer networks insoluble in aqueous media and capable to absorb vast amounts of water or biological fluids by swelling [83]. Physical properties of hydrogels such as soft consistency, porosity, and high water content mimic the properties of living soft tissues in the body better than other synthetic biomaterials [82]. Drug release from hydrogels is strongly dependent on the main characteristics of the hydrogel network such as the polymer volume fraction in the swollen state and pore size [83], but also on the fundamental properties of the drug such as molecular weight and state of charge. Permeation and release of the drug also depend on the nature and intensity of interactions between the hydrogel chains and the drug [84]. In response to different stimuli, hydrogels can change their structure, permeability, swelling behavior, and mechanical properties [85]. Such changes can be induced intentionally and exploited to modulate drug release from hydrogels. The use of hydrogels in controlled drug release systems is favored due to some of their main advantages including tunable physical properties, controllable degradation behavior, typically good biocompatibility, and the ease of hydrophilic drug encapsulation [4]. Although hydrogels allow enhanced drug permeation due to high water content and may provide the possibility for sustained drug release, the high water content in common hydrogels can be coupled with large pore size and lead to the undesirably fast release of the drug [86]. Major limitations in the use of hydrogels arise from difficult handling and mechanical instability [24]. Typical hydrogels tend to exhibit spatial gel inhomogeneities [87]. Even though multiple strategies exist for engineering strong and tough hydrogels with tunable mechanical properties [88], [89], patches that are not based on hydrogels for transdermal drug delivery commonly show better mechanical resistance [24]. Photo-induced polymerization using ultraviolet (UV) irradiation is a common technique used to prepare hydrogels for biomedical applications [90]. However, hydrogels can be also obtained by different chemical and physical cross-linking methods including radiation-induced synthesis which often involves gamma irradiation [91]–[94].

1.1.8 Gamma irradiation and polymeric biomaterials

Gamma irradiation can induce manifold chemical effects including chain scission, cross-linking, polymerization, grafting, and oxidation [95]. Medium-level doses of gamma irradiation are sufficient for chain reactions leading to polymerization, while much higher absorbed doses are necessary for single-step processes or short chain length reactions (*e.g.* in the case of radiation cross-linking) [95]. For a long time, gamma irradiation was known for its capability to induce polymerization of monomers in solution without any additives (commonly serving as initiators or cross-linkers) [96]. Hence, gamma irradiation can be a powerful tool for the simultaneous synthesis, processing, and sterilization of polymeric materials. The use of gamma irradiation can be particularly beneficial in the production of implantable drug delivery systems based on polymeric biomaterials as it may facilitate the processes of fabrication and sterilization (or even combine them in a single step).

1.1.9 Fabrication of membranes using phase inversion

Commercially available polymeric membranes are commonly fabricated by using the methods of phase inversion as they are characterized by low cost, ease of processing, and flexibility in terms of production scale [97]. The process of phase inversion was introduced in membrane technology in the 1960s [98]. This process presents a controlled transformation of a thermodynamically stable polymer solution from liquid to a solid state where solidification takes place after liquid-liquid demixing [99]. Although the demixing can be induced by different means, the most widely used technique is the immersion in a nonsolvent bath, which leads to nonsolvent induced phase separation (known also as immersion precipitation [100]). The technique can be applied to almost any polymer type as long as it can be dissolved in a solvent or mixture of solvents [99]. Nonsolvent induced phase separation is a complex process governed by thermodynamic and kinetic phenomena while also being determined by the interplay of many experimental parameters as discussed in detail in the review by Tan and Rodrigue [101]. The support material used in membrane fabrication by immersion precipitation adds to the complexity by introducing additional wetting phenomena to the process of polymer solidification [102]. Type of the support material can also have an impact on the demixing speed during immersion precipitation [103]. All of the mentioned aspects ultimately affect membrane morphology and functionality.

1.1.10 Composite hydrogel membranes

Composite membranes comprising different functional polymers are in the focus of many research efforts due to the possibility of versatile applications [104]. A combination of a rigid porous membrane and a soft functional hydrogel is especially interesting as it can uniquely exploit the benefits of hydrogels for applications in important fields such as biomedical engineering, sensing, separation, and catalysis [105]. Reduced size of the hydrogel component combined with its hydrophilic nature can provide a more rapid response to external stimuli and enhanced antifouling properties, while the rigid porous membrane may provide mechanical support, spatial confinement within macropores, or act as a size-selective barrier [105]. Improved hydrogel response to external stimuli is of special interest in drug delivery whether they come from the local environment or they are intentionally applied to modulate the release. Among different applied stimuli for the control of drug release, electrical stimuli can be easily produced, programmed, and controlled to achieve modulation of drug release in real-time. Mechanisms of drug transport through hydrogel-based membranes driven by electrical phenomena and the concepts of electrically controlled drug delivery devices are reviewed in detail by Kulkarni and Biswanath [106]. Only few notable attempts have been made so far to fabricate composite hydrogel membranes that enable electrically modulated transport of molecules [107]–[111]. All of these attempts were focused on the permeation control mainly for the purpose of solute separation, and not for applications in controlled drug delivery.

1.1.11 Composite membranes based on polyethersulfone and poly(acrylic acid) as functional components

Composite membranes comprising polyethersulfone (PES) or poly(acrylic acid) (PAA) as one of the main constituents, or a combination of both, have been fabricated in the past for different applications (including mainly stimuli-responsive materials, separation, and purification) using various synthesis methods. Acrylic acid (AA) was polymerized and cross-linked *in situ* within the pores of a poly(1,1-difluoroethylene) membrane to form pH-responsive valves [112]. pH-responsive valves were also fabricated by grafting PAA onto the composite membrane composed of silica and anodic aluminum oxide [113]. Composite membranes obtained by blending PES with amphiphilic diblock copolymers of polystyrene and PAA were fabricated for pH-switching applications [114]. Photo-responsive permeability of PES-based membranes was attained by modifying the PES with the host-guest complex between azobenzene and β-cyclodextrin [115]. PES membranes subjected to surface modification by using hydrophilic chains were also fabricated for purposes of separation and blood purification [116]. Ion-exchange ultrafiltration membranes for water purification were synthesized from the mixtures of polysulfone and PAA solutions via liquid phase inversion of the cast films [117]. pH-sensitive composite membranes with a good potential for ion exchange were obtained by blending PAA microgels with PES solution and subsequent preparation via mixture spin coating coupled with liquid-liquid phase separation [118]. Multifunctional composite membranes were fabricated by exploiting *in situ* cross-linked copolymerization of N-vinylpyrrolidone and AA in PES solutions [119]. Thermal copolymerization was followed by spin coating and liquid-liquid phase inversion in order to form membranes that exhibit improved biocompatibility, good protein antifouling, and capability for cationic dye adsorption [119].

Radovanović and coworkers have established an interesting technique for the fabrication of composite membranes, which combines photopolymerization and cross-linking of functional monomers with the traditional liquid phase inversion for proton-conducting applications related to fuel cells [120] and heavy metal removal from aqueous solutions [121]. In our research, we used a similar concept and optimized this technique in terms of precursors and synthesis parameters to achieve biomaterial properties adequate for iontophoretic and subcutaneous drug delivery.

1.1.12 Electro-responsive composite hydrogels based on PAA

PAA was used in composite hydrogels to improve responsivity to electrical stimuli for drug delivery purposes. A monolithic gel matrix composed of calcium alginate and PAA was used for electrically stimulated drug delivery of hydrocortisone [122]. Interpenetrating polymer networks of poly(vinyl alcohol) (PVA) and PAA were investigated for the electrically modulated drug delivery of cefazoline and theophylline [123]. Osada and coworkers have introduced the concept of electrically controlled solute permeation and separation using composite hydrogel membranes composed of PVA and PAA [110], [111]. Yamauchi et al. have reported electrical switching and modulation of protein permeation due to reversible volume changes of composite PVA/PAA membranes that were fabricated by iterative freezing and thawing of the aqueous solution containing PVA and PAA [111]. Kokufuta et al. exploited similar composite PVA/PAA membranes for the separation of maleic acid and fumaric acid under specified conditions of pH and applied electric potential gradient [110].

Although these composite hydrogels containing PAA have shown a good response to electrical stimuli, they either suffered from poor mechanical properties or required tedious fabrication involving many cycles of freezing and thawing.

1.1.13 Ion-exchange materials in iontophoretic drug delivery systems

As mentioned earlier, ion-exchange materials in drug delivery (used mainly in iontophoresis) can come in many forms including resins, membranes, and fibers. Several studies of Hirvonen and coworkers have reported advantages of using ion-exchange fibers for iontophoresis [75], [78], [79]. Jaskari et al. showed that ion-exchange fibers can be suitable drug reservoirs in iontophoresis [75]. Malinovskaja et al. have demonstrated the efficient use of ion-exchange fibers in iontophoretic delivery of apomorphine and leuprorelin [78], [79]. In addition to these studies, Gao et al. have performed a more detailed analysis of ion-exchange fibers in terms of drug loading, drug release, and iontophoretic properties where they used tramadol as the model drug [80]. Their findings indicate the benefits of ion-exchange fibers such as uniform loading of the drug and the possibility of controllable delivery via iontophoresis [80]. Vispute et al. found that ion-exchange fibers have better iontophoretic properties concerning the loading and release of cationic drugs in comparison with ion-exchange resins [124].

It is clear from the research findings that ion-exchange fibers have suitable properties for iontophoretic drug delivery and a high capacity for drug loading. However, the properties of ion-exchange fibers related to drug delivery are not easily tunable when aiming at specific applications. Ion-exchange fibers also require special packing and appropriate enclosure to form mechanically stable reservoirs of a predetermined geometry. On the other hand, composite hydrogel membranes offer a high degree of customization and adjustment already during the synthesis. Reservoirs in the form of composite hydrogel membranes can be prepared with defined thickness and molded into different shapes while the mechanical support is already incorporated during fabrication.

1.1.14 Composite hydrogels based on PAA and biodegradable polymers

Composite hydrogel implants composed of PAA and a biodegradable polymer matrix can be interesting materials for implantable reservoirs intended to perform subcutaneous passive delivery of cationic drugs governed by ion exchange. The presence of abundant carboxyl groups on the surface of implantable reservoirs may be beneficial for drug release since they can weaken the inflammatory response and inhibit the formation of a fibrotic capsule around the implant [125]. Magnetic microspheres [126] and composite membranes with antibacterial properties [127] were obtained in previous studies by exploiting copolymerization of PAA and chitosan. PAA was also immobilized on the surface of poly(lactic acid) as a chemically reactive cross-linker to open possibilities for diverse biomedical applications [128].

The use of gamma irradiation besides being interesting from the biomaterial sterilization point of view has interesting properties as it can simultaneously modify the properties of hydrophobic biodegradable poly(esters) comprising the polymer matrix and cause polymerization of the hydrogel (even without additional initiators). PAA hydrogels of different sizes and properties [129], [130] can be synthesized by gamma irradiation-induced polymerization of AA. Microgels of PAA can be also synthesized from dilute and acidified aqueous solutions of PAA when they are subjected to gamma irradiation from a ^{60}Co source [131]. Poly(DL-lactide-*co*-glycolide) (PLGA) is used extensively in the applications related to drug delivery due to its excellent biocompatibility and degradability under physiological conditions through the mechanisms of enzymatic chain scission and hydrolysis [132], [133]. The effects of gamma irradiation on the behavior and properties of PLGA were widely investigated and well-documented in the previous studies [134]–[140]. N-methyl-2-pyrrolidone (NMP) was used as a suitable PLGA solvent in the fabrication of *in situ* formed implantable reservoirs for drug delivery (which essentially exploits the process of liquid phase inversion) using a gamma irradiation dose of 25 kGy [141], [142], but also without the use of gamma irradiation [143]. Previous studies showed the interesting phase inversion dynamics of PLGA which leads to the formation of porous PLGA matrices after the quenching of PLGA solutions in NMP with aqueous solutions to induce liquid phase inversion [144]–[146]. The porosity of the PLGA matrix can affect other important parameters related to drug delivery including degradation rate, mechanism of drug release, and drug release kinetics [147], [148].

In composite hydrogel materials, cross-linked PAA hydrogel can provide controlled release of cationic drugs via ion exchange, while the drug release rate can be additionally reduced by manipulating the microstructure of the biodegradable hydrophobic matrix to obtain a rate-limiting barrier. On the other hand, tunable porosity of the hydrophobic matrix can be also used to achieve the electrical responsivity of implantable drug reservoirs.

1.2 Research motivation and our approach

1.2.1 Our concept of composite hydrogel reservoirs

Several fundamental concepts and diverse beneficial properties of biomaterials can be exploited in transdermal or subcutaneous controlled drug delivery as evidenced by the relevant findings of the aforementioned studies. Hence, in order to design and fabricate innovative drug delivery systems, one must adopt a multifaceted approach. Our research was mainly inspired by the concepts of ion exchange (enabling good control over drug release through non-specific electrical phenomena) and composite hydrogel membranes (opening the possibility for the fabrication of compact mechanically stable structures that respond rapidly to external stimuli). A combination of these concepts with the appropriate selection of biomaterials and synthesis methods can lead to a new class of versatile cationic drug reservoirs suitable for passive or iontophoretic drug delivery. Our aim in a broader context was to fill the gap in the development of stand-alone cationic drug reservoirs composed of composite hydrogel materials for the purpose of controlled transdermal and subcutaneous drug delivery.

Our idea was to use a relatively rigid hydrophobic polymer matrix as the mechanical support and rate-limiting barrier for controlled drug release, while a soft cross-linked hydrogel should store the hydrophilic cationic drug and act as an ion exchanger. This idea underpins the concept of composite hydrogel reservoirs (**Figure 1.2**).

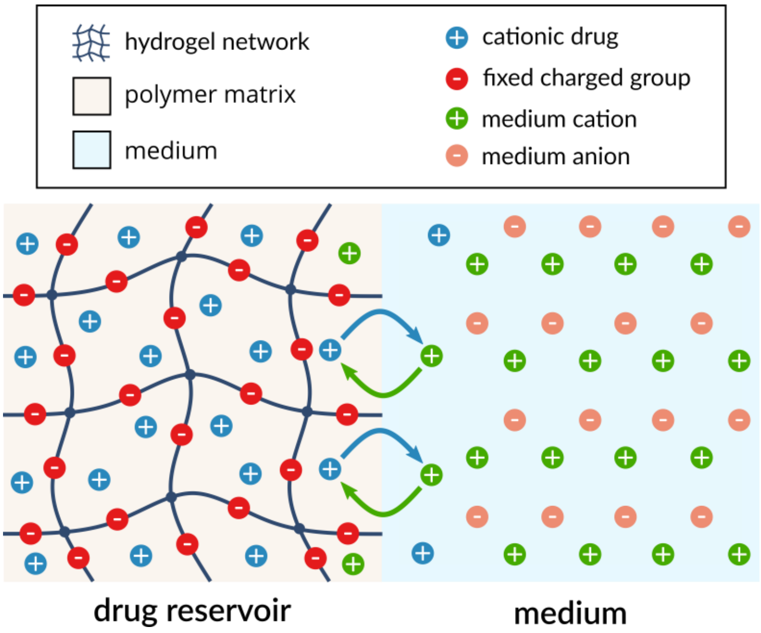

Figure 1.2. Illustration of our composite hydrogel reservoir concept.

In order to fabricate composite hydrogel membranes and implants of a suitable microstructure and functionality, we turned to modification of the traditional liquid phase inversion process ubiquitous in membrane technology. We triggered polymerization of a hydrogel by irradiation of the initial homogeneous solution containing all precursor materials and subsequently finalized the solidification process through nonsolvent induced phase separation.

Careful selection of precursor materials and functional components for composite hydrogel reservoirs should be performed in order to obtain adequate properties suitable for versatile applications including passive or iontophoretic drug delivery.

1.2.2 Selection of precursor materials and functional components

We required a biocompatible and powerful solubilizing agent for the formation of a homogeneous initial solution containing diverse precursor materials including hydrophobic polymers, hydrophilic monomers, cross-linkers, and photoinitiators. Therefore, we selected NMP as a common solvent for all precursors used in the synthesis. NMP is an aprotic solvent miscible with water, approved by the Food and Drug Administration, adequate for fast solidification of polymer-based implants, and tested in numerous pharmaceutical applications [149]. **Figure 1.3** shows the structure of NMP.

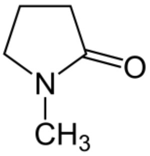

Figure 1.3. Structure of NMP. Source: [150].

As a polymer matrix for composite membranes, we selected PES that is abundantly used as the main constituent of rigid porous membranes in various applications. PES is an amorphous high-performance thermoplastic polymer characterized by good thermal stability, high glass transition temperature (above

190 °C), good mechanical properties and excellent chemical resistance in the wide range of pH values [116], [151]–[153]. By selecting the molecular weight of PES, one can alter the local pore size and overall porosity of the synthesized membrane [154]. Although PES is considered a promising material for biomedical applications, its hydrophilicity and biocompatibility need to be improved to avoid biofouling of PES-based membranes, and this is commonly performed by chemical surface modification [116], [151]. **Figure 1.4** illustrates the structure of PES.

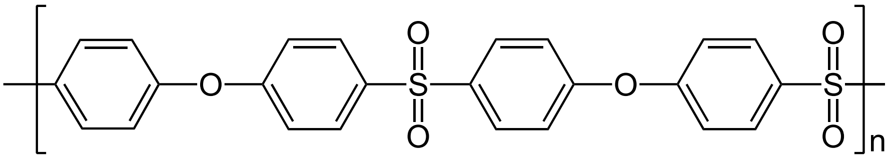

Figure 1.4. Structure of the PES repeating unit. Source: [155].

We selected poly(DL-lactide-*co*-ε-caprolactone) (DL-PLCL) and PLGA as biodegradable polymer matrices for composite implants. These materials are block copolymers of poly(esters) well-known for their biocompatibility, safety, and widespread use in implantable polymeric drug delivery systems. These two amorphous polymers have different expected degradation times and significantly different glass transition temperatures (between -50 °C and -40 °C for 25:75 DL-PLCL [156] and typically reported to be above 37 °C for PLGA [157]). **Figures 1.5** and **1.6** show the structures of DL-PLCL and PLGA, respectively.

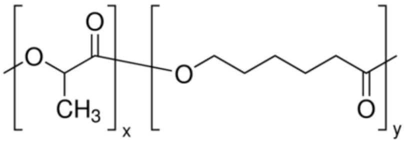

Figure 1.5. Structure of the DL-PLCL block copolymer. Numbers of lactic acid and caprolactone units are designated as x and y, respectively. Source: [158].

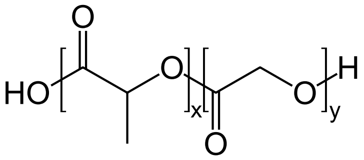

Figure 1.6. Structure of the PLGA block copolymer. Numbers of lactic acid and glycolic acid units are designated as x and y, respectively. Source: [159].

As the soft hydrogel component of composite hydrogel reservoirs, we selected PAA. PAA hydrogel is a promising material for the storage of cationic drugs since it contains fixed ionizable groups and can act as a polyelectrolyte in aqueous solutions. Polyelectrolyte behavior of hydrogels can be advantageous for the control of drug release governed by non-specific electrostatic interactions [160], [161]. The abundance of ionizable carboxyl groups in PAA enables cation exchange [69], imparts electrical conductivity [162], and leads to the pH-responsive behavior if the molecular weight is sufficiently high (above 16.5 kDa) [163]. Considering its interesting properties, PAA can be employed as a versatile cationic drug storage component suitable for passive delivery governed by ion exchange or iontophoretic delivery driven by the application of electric current. However, PAA generally exhibits a quite high swelling degree in the physiological environment and survives extensive volume expansion when the electric field is applied under physiological conditions [164]. Reinforcement of PAA with a mechanically stronger polymer matrix through the formation of a composite hydrogel material can be a good option for the reduction of mechanical instability. **Figure 1.7** illustrates the structure of PAA.

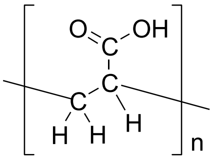

Figure 1.7. Structure of the PAA repeating unit. Source: [165].

For *in vitro* investigations of controlled cationic drug release from our composite hydrogel reservoirs, we selected methylene blue (MB) as the model drug. MB is a phenothiazinium dye placed on the World Health Organization's List of Essential Medicines [166]. MB was selected due to its cationic nature in aqueous solutions, low molecular weight, ease of spectrophotometric detection, and previous use in iontophoretic studies [167]–[169]. Controlled delivery of MB sparked additional interest due to the promising results obtained with antibacterial dressings containing MB in the management of chronic wounds including pressure injuries and diabetic ulcers [170], [171]. **Figure 1.8** shows the structure of MB.

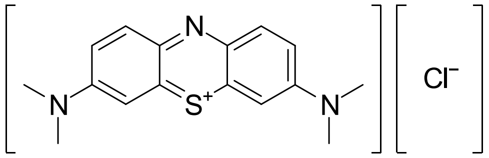

Figure 1.8. Structure of the MB molecule. Source: [172].

1.3 Aims, scope, and organization of the dissertation

Main aims of this dissertation are the following:

- to synthesize and characterize a new class of improved composite hydrogel reservoirs suitable for the use in transdermal and subcutaneous drug delivery systems,
- to develop a robust and scalable method for the synthesis of composite cationic drug reservoirs based on a cross-linked PAA hydrogel as the main storage component and the hydrophobic polymer matrix as the supporting component,
- to analyze the influence of electrical excitation on the iontophoretic delivery of cationic drugs from composite hydrogel reservoirs intended for transdermal drug delivery,
- to establish a modeling approach that adequately describes the release of cationic drugs from composite hydrogel reservoirs, and
- to engineer customized electronic devices for *in vitro* iontophoresis and electrical characterization.

This dissertation is mainly based on the following publications [173]–[176]:

I **Ž. Janićijević** and F. Radovanović, "Polyethersulfone/poly(acrylic acid) composite hydrogel membrane reservoirs for controlled delivery of cationic drug formulations," *Polymer (Guildf).*, vol. 147, pp. 56–66, Jul. 2018, doi: 10.1016/j.polymer.2018.05.065.

II **Ž. Janićijević**, M. Ninkov, M. Kataranovski, and F. Radovanović, "Poly(DL-Lactide-*co*-ε-Caprolactone)/Poly(Acrylic Acid) Composite Implant for Controlled Delivery of Cationic Drugs," *Macromol. Biosci.*, vol. 19, no. 2, p. 1800322, Feb. 2019, doi: 10.1002/mabi.201800322.

III **Ž. Janićijević**, I. Vujčić, Đ. Veljović, M. Vujisić, and F. Radovanović, "Composite poly(DL-lactide-*co*-glycolide)/poly(acrylic acid) hydrogels synthesized using UV and gamma irradiation: comparison of material properties," *Radiat. Phys. Chem.*, vol. 166, p. 108466, Jan. 2020, doi: 10.1016/j.radphyschem.2019.108466.

IV P. Atanasijević and **Ž. Janićijević**, "Programabilni pulsni strujni izvor za *in vitro* ispitivanja jontoforeze [Programmable pulse current source for *in vitro* investigations of iontophoresis]," u *Zborniku 61. Konferencije za elektroniku, telekomunikacije, računarstvo, automatiku i nuklearnu tehniku, ETRAN 2017*, 2017, pp. BT1.2.1-5.

The content of these publications is reused in accordance with the kind permissions of the publishers. The publications are referred to by the corresponding Roman numerals provided at the end of each section title and also cited directly in the text when necessary for clarity.

It is important to note that the investigations of composite hydrogel implant biocompatibility (part of the journal article **II**[1]) fall outside of the scope of this dissertation as the author had only a minor contribution in this part of the research. We shall briefly summarize the findings of biocompatibility tests in the final section of the results (**4.9 Biocompatibility of composite DL-PLCL/PAA implants**) for completeness.

The dissertation is organized into the following chapters:

- **Chapter 2** provides a list of materials used for experiments in the dissertation and gives a detailed description of employed experimental, numerical, and statistical methods.
- **Chapter 3** describes the design of custom-built electronic devices used in experimental setups for electrical characterization and *in vitro* iontophoretic drug delivery.
- **Chapter 4** comprises all results and findings of the dissertation regarding the characterization of the composite hydrogel materials, analysis of composite hydrogel properties relevant for passive and iontophoretic drug delivery, and investigations of *in vitro* release of MB as the model drug from the composite hydrogel reservoirs.
- **Chapter 5** explains in detail the modeling approaches used in this dissertation. The first part of the chapter explains the use of the gel correlation length model in the estimation of the composite hydrogel pore size. Latter parts of the chapter focus on the models of cationic drug release from composite hydrogel reservoirs where we combine the analytical models of diffusion from monolithic drug reservoirs with the empirical Weber-Morris model.
- **Chapter 6** presents the discussion of the results and findings from this dissertation in the broader context and provides some relevant comparisons with other available materials. This chapter also points out important knowledge gaps that should be the topics of further research.
- **Chapter 7** summarizes the contributions of the dissertation and provides recommendations for further research.

---

[1] [174] Ž. Janićijević, M. Ninkov, M. Kataranovski, and F. Radovanović, "Poly(DL-Lactide-*co*-ε-Caprolactone)/Poly(Acrylic Acid) Composite Implant for Controlled Delivery of Cationic Drugs," *Macromol. Biosci.*, vol. 19, no. 2, p. 1800322, Feb. 2019, doi: 10.1002/mabi.201800322.

Chapter 2: Materials and Methods

2.1 Materials (I-III)

Materials used in the experiments conducted as part of this dissertation are listed below with their corresponding details (M_w designates the mass-average molecular weight, M_n designates the number-average molecular weight, and PDI the polydispersity index of the polymer):

- N-methyl-2-pyrrolidone (NMP) (purity 99%), Sigma-Aldrich, Germany
- acrylic acid (AA) (purity 99%), Sigma-Aldrich, Germany
- polyethersulfone (PES) (Ultrason E 6020P, M_w = 75 kDa, PDI = 3.4), BASF, Germany
- poly(DL-lactide-*co*-ε-caprolactone) (DL-PLCL) (25:75, M_w = 96.7 kDa, PDI = 1.61), DURECT Corporation, USA
- poly(DL-lactide-*co*-glycolide) (PLGA) (50:50, M_w = (31.3-57.6) kDa, ester-terminated), DURECT Corporation, USA
- acrylamide (AAm) (purity ≥99%), Sigma-Aldrich, Germany
- *N,N'*-methylenebis(acrylamide) (MBAA) (purity 99%), Sigma-Aldrich, Germany
- trimethylolpropane ethoxylate triacrylate (TMPTA) (average M_n ~912 Da), Sigma-Aldrich, Germany
- bis(2,4,6-trimethylbenzoyl)-phenylphosphineoxide (Irgacure 819), Ciba SC, Switzerland
- potassium persulfate ($K_2S_2O_8$) (purity ≥99%), Sigma-Aldrich, Germany
- methylene blue (MB) (powder, Reag. Ph.Eur.), E. Merck, Germany
- potassium dihydrogen phosphate (KH_2PO_4) (purity p.a., >99%), Centrohem, Serbia
- potassium chloride (KCl) (purity p.a., >99%), Centrohem, Serbia
- citric acid monohydrate (CA) (Ph.Eur.), Alkaloid, Republic of North Macedonia
- sodium hydroxide (NaOH) (purity p.a., >98%), Centrohem, Serbia
- hydrochloric acid (HCl) (37%), VWR Chemicals, France
- *n*-heptane (purity ≥99%), VWR Chemicals, France
- ethanol (purity p.a. or 96 vol%), Zorka Pharma, Serbia
- Teflon rings (PTFE Flat Washer, thickness 0.787 mm, inside diameter 11.11 mm), USA
- Teflon rings (PTFE Flat Washer, thickness 1.575 mm, inside diameter 11.252 mm), USA
- fluorinated ethylene propylene non-stick film (thickness 25 μm), Scientific Commodities, Inc., USA
- polyester spunbond nonwoven fabric (Type 078/20, area weight 21 $g \cdot m^{-2}$), Johns Manville Sales GmbH, Germany
- intravenous (IV) tubing (3 mm inside diameter), Van Oostveen Medical B.V. - Romed Holland, Netherlands
- platinum wire (purity 99.9%, 0.5 mm diameter), uGems, USA
- stainless steel plate electrodes (AISI304L, 0.5 mm thickness), Latifović d.o.o., Serbia

- pencil lead graphite (Mars micro carbon 250, degree 2B, 0.5 mm diameter), STAEDTLER Mars GmbH & Co. KG, Germany
- glass plates (length 100 mm, width 100 mm, thickness 3 mm), Serbia

All materials were used as supplied without additional treatment or modifications. Aqueous solutions were prepared using distilled water.

2.2 Methods (I-III)

2.2.1 Formulation of casting solutions for membranes and implants (I-III)

In this dissertation, concentrations of different components in the casting solution are expressed as follows:

- polymer base (PB) concentration is designated in wt%,
- monomer (MM) concentration is designated in mmol·g^{-1} of the dry product assuming the reactant conversion yield of 100%, and
- cross-linker (CL) concentration is designated in mol% with respect to the MM concentration.

The formulations are then presented with the code xPB-yMM-zCL where x, y, and z denote the numerical values of corresponding PB, MM, and CL concentrations, respectively. All casting solutions were prepared using NMP as a common solvent for all components.

2.2.2 Protocol for buffer preparation (I-III)

Two types of buffered solutions were prepared for the experiments: citrate buffer (CB) and phosphate-buffered saline (PBS). At first, the predetermined amounts of CA or KH_2PO_4 were weighed and dissolved in 950 cm^3 of distilled water in a beaker. Small amounts of solid NaOH were gradually added to the stirred solution while the pH was monitored using a pH-meter (HI 3222, Hanna Instruments, Romania). After the desired buffer pH was reached, the obtained solution was transferred to a 1 dm^3 volumetric flask. Finally, distilled water was added to the volumetric flask up to the graduation mark to obtain the buffer solution with defined pH (pH = 3 (for CB), 7.4, and 8 (for PBS)) and ionic strength (I) ($I = 0.154$ M (for PBS) and 0.2 M (for CB or PBS)).

2.2.3 Synthesis of composite hydrogel membranes (I)

Composite hydrogel membranes were synthesized using the modified protocol of conventional liquid phase inversion [100]. Hydrogel MM and CL were mixed with the hydrophobic PB solution and copolymerized using UV irradiation, before the immersion into the nonsolvent aqueous bath which finalized phase separation and solidification (**Figure 2.1**). The AA MM was copolymerized with a bifunctional (MBAA) or trifunctional (TMPTA) CL to obtain membranes with different properties.

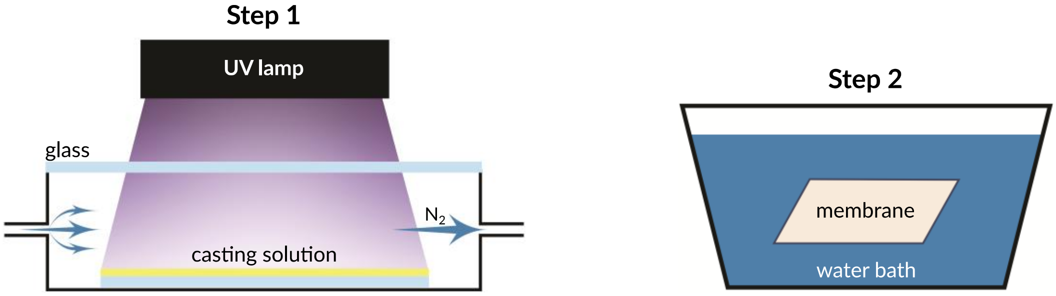

Figure 2.1. Illustration of the composite PES/PAA membrane synthesis process comprising two main steps: 1) UV irradiation of the casting solution and 2) phase separation and solidification in the water bath.

30 wt% PB solution of PES in NMP was prepared by overnight stirring at the elevated temperature of 80 °C. Solutions of photopolymerizable components (AA, MBAA or TMPTA, and photoinitiator Irgacure 819 (PI)) in NMP were freshly prepared before the synthesis. Casting solutions for membrane fabrication were obtained by mixing the predetermined quantities of PES solution and solutions of

photopolymerizable components. Composite PES/PAA membranes were synthesized using four different formulations of the casting solution (12PES-7AA-10MBAA, 14PES-6.5AA-10MBAA, 12PES-5.3AA-5TMPTA, and 14PES-5AA-5TMPTA). Compositions of the casting solutions for the synthesis are listed in **Table 2.1**. Final casting solutions were viscous and transparent which confirmed that all functional components are miscible in given quantities.

Prepared solutions for membrane synthesis were cast on a glass plate with a film applicator (blade width 7.62 cm, clearance 200 µm, BYK Gardner, Germany) and then the glass plate was placed within an enclosure purged with nitrogen gas. The cast film was exposed to UV irradiation through a 3 mm thick glass window on top of the enclosure for 3 min to reach the exposure dose of 1.5 $J \cdot cm^{-2}$ (mostly in the UVA spectral region). The exposure dose was measured by a UV light meter (Lutron YK-35UV, Lutron Electronic Enterprise Co., Taiwan). Cast solutions turned cloudy due to gel formation in the cast film. Membranes were subsequently formed by swift immersion of glass plates with UV cured cast films into the water bath. At least 10 min in the water bath was allowed for the completion of phase separation and solidification processes. After solidification in the water bath, membranes were separated from the glass plate and transferred to a beaker with distilled water for further overnight extraction of the residual solvent and unreacted components. Finally, the membranes were transferred to a storage solution (ethanol-water 1:1 (v/v) mixture) to prevent biological contamination during long-term use. Obtained membranes had a nominal size of approximately 100 mm × 76 mm × 0.2 mm.

Table 2.1. Compositions of the casting solutions used for the synthesis of composite hydrogel membranes.

Formulation code	PES (wt%)	AA (wt%)	CL (wt%)	PI (wt%)	NMP (wt%)
12PES-7AA-10MBAA	11.98	15.58	3.35[a]	0.16	68.93
14PES-6.5AA-10MBAA	13.97	15.18	3.26[a]	0.19	67.40
12PES-5.3AA-5TMPTA	11.99	12.15	7.67[b]	0.16	68.03
14PES-5AA-5TMPTA	13.98	12.21	7.74[b]	0.19	65.88

[a] CL is MBAA; [b] CL is TMPTA.

2.2.4 Synthesis of composite hydrogel implants using UV irradiation (II, III)

Composite hydrogel implants were synthesized using a similar approach as for the synthesis of composite hydrogel membranes (**Figure 2.2**).

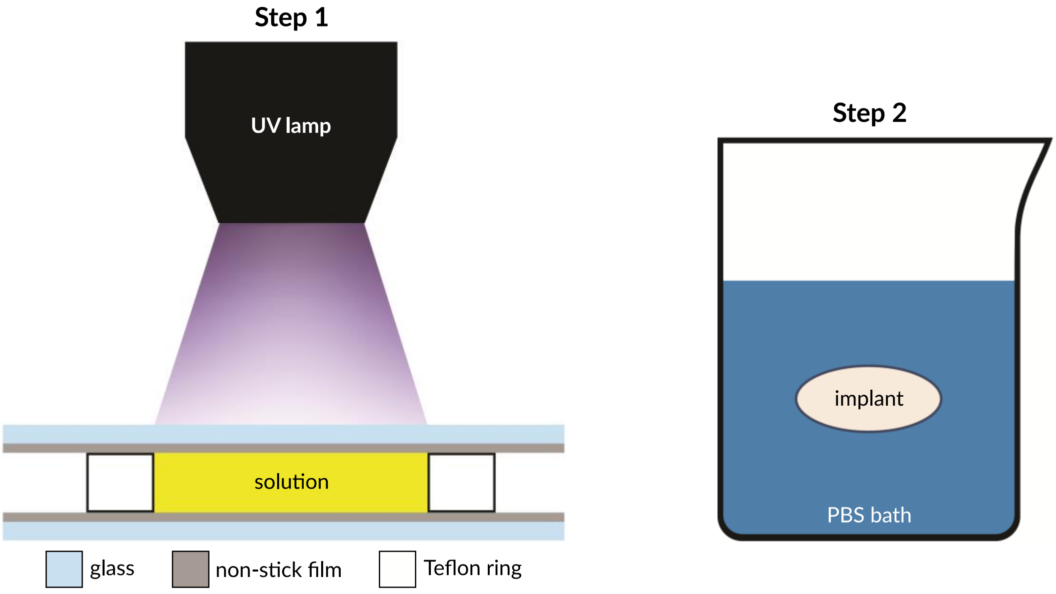

Figure 2.2. Illustration of the composite hydrogel implant synthesis process comprising two main steps: 1) UV irradiation of the dispensed solution and 2) phase separation and solidification in the PBS bath.

30 wt% solution of PB (DL-PLCL or PLGA) in NMP was prepared by overnight stirring at ambient temperature. Solutions of photopolymerizable components contained predefined amounts of AA, TMPTA and PI dissolved in NMP as a common solvent. Final precursor solutions for the synthesis were obtained by combining the predefined quantities of PB solutions and solutions of photopolymerizable components. Compositions of the final precursor solutions for the synthesis are listed in **Table 2.2**. Predetermined volumes of obtained precursor solutions were inserted with a pipette into the molds. Constructed molds comprised a Teflon ring sealed with single sheets of transparent fluorinated ethylene propylene non-stick film at the top and bottom. Such molds prevented the leakage of precursor solutions, minimized oxygen penetration, and enabled UV irradiation. Teflon rings of 0.787 mm thickness and 11.11 mm inside diameter were used to form the mold for ~0.08 cm^3 of the solution with DL-PLCL as PB. Teflon rings of 1.575 mm thickness and 11.252 mm inside diameter were used to form the mold for ~0.16 cm^3 of the solution with PLGA as PB. Solutions within the molds were exposed to UV irradiation (wavelength $\lambda = 365$ nm) through a 3 mm thick glass window for 3 min to reach the exposure dose of 3.6 $J \cdot cm^{-2}$ as recorded by the UV light meter (Lutron YK-35UV, Lutron Electronic Enterprise Co., Taiwan). The precursor solution became nontransparent after UV curing and the solidified gel was formed in the mold. The obtained gel was released from the mold and quickly dropped in the PBS solution (pH = 7.4 and $I = 0.154$ M) using a non-stick plunger. This step was performed to finalize the processes of phase separation and solidification, which resulted in the formation of white disk-shaped composite implants comprising PB combined with PAA hydrogel. Synthesized composite implants were left in the PBS solution for overnight extraction. After the extraction of unreacted components and solvent, composite hydrogel implants were transferred into the fresh PBS solution. Synthesized implants were stored either refrigerated or dried (depending on further experiments) to slow down the degradation process and minimize the possibility of biological contamination. Obtained wet composite DL-PLCL/PAA implants had a thickness of approximately 1 mm and a nominal diameter of 14.1 mm, while the wet composite PLGA/PAA implants had a thickness of approximately 2.2 mm and a nominal diameter of 13.8 mm.

Composite PLGA/PAA implants fabricated using UV irradiation are denoted in the further text as UV-PLGA-PAAs.

2.2.5 Synthesis of composite hydrogel implants using gamma irradiation (III)

Composite hydrogel implants comprising PLGA as the PB were also synthesized using gamma irradiation. The initial precursor solution and molds were prepared in the same manner as for the synthesis using UV irradiation. The only difference was the absence of the PI component from the precursor solution. The composition of the final precursor solution for the synthesis is listed in **Table 2.2**.

Table 2.2. Compositions of the solutions used for the synthesis of composite hydrogel implants. G denotes the use of gamma instead of UV irradiation for the synthesis using the formulated solution.

Formulation code	PB (wt%)	AA (wt%)	TMPTA (wt%)	PI (wt%)	NMP (wt%)
16DL-PLCL-3.41AA-10TMPTA	15.97[b]	8.84	11.18	0.21	63.80
16PLGA-3.41AA-10TMPTA	15.97[c]	8.84	11.18	0.21	63.80
16PLGA-3.41AA-10TMPTA (G)[a]	16.01[c]	8.86	11.21	0	63.92

[a] Formulation is not exactly equivalent (PI is not added to the solution); [b] PB is DL-PLCL; [c] PB is PLGA.

Teflon rings of 1.575 mm thickness and 11.252 mm inside diameter were used to form the mold for ~0.16 cm^3 of the final precursor solution. Molds containing the initial precursor solution were inserted into polypropylene ziplock bags and placed forward of the ^{60}Co source of gamma rays at predetermined positions to obtain desired irradiation parameters. Initial precursor solutions were subjected to gamma irradiation using five different combinations of dose and dose rate parameters (dose (dose rate)): 17 kGy

(8.1 kGy·h^{-1}), 25 kGy (6.1 kGy·h^{-1}), 25 kGy (8.1 kGy·h^{-1}), 25 kGy (10.1 kGy·h^{-1}), and 33 kGy (8.1 kGy·h^{-1}). The synthesis process is depicted in **Figure 2.3**.

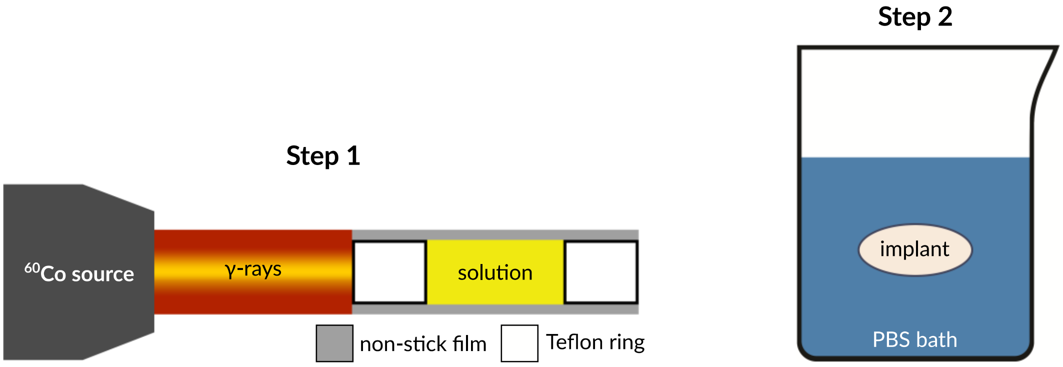

Figure 2.3. Illustration of the composite PLGA/PAA implant synthesis process comprising two main steps: 1) gamma irradiation of the dispensed solution and 2) phase separation and solidification in the PBS bath.

Irradiation of samples was carried out at ambient temperature (~25 °C) in an air atmosphere using the ^{60}Co source at the Radiation Unit for Industrial Sterilization and Conservation, Vinča Institute of Nuclear Sciences. The activity of the ^{60}Co source of gamma rays at the time was about $3.7 \cdot 10^{15}$ Bq. Gamma-ray field mapping was performed using the ethanol-chlorobenzene solution (ECB) dosimetry system [177]. An absorbed dose of high-energy radiation is routinely examined with the ECB solution which is considered as a standard dosimeter [178], [179]. Oscillotitrator (OK-302/1, Radeliks Electrochemical Instruments, Hungary) was used to perform the dosimetry measurements. Calibration of the device was carried out with ECB dosimeters irradiated at the High Dose Reference Laboratory of Risø National Laboratory, Denmark.

Curing with gamma rays resulted in solidified nontransparent yellowish gels in the molds. Obtained gels were further treated and stored in the same manner as the implants synthesized using UV irradiation. The final product of the synthesis was the disk-shaped composite implant of pale-yellow color comprising PLGA combined with PAA hydrogel. Obtained wet PLGA/PAA implants had a thickness of approximately 2.1 mm and a nominal diameter of 13.8 mm.

Composite PLGA/PAA implants fabricated using gamma irradiation are denoted in the further text as G-PLGA-PAAs.

2.2.6 Characterization of membrane and implant materials (I-III)

Materials fabricated in this dissertation were characterized using the techniques of Fourier Transform Infrared Spectroscopy-Attenuated Total Reflectance (FTIR-ATR), Scanning Electron Microscopy (SEM), and Differential Scanning Calorimetry (DSC).

Dry samples required for material characterization measurements were prepared via a dedicated solvent exchange protocol to minimize the effects of pore collapse. The wet sample for characterization was immersed in pure ethanol for 1 h and then dipped in *n*-heptane for 1 h. Finally, the sample was air-dried under ambient conditions for at least 24 h in the case of membranes or at least 72 h in the case of implants. Wet samples of composite membranes and implants were also characterized directly using FTIR-ATR.

The chemical compositions of both (top and bottom) sides of PES/PAA membranes were investigated using the Thermo Scientific Nicolet 6700 FTIR Spectrometer with Smart ATR Diamond accessory, Thermo Fisher Scientific Inc., USA (range from 525 cm^{-1} to 4000 cm^{-1}; resolution of 0.5 cm^{-1}). The top side of the membrane corresponds to the top surface of the cast film immersed in the water bath (in direct contact with the surrounding medium), while the bottom side of the membrane corresponds to the bottom surface of the cast film immersed in the water bath (initially in direct contact with the glass plate). FTIR-ATR spectra of DL-PLCL/PAA and PLGA/PAA implants were recorded using the Thermo Scientific Nicolet iS10 FTIR Spectrometer with Smart iTX ATR Diamond accessory, Thermo Fisher Scientific Inc., USA (range from 400 cm^{-1} to 4000 cm^{-1}; resolution of 0.5 cm^{-1}). Acquired spectra were normalized to the highest peak intensity in absorbance mode for qualitative interpretation and presentation except where stated otherwise.

Microstructure and morphology of the dry samples were examined using the field emission scanning electron microscope (FESEM) (TESCAN MIRA 3 XMU, TESCAN, Czech Republic) operated at the voltage of 20 kV. Before imaging, the samples were cooled in liquid nitrogen and fractured to reveal cross-sectional surfaces. All surfaces to be imaged were sputtered with a thin layer of gold or carbon. Where reported, the average particle size was determined by measuring the Feret diameter of 40-200 particles using the ImageJ 1.52j software for image processing [180].

Glass transitions in PLGA/PAA implants were recorded using the device DSC131 EVO, SETARAM, France, which is operated via the CALISTO software. Dry samples for the analysis were hermetically sealed within aluminum pans of 30 mm^3 volume and subjected to controlled heating in a chamber purged with nitrogen (range from 10 °C to 140 °C; the heating rate of 10 $°\text{C}\cdot\text{min}^{-1}$). Acquired DSC thermograms were normalized to the PLGA content in the sample with respect to its weight fraction. Halfwidth of the enthalpic relaxation peak coupled with the glass transition was used to determine the value of glass transition temperature (T_g).

2.2.7 Mass swelling degree of composite membranes and implants (I-III)

Adequate volumes of the swelling solutions, equilibration period, and drying parameters for the samples of composite membranes and implants were determined in the preliminary experiments. Before the measurement of mass swelling degree (MSD), a sample (membrane sheet of ~1 cm^2 area or a single implant) was immersed and equilibrated for 24 h in the excess amount (50-100 cm^3) of swelling solution. After this period, the wet sample was weighed and then left in the oven to dry for 2 h at 100 °C. Finally, the dry sample was weighed.

MSD of the sample was calculated using the following expression:

$$\text{MSD (\%)} = \frac{(m_\text{w} - m_\text{d})}{m_\text{d}} \cdot 100\% \tag{2.1}$$

where m_w is the wet sample weight and m_d the dry sample weight.

MSDs of composite membranes were investigated in distilled water, PBS (pH = 8 and I = 0.2 M), CB (pH = 3 and I = 0.2 M), and MB solutions of different initial concentrations (in the approximate range from 0.05 $\text{g}\cdot\text{dm}^{-3}$ to 0.45 $\text{g}\cdot\text{dm}^{-3}$). MSDs of all composite implants were investigated in PBS only.

The experiments were performed in triplicate for composite PES/PAA membranes and DL-PLCL/PAA implants. For the composite PLGA/PAA implants, the experiments were carried out in duplicate.

2.2.8 Swelling kinetics of composite implants (II, III)

All composite hydrogel implants were prepared for swelling kinetics measurements by equilibration in PBS and subsequent drying. As a first step of the preparation, the implant was equilibrated in PBS for 24 h, carefully blotted with filter paper, and then weighed. After weighing, the implant was dried at ambient temperature under atmospheric pressure for 72 h. At the beginning of the experiment, the dry implant was weighed and then immersed in the excess amount (~80 cm^3) of PBS within a large Petri dish. Implant weight (in the approximate range from 30 mg to 330 mg) was monitored at predetermined time intervals until MSD approached the equilibrium value. For each weighing, the implant was taken out of the Petri dish, carefully blotted with filter paper, weighed, and then quickly immersed again in the PBS solution. The swelling kinetics experiments were performed in triplicate for all composite implants.

2.2.9 Ion-exchange capacity of composite membranes and implants (I-III)

Ion-exchange capacity (IEC) corresponds to the concentration of carboxyl groups (C_cg) which act as weak cation exchangers. The C_cg was determined using the acid-base titration method. At the beginning of the experiment, samples of all composite membranes and implants (approximately 15-70 mg of dry weight) were cut into smaller pieces, immersed in the solution of HCl (membranes in 10 cm^3 of 1 M HCl and implants in 100 cm^3 of 0.1 M HCl), and stirred for 1 h on a magnetic stirrer to protonate carboxyl groups. The samples were then removed from the HCl solution, rinsed with copious amounts of distilled water, and carefully blotted using tissue paper. After blotting, the protonated samples were immersed in 40 cm^3 of 0.01 M NaOH solution and stirred for 1 h in a capped beaker on a magnetic stirrer. The samples were then removed from the residual solution, washed with distilled water, and left to dry in the oven at 100 °C under atmospheric pressure for 2 h. Finally, the dry weights of the samples were measured.

Measurements were carried out by titrating two 15 cm^3 aliquots of the residual solution with 0.01 M HCl and two 15 cm^3 aliquots of the initial 0.01 M NaOH solution as blank probes. Potentiometric (pH-meter HI3222, Hanna Instruments, Romania) or conductometric (conductometer TDS-EC Meter, Digital Aid, USA) titration curves were recorded and the equivalence point was calculated using the MATLAB programming package.

C_{cg} was calculated by using the expression:

$$C_{\mathrm{cg}}\ (\mathrm{mmol}\cdot\mathrm{g}^{-1}) = \frac{0.4\cdot\left(1-\frac{V_{\mathrm{r}}}{V_{\mathrm{b}}}\right)}{m_{\mathrm{d}}} \tag{2.2}$$

where V_{r} is the average volume of 0.01 M HCl solution consumed to titrate the residual solution, V_{b} is the average volume of 0.01 M HCl solution consumed to titrate the blank probe solution, and m_{d} is the dry sample weight.

Reaction yield (RY) of composite membranes and implants was calculated as a ratio of C_{cg} and concentration of AA corresponding to the casting solution formulation expressed in mmol·g^{-1} within the final dry product assuming the reactant conversion yield of 100%.

The experiments were performed in duplicate for all composite membranes and implants.

2.2.10 Measurement of ionic conductivity of composite PES/PAA membranes

Ionic conductivity of composite PES/PAA membranes (12PES-5.3AA-5TMPTA) was measured at an ambient temperature of 22 °C using the method of Electrical Impedance Spectroscopy (EIS). The geometry of the experimental setup was similar to the one used for the EIS measurements on polymer electrolyte films [181]. EIS measurements were performed in the frequency range above 1 kHz where the dominantly resistive response is expected for ion-exchange membranes as shown by previous research [182].

At first, the wet composite PES/PAA membrane (12PES-5.3AA-5TMPTA) samples equilibrated in PBS (pH = 7.4 and I = 0.154 M) for 24 h were cut to match the shape of stainless steel blocking electrodes (2.1 cm × 2.1 cm × 0.05 cm). Subsequently, each of the samples was mounted between the electrodes and kept under constant pressure using a spring clamp during the measurement. The thickness of the membrane samples was determined indirectly by subtracting the thickness of the electrodes without the sample from the thickness of the setup containing the membrane sample sandwiched between the electrodes. Individual thicknesses were determined using the vernier caliper.

Setup for EIS measurements comprised the digital lock-in amplifier (SR850, Stanford Research Systems, USA) and a custom-built analog front end constructed to enable four-terminal impedance sensing (for details refer to section **3.1 Analog front-end for the lock-in amplifier**). The measurements were carried out in the frequency range from 75 to 100 kHz with the step of 5 kHz using the excitation amplitude of 150 mV RMS. Measured impedance magnitude was averaged over the frequency range for each of the membrane samples under test and defined as the bulk resistance of the membrane sample R_{B}. The value of R_{B} can then be used to calculate the membrane resistance:

$$R_{\mathrm{m}} = R_{\mathrm{B}}\cdot S_{\mathrm{e}} \tag{2.3}$$

where S_{e} designates the surface area of the stainless steel blocking electrodes.

Bulk ionic conductivity of the composite PES/PAA membrane σ_m can then be calculated in the same manner as for polymer electrolyte films [181] and is given by:

$$\sigma_{\mathrm{m}} = \frac{d_{\mathrm{m}}}{R_{\mathrm{m}}} \tag{2.4}$$

where d_m designates the clamped membrane sample thickness during the EIS measurement.

The experiments were performed in triplicate.

2.2.11 Loading of composite membranes and implants with MB (I, II)

Loading with MB was carried out for composite PES/PAA membranes (12PES-5.3AA-5TMPTA) and composite DL-PLCL/PAA implants (16DL-PLCL-3.41AA-10TMPTA).

Each of the wet membrane samples of approximately 1 cm^2 area was initially equilibrated in 50 cm^3 of PBS (pH = 8.0 and I = 0.2 M) for 24 h to deprotonate carboxyl groups. The samples were then rinsed with distilled water, blotted with tissue paper, and weighed. After weighing, each sample was immersed in 50 cm^3 of a predetermined MB aqueous solution for 24 h. The loading solution with the sample was kept in a dark space to avoid MB photolysis.

MB solutions were prepared with different concentrations to study the loading efficiency and *in vitro* release performance at different loadings. MB solution concentrations were adjusted to achieve predetermined molar ratios of MB cations (MB$^+$) and carboxyl groups (-COOH) in the membrane (n(MB$^+$)/n(-COOH) = 0.5, 1, or 1.5) assuming the 100% reactant conversion yield. For typical values of MB concentrations refer to **Table 2.3**. A similar experimental approach was used by Gao et al. in the investigation of ion-exchange fiber loading efficiency [80]. Initial MB concentrations were calculated by utilizing wet membrane weight, mean MSD, and mean C_{cg} values determined in previous experiments conducted as described in sections **2.2.7 Mass swelling degree of composite membranes and implants** and **2.2.9 Ion-exchange capacity of composite membranes and implants**. For calculation details refer to section **Appendix A: Calculation of MB amount in the loading solutions**.

Table 2.3. Typical initial concentrations of MB solutions used for the loading of composite PES/PAA membrane (12PES-5.3AA-5TMPTA) samples. The listed MB concentrations were used for the membrane samples with an estimated dry weight of 10 mg that were immersed in 50 cm^3 of the loading solution.

n(MB$^+$)/n(-COOH)	MB concentration (g·dm^{-3})
0.5	0.14
1	0.28
1.5	0.42

Wet implant samples were equilibrated in 50 cm^3 of PBS (pH = 7.4 and I = 0.154 M) for 24 h. After this period, samples were washed with distilled water, blotted with filter paper, and weighed. Each implant was then immersed in 25 cm^3 of 1 g·dm^{-3} MB aqueous solution for 120 h. The loading solution with the implant was kept in a dark space to avoid MB photolysis. The weight of MB in aqueous solution corresponded to the molar ratio n(MB$^+$)/n(-COOH) = 1. Initial MB concentration was calculated in the same manner as for membranes.

The maximum loading efficiency of 100% was defined as equivalent to the measured mean IEC of the corresponding composite hydrogel material. The measured amount of loaded MB per unit weight of the dry composite hydrogel was normalized with respect to the mean IEC and reported as the loading efficiency.

All MB loading experiments were performed in triplicate.

2.2.12 Passive MB release *in vitro* from composite membranes and implants (I, II)

After the MB loading experiments, composite PES/PAA membranes (12PES-5.3AA-5TMPTA) and composite DL-PLCL/PAA implants (16DL-PLCL-3.41AA-10TMPTA) loaded with MB were rinsed with distilled water and their surface was blotted with tissue paper.

Membrane samples were then immersed in 200 cm^3 of buffered solution (PBS (pH = 8 and I = 0.2 M) or CB (pH = 3 and I = 0.2 M)), which was stirred at 500 rpm on a magnetic stirrer at ambient temperature. MB release kinetics was monitored by measuring the MB content in 3 cm^3 solution aliquots taken at predetermined time intervals which were immediately replaced with the same volume of a fresh buffered solution. MB concentration in the aliquots was determined from absorbance values recorded at the wavelength of 664 nm using the UV-Vis Spectrometer (Cintra 101, GBC Scientific Equipment Ltd., Australia). When the point of saturation in MB release kinetics was approached, stirring was stopped and the obtained solutions were placed in the dark to equilibrate with the membrane samples for at least 48 h. Finally, the released amount of MB in equilibrium was recorded.

After MB release in the buffered aqueous solution, membrane samples were again washed with distilled water and carefully blotted. The MB release experiments were continued by immersing each sample in 50 cm^3 of 96 vol% ethanol and stirring the new solutions with membranes at 1100 rpm on a magnetic stirrer at ambient temperature for 3 h. MB content in the obtained solutions was determined spectrophotometrically at the end of this experimental step. Membrane samples were dried in the oven at 100 °C for 1 h after the MB release experiments and then weighed.

Prepared implants previously loaded with MB (which had a mean thickness of 1.258 mm, mean diameter of 13 mm and approximate weight of 167 mg) were immersed in 50 cm^3 of PBS (pH = 7.4 and I = 0.154 M). Beakers containing the solution and implant were kept at 37 ± 0.1 °C inside a water bath without stirring during the entire period of MB release experiments. MB release kinetics was monitored for 28 days by measuring the MB content in 3 cm^3 solution aliquots taken at predetermined time intervals. MB concentration in the aliquots was calculated from the absorbance recorded at the wavelength of 664 nm by using the UV-Vis Spectrometer (Cintra 101, GBC Scientific Equipment Ltd., Australia). After each sampling of the solution, its entire volume was discarded and quickly replaced with 50 cm^3 of fresh PBS previously heated up to 37 °C.

Experiments of passive MB release *in vitro* from composite PES/PAA membranes were performed in duplicate, while the experiments of passive MB release *in vitro* from composite DL-PLCL/PAA implants were carried out in triplicate.

2.2.13 Protocol for the preparation of the conductive polyacrylamide hydrogel

The conductive gel was synthesized for the salt bridges in the experiments of iontophoretic MB release. The gel was based on the thermally cross-linked polyacrylamide (PAAm) hydrogel containing a concentrated solution of KCl. To prepare the conductive gel, 0.287 g of AAm MM, 0.01 g of MBAA CL, 0.6 cm^3 of 10 g·dm^{-3} $K_2S_2O_8$ thermal initiator solution, and 5.34 cm^3 of 2 M KCl solution were mixed to form a transparent homogeneous aqueous solution. The obtained solution was then injected into multiple pieces of IV tubing (each of ~5 cm length and 3 mm inside diameter) using the syringe and needle to fill approximately 2/3 of the volume. The pieces of IV tubing filled with the precursor solution were subsequently clamped on both sides and placed in the oven at 80 °C for 30 min to form the hydrogel by thermal cross-linking. Pieces of IV tubing with the formed hydrogel were unclamped and finally submerged in 200 cm^3 of 2 M KCl solution for 24 h to extract the unreacted components and saturate the hydrogel with the solution. The IV tubings with prepared conductive hydrogel were stored in a fresh 2 M KCl solution at ambient temperature for further use.

2.2.14 Iontophoretic *in vitro* release of MB from composite PES/PAA membranes

Circular wet samples of composite PES/PAA membranes (12PES-5.3AA-5TMPTA) having a nominal thickness of 0.02 mm and an approximate diameter of 1.9 cm were at first equilibrated in 50 cm^3 of PBS (pH = 7.4 and I = 0.154 M) for 24 h to deprotonate carboxyl groups. The samples were subsequently rinsed with distilled water, carefully blotted with tissue paper, and weighed. After weighing, each of the membrane samples was immersed in 1 g·dm^{-3} MB aqueous solution for loading. The volume of MB solution was calculated based on the wet membrane weight, mean MSD, and mean C_{cg} separately for each sample to achieve the molar ratio n(MB$^+$)/n(-COOH) = 1. For calculation details refer to section **Appendix A: Calculation of MB amount in the loading solutions**. The membrane samples were left to absorb MB for at least 120 h in the dark to reach equilibrium loading. Loading efficiency was defined as described in section **2.2.11 Loading of composite membranes and implants with MB**. After MB loading, membrane samples were rinsed with copious amounts of distilled water to remove weakly bound MB from the surface and carefully blotted with tissue paper. Iontophoresis experiments were performed in an experimental setup illustrated in **Figure 2.4**.

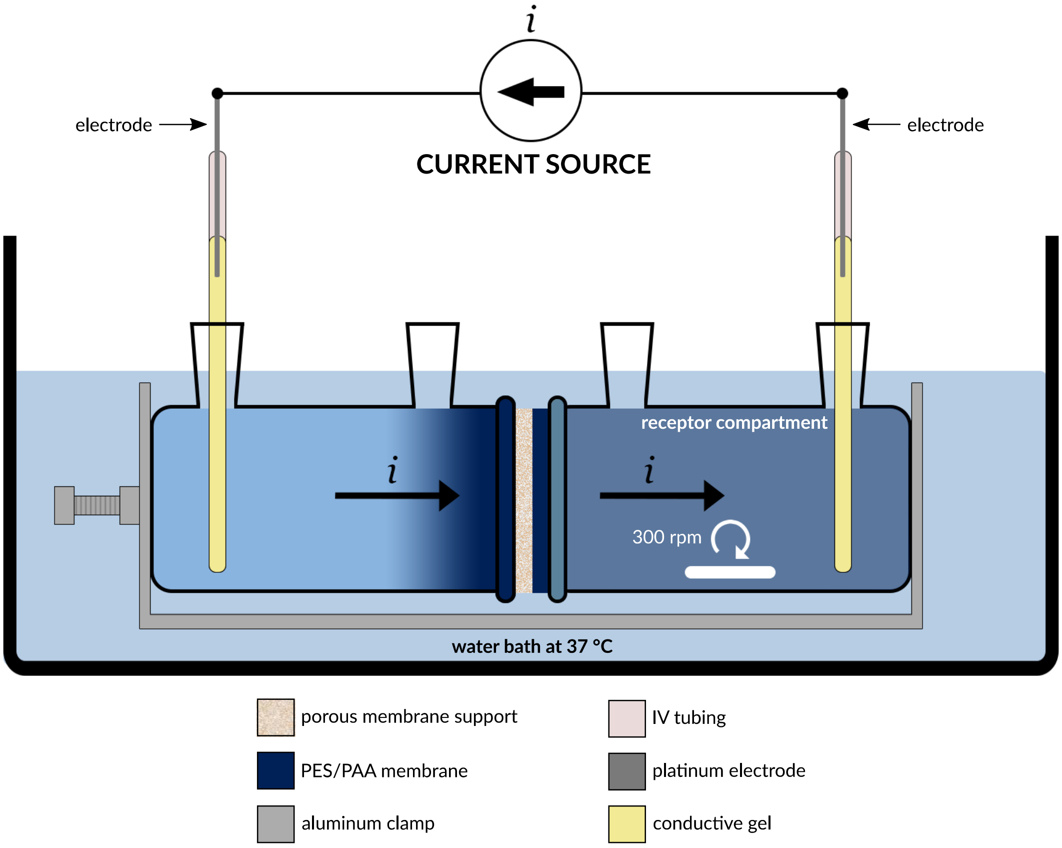

Figure 2.4. Illustration of the custom-built experimental setup for *in vitro* iontophoretic release of MB.

As the main part of the setup, we used a custom-built side-by-side diffusion cell with side-chamber volumes of 5 cm^3. Prepared membrane sample and polyester spunbond nonwoven fabric of the same size and shape were sandwiched between the chambers, and subsequently, the cell was sealed using a custom-built aluminum clamp to prevent leakage. Each of the chambers was initially filled with 5 cm^3 of PBS (pH = 7.4 and I = 0.154 M). IV tubing (~5 cm length and 3 mm inside diameter) filled with conductive cross-linked PAAm hydrogel was then inserted in each of the chambers through lateral orifices of the side-by-side cell. Platinum wire electrodes of 0.5 mm diameter were brought into direct contact with the conductive hydrogel to form terminals for external electrical connections with the custom-built current source for iontophoresis (described in section **3.2 Programmable current source for iontophoresis experiments**). Assembled side-by-side cell was subsequently placed above a hot plate with a magnetic stirrer and partially submerged in an aqueous bath. For the entire duration of the experiments, the solution within the side-chamber serving as the receptor compartment was stirred at 300 rpm, and the temperature in the aqueous bath was kept at (37 ± 1) °C. To initiate iontophoresis, platinum wire electrodes were connected with the dedicated custom-built current source via alligator clips, and the parameters of applied electric current were adjusted using a LabVIEW (LabVIEW 2014, National Instruments, USA) based interface.

The electric current was applied through the exposed membrane area of 1.13 cm^2 either in the continuous regime (with the amplitude i = 0.2 mA) or pulse regime (square wave with duty cycle DC = 50%, frequency f = 1 kHz, and amplitude i = 0.2 mA) for 100 min. MB release kinetics was monitored by measuring the content of MB in 3 cm^3 solution aliquots taken every 10 min with a micropipette through the middle orifice of the receptor chamber. Each sampled aliquot of 3 cm^3 volume was immediately replaced with the equivalent volume of fresh PBS. The absorbance of the sampled aliquots was measured at the wavelength of 664 nm by the UV-Vis Spectrometer (Cintra 101, GBC Scientific Equipment Ltd., Australia) and the concentration of MB was calculated using the appropriate calibration curve.

PBS was chosen for the chamber solutions to mimic the expected contact of the composite PES/PAA membrane reservoir with conductive gels typically used in electrotherapy. Conductive PAAm-based hydrogel served as a salt bridge separating the electrodes from the solutions in the chambers in order to minimize the influence of possible electrode reactions on the chemical composition and pH of the chamber solutions. Polyester spunbond nonwoven fabric was used to prevent membrane bending in the direction opposite to the flow of electric current. Parameters of electrical excitation were chosen to simulate common iontophoretic treatment conditions and to exploit the beneficial electrical properties of ion-exchange membranes when the pulsed excitation was used.

Experiments of iontophoretic MB release *in vitro* were performed in duplicate for each of the applied electric current regimes (continuous or pulse).

2.2.15 Numerical methods

Basic data analysis and related numerical calculations were carried out using a set of custom scripts. The curve fitting was performed using the standard methods of linear and nonlinear regression. In addition, the custom simplified gradient descent optimization algorithm for nonlinear regression was implemented in the form of a script to determine the apparent diffusion coefficient (D_a) of composite DL-PLCL/PAA implants (**Appendix D: Script for the determination of D_a for the composite DL-PLCL/PAA implants**). For details about the D_a calculation for composite DL-PLCL/PAA implants refer to section **5.4.2 Determination of D_a for the composite DL-PLCL/PAA implants**. Numerical analysis in this dissertation was performed using the MATLAB programming package (R2016b, The MathWorks, Inc., USA).

2.2.16 Statistical methods

Quantitative data in this dissertation are reported in the form (MV ± SD) for the investigated sample unless otherwise indicated, where MV designates the mean value and SD the standard deviation of the sample. The number of measurements (*i.e.* replicates) N is stated individually for each of the used experimental methods.

When required, statistical significance between two sample groups was calculated using the *t*-test and between multiple sample groups using the one-way analysis of variance (one-way ANOVA) followed by Tukey's or Dunnett's multiple comparisons test. Homoscedasticity assumption was assessed using the Bartlett's or Levene's test. In all cases, the P-value of 0.05 was taken as the significance level and $P < 0.05$ was considered as statistically significant. Statistical analysis was performed using Minitab software (Version 17.1.0, Minitab, Inc., USA) and GraphPad Prism software (Version 6.01, GraphPad Software, Inc., USA).

Chapter 3: Custom-built electronic devices used in experimental measurements

3.1 Analog front-end for the lock-in amplifier

The schematic of the analog front end of the lock-in amplifier is illustrated in **Figure 3.1**. The design revolved around the high-performance rail-to-rail input and output operational amplifiers MCP6021 and MCP6022 (Microchip Technology Inc., USA). These operational amplifiers feature wide bandwidth, stability at unity gain, low noise, low distortion, low input offset voltage, and low supply current [183]. Their favorable properties allowed for a stable battery-powered circuit that does not require decoupling capacitors for proper operation. The supply voltage of 3 V (two AA batteries) was used during all measurements and the common ground reference point was set at 1.5 V. The unknown impedance under test Z_x was connected between the pins JP_M1 and JP_M2 and the reference voltage signal of 150 mV RMS amplitude from the lock-in amplifier was applied between the pins JP_EXC1 and JP_EXC_GND (connected to the common ground of the circuit). MCP6022 package contains two operational amplifiers which served as buffers at unity gain for the voltage measurement between the pins JP_M1 and JP_M2. Buffered voltage V_U between the pins JP_V1 and JP_V2 was measured using the differential input of the lock-in amplifier.

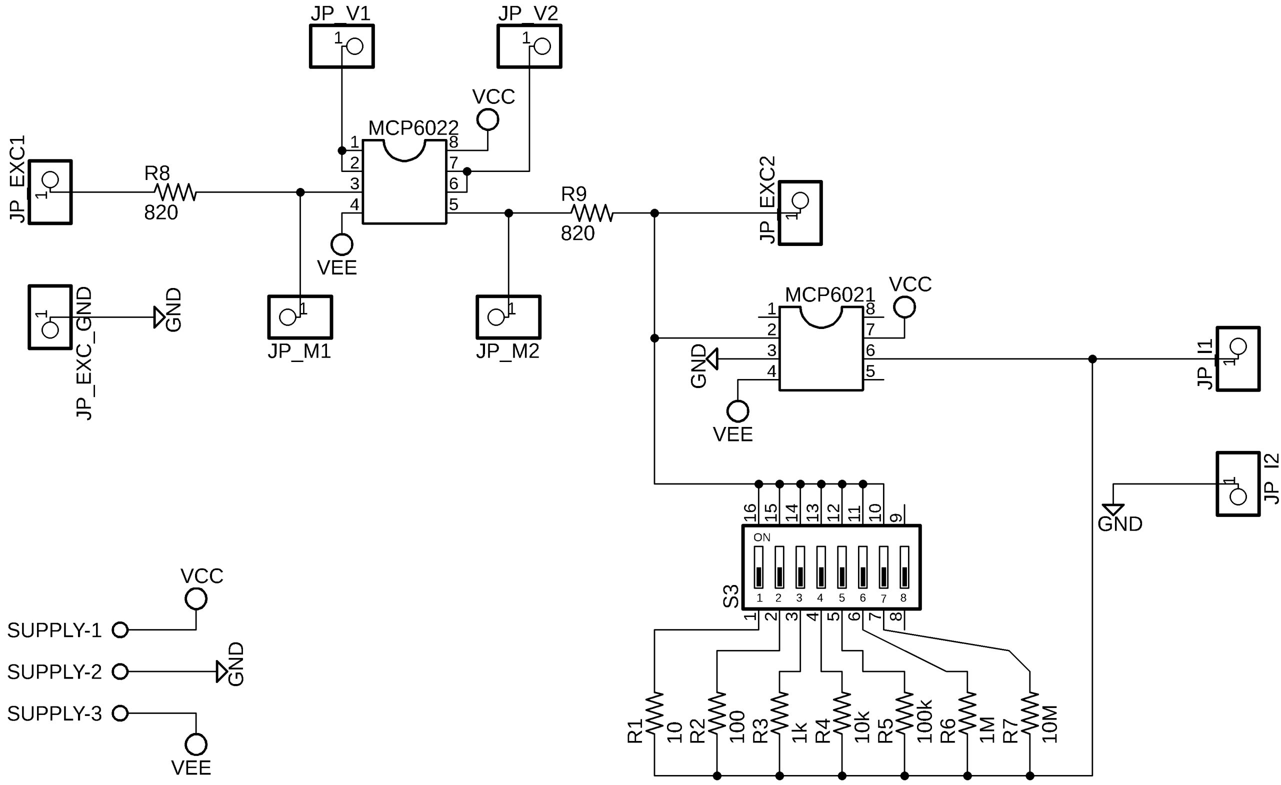

Figure 3.1. Schematic of the analog front end for the lock-in amplifier.

Current through Z_x was measured indirectly after the conversion to voltage with a transimpedance amplifier comprising an MCP6021 operational amplifier and selectable feedback resistor R_f. For the sake of simplicity, the selection of the suitable feedback resistor was performed manually by the slide-style 8-pole dual in-line package (DIP) switch. The voltage V_I between the pins JP_I1 and JP_I2 obtained by current conversion was also measured using the differential input of the lock-in amplifier. Values of measured voltages V_U and V_I can be used to determine Z_x with the following expression:

$$Z_{\mathrm{x}} = -R_{\mathrm{f}}\frac{V_{\mathrm{U}}}{V_{\mathrm{I}}} \tag{3.1}$$

Note that the values of V_{U}, V_{I}, and Z_{x} are complex numbers defined by the magnitude and phase. However, if the impedance exhibits dominantly resistive behavior (when the voltage and current are approximately in phase) the phase contribution can be neglected and the magnitude of Z_{x} can be calculated directly by substituting the magnitudes of V_{U} and V_{I} in **Equation (3.1)**.

3.2 Programmable current source for iontophoresis experiments (IV)

A custom programmable current source was designed and constructed for *in vitro* investigations of iontophoresis. The main concepts, properties, and functionality of the device will be briefly presented here, while the details of device hardware and software realization can be found in paper **IV**[2].

3.2.1 Device hardware

The schematic of device hardware is shown in **Figure 3.2**. Hardware design revolved around the Arduino UNO R3 open-source microcontroller board used for the generation of rectangular voltage pulses with adjustable width and frequency through pulse width modulation (PWM). The amplitude of voltage pulses was modulated by using the voltage divider comprising a p-channel junction gate field-effect transistor (p-JFET) as a voltage-controlled resistor.

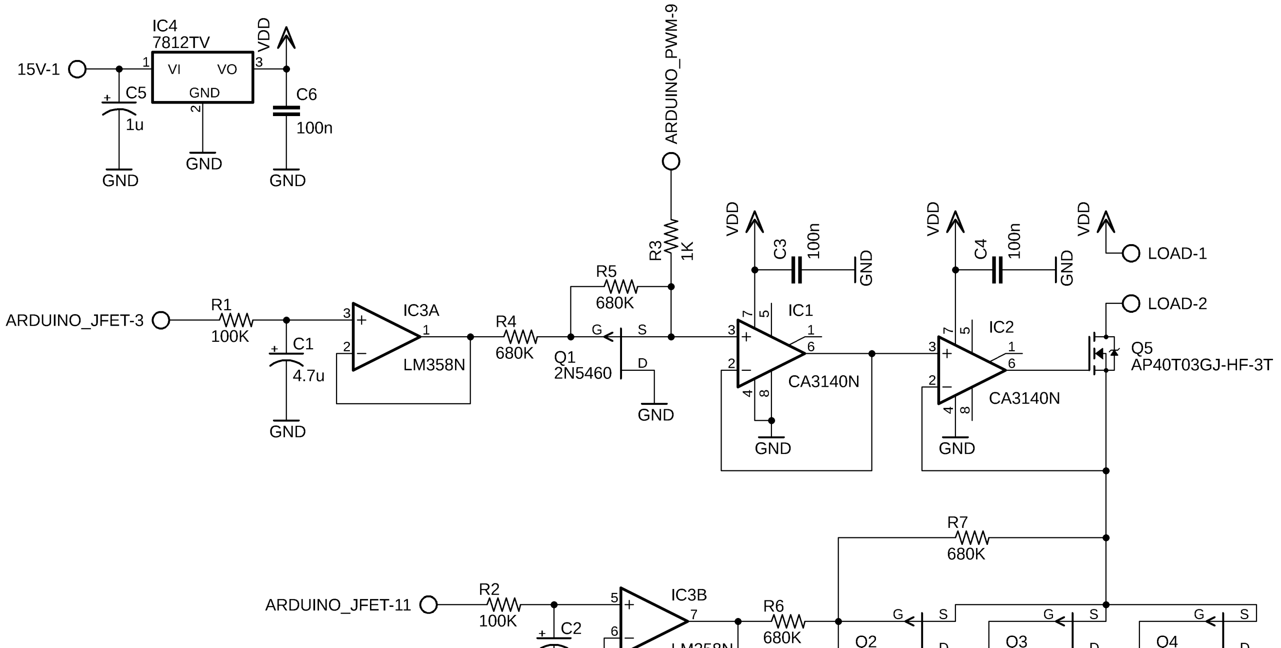

Figure 3.2. Schematic of the programmable current source for *in vitro* iontophoresis experiments.

For small values of the source-to-drain voltage (V_{SD}), the p-JFETs can be biased to operate in the linear ohmic region. In this region, p-JFETs approximately behave as variable resistors and their resistance can be adjusted by varying gate-to-source voltage (V_{GS}). The nonlinearity of the p-JFET current-voltage characteristic in the ohmic region was compensated for by adding a feedback loop composed of two 680

---

[2] [176] P. Atanasijević and Ž. Janićijević, "Programabilni pulsni strujni izvor za *in vitro* ispitivanja jontoforeze [Programmable pulse current source for *in vitro* investigations of iontophoresis]," u *Zborniku 61. Konferencije za elektroniku, telekomunikacije, računarstvo, automatiku i nuklearnu tehniku, ETRAN 2017*, 2017, pp. BT1.2.1-5.

kΩ resistors. In addition, this feedback loop increases the V_{SD} range in which p-JFET behaves as the controllable resistor and minimizes signal distortion as explained by Horowitz and Hill [184].

The constant voltage required to control the resistance of p-JFETs was generated by applying active low-pass filters to the default PWM outputs of the Arduino UNO R3 board (having the amplitude of 5 V and frequency of 490 Hz). The value of the constant voltage in the range of 0-5 V was regulated by adjusting the duty cycle of the pulses. Hence, the control of p-JFET resistance could be performed digitally in the software by assigning the adequate duty cycle.

Voltage pulse with defined amplitude and duty cycle at the output of the voltage divider was further buffered and brought to the input of the final stage for the current generation comprising an operational amplifier, n-channel metal-oxide-semiconductor field-effect transistor (n-MOSFET), and three p-JFETs connected in parallel. Generated output current flows through the load connected between the drain of the n-MOSFET and the positive supply rail (VDD in **Figure 3.2**). The final stage behaves as a voltage-controlled current source where the generated current flowing through the load I_L is given by the expression:

$$I_{\mathrm{L}} = \frac{V_{\mathrm{IN}}}{3R_{\mathrm{JFET}}} \tag{3.2}$$

where V_{IN} designates the voltage at the output of the voltage divider used for pulse amplitude adjustment and R_{JFET} designates the voltage-controlled resistance of the individual p-JFET in the stage for the current generation.

Note that the output current amplitude can be modulated by either one of the parameters in the **Equation (3.2)** or both separately depending on the requirements. Three p-JFETs in the stage for the current generation are connected in parallel to reduce the total resistance value used to control the current amplitude and limit the current flowing through individual p-JFETs.

3.2.2 Device software

The software of the pulsed current source consists of two main parts. The first part is implemented and executed on the microcontroller (Atmel ATmega328P on the Arduino UNO R3 board). The microcontroller programming was carried out in the integrated development environment Arduino 1.6.9.

The program uploaded to the microcontroller enabled the adjustment of the following parameters of the output current pulses: frequency, duty cycle, period, and pulse width. In addition, the program provided the regulation of the duty cycles of the voltage signals used to control the p-JFET resistances. Two data acquisition modes were supported by the microcontroller program: acquisition of the fixed number of samples and continuous acquisition.

Application of the current source in practice requires a reliable continuous generation of voltage pulses occurring independently from other segments of program execution. To provide such a feature, the first hardware timer of the microcontroller with the 16-bit resolution was directly accessed. This timer controls the digital output at the PWM pin 9. The adjustment of pulse signal properties was enabled by including the available library TimerOne.h. The second hardware timer with the 8-bit resolution was used to control the digital output at the PWM pins 3 and 11 employed to adjust the resistance of p-JFETs.

The acquisition of the voltage signals was enabled at the specified analog input of the Arduino UNO R3 board. Analog-to-digital (AD) conversion time was shortened to about 20 μs by accessing the ADCSRA register for configuring the Arduino AD converter. Such an approach slightly reduces the resolution of AD conversion, but this change proved to be negligible for the intended application.

The second part of the software was implemented and executed on a personal computer. This part of the software was designed to provide a simplified and intuitive graphical user interface for the adjustment of pulse current source operation and data acquisition. The second part of the software was created using the software for the graphical programming of measurement and control systems LabVIEW (LabVIEW 2014, National Instruments, USA).

The graphical user interface provided the possibility to directly set and fine-tune properties of the output current in real-time according to the implemented calibration functions without changing the program uploaded to the microcontroller.

Two parts of the software exchange the information through the Universal Serial Bus (USB) connection established between the personal computer and the Arduino UNO R3 board.

Communication between the LabVIEW and the microcontroller Atmel ATmega328P through USB was configured using the subprograms available as part of the Virtual Instrument Software Architecture (VISA) standard. Such interface for communication enables the use of an arbitrary microcontroller which only should be programmed to retain the same form of communication with the personal computer.

3.2.3 Performance evaluation

Basic performance characteristics of the device were measured using the digital multimeter (SMA92, Somogyi Elektronic, China) and the digital oscilloscope (INSTRUSTAR ISDS205A, Harbin Instrustar Electronic Technology, China). The properties are listed in **Table 3.1**.

Table 3.1. Basic performance characteristics of the constructed programmable current source.

Current amplitude range	(0.1-4.5) mA
Pulse frequency range	(1-10000) Hz
Duty cycle	(0-100) %
Pulse rise time	0.81 μs
Pulse fall time	1.14 μs
Pulse settling time	2.1 μs

The device was also tested under realistic experimental conditions using the following parameters of pulsed current excitation: amplitude $i = 2$ mA, frequency $f = 1$ kHz, and duty cycle $DC = 50\%$. The experiment was conducted for 60 min on the simulated load with slowly changing impedance in the range of 3-3.5 kΩ. Under these experimental conditions, the pulsed current excitation showed the dynamic stability of the mean current amplitude of ±0.2%. Therefore, the constructed programmable current source was considered as suitable for the *in vitro* tests of iontophoresis in the research setting.

Chapter 4: Results

4.1 FTIR-ATR analysis of composite hydrogels (I-III)

We analyzed the chemical composition of composite hydrogel membranes and implants using the recorded FTIR-ATR spectra. Such analysis should provide useful insights into the influence of synthesis parameters on the distribution of hydrophobic and hydrophilic components within the composites and their physicochemical interactions.

4.1.1 FTIR-ATR analysis of composite PES/PAA membranes (I)

Figures 4.1 and **4.2** show the spectra of representative composite PES/PAA membranes in the wet state.

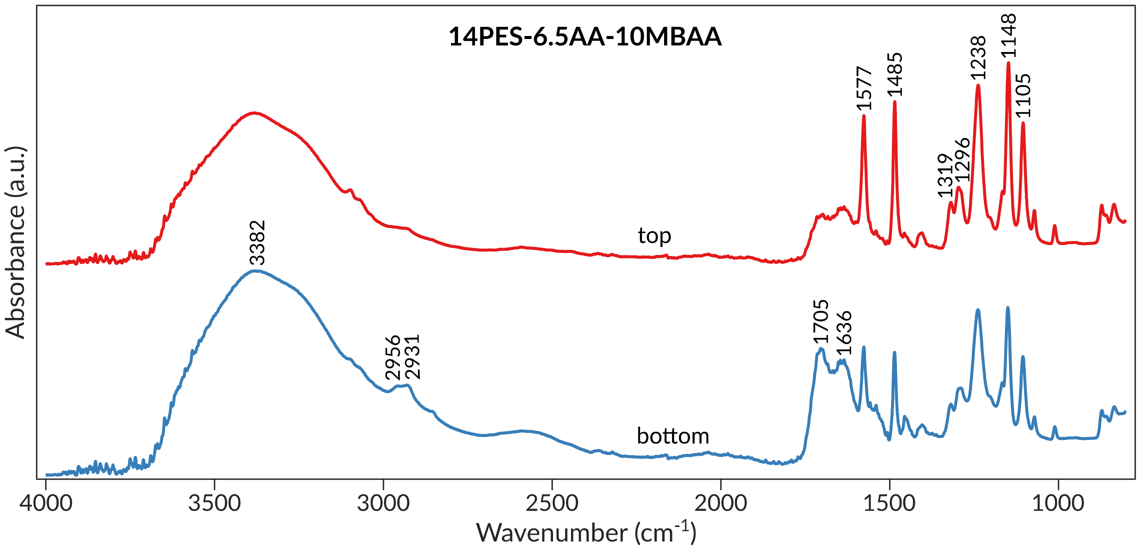

Figure 4.1. FTIR-ATR spectra of the composite PES/PAA membrane (14PES-6.5AA-10MBAA) top and bottom sides in the wet state.

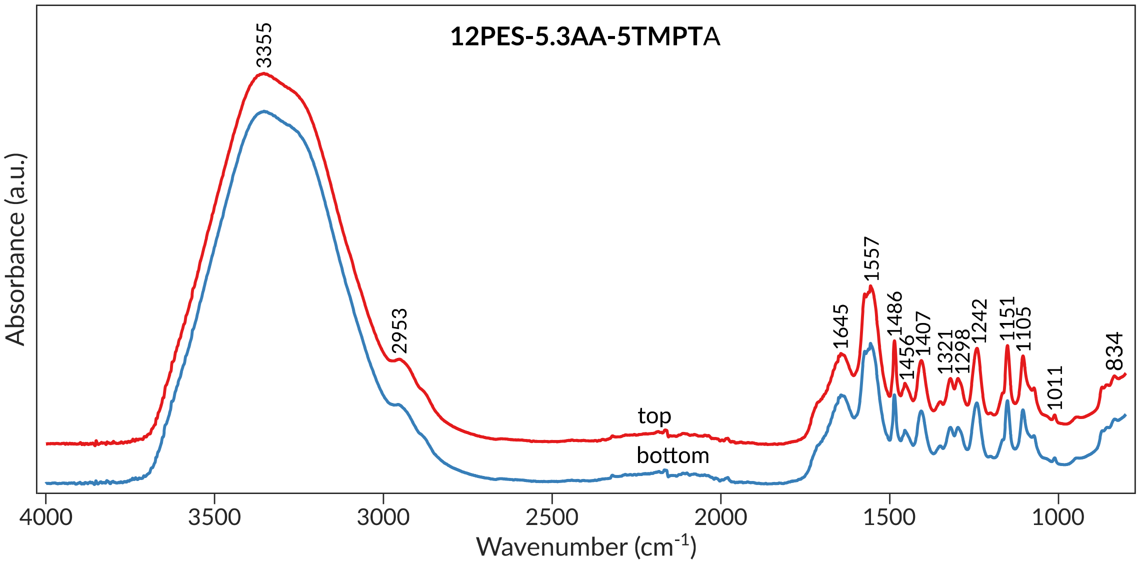

Figure 4.2. FTIR-ATR spectra of the composite PES/PAA membrane (12PES-5.3AA-5TMPTA) top and bottom sides in the wet state.

Composite PES/PAA membranes synthesized using the hydrophobic bifunctional CL MBAA exhibited different chemical compositions in the wet state at the top and bottom sides of the membrane as shown by FTIR-ATR spectra in **Figure 4.1**. The top side of the membrane contained more PES, while the bottom side contained more PAA hydrogel as evidenced by the relative intensity of characteristic bands.

Characteristic absorption bands of PES that we detected in the spectra are the C-O stretching at 1105 cm^{-1}, C-O-C stretching of the aromatic ether band at 1238 cm^{-1}, symmetric O=S=O stretching band at 1148 cm^{-1}, asymmetric O=S=O stretching bands at 1296 and 1319 cm^{-1}, and the bands corresponding to the aromatic polysulfone ring at 1485 and 1577 cm^{-1}. We also observed the characteristic bands of PAA hydrogel which are the band characteristic for hydrogen-bonded carboxyl groups forming dimers and oligomers at 1636 cm^{-1}, C=O stretching band of protonated carboxyl groups at 1705 cm^{-1}, and symmetric H-O-H stretching band at 3382 cm^{-1} arising from hydrogen-bonded water molecules. CH_2 stretching bands at 2931 and 2956 cm^{-1} also appeared in the spectra.

Composite PES/PAA membranes synthesized using the hydrophilic trifunctional CL TMPTA exhibited almost identical chemical composition at the top and bottom sides of the membrane in its wet state as illustrated by FTIR-ATR spectra in **Figure 4.2**. Qualitatively the spectral bands were similar to the ones shown in **Figure 4.1**. We observed that the H-O-H stretching band situated at 3355 cm^{-1} had greater intensity compared to the same band in the spectra of membranes synthesized using the MBAA as the CL. Such a finding could originate from the higher water content of composite PES/PAA membranes synthesized using TMPTA.

We compared the FTIR-ATR spectra of composite PES/PAA membranes synthesized using TMPTA in the wet and dry state as depicted in **Figure 4.3**. Prominent bands characteristic for PAA hydrogel formation disappeared after membrane drying in air. However, the distinct C=O stretching band of protonated carboxyl groups at 1716 cm^{-1} confirmed the presence of PAA in the air-dried membrane. The CH_2 stretching bands at 2877 and 2924 cm^{-1} also became more pronounced in the spectra of the air-dried membrane.

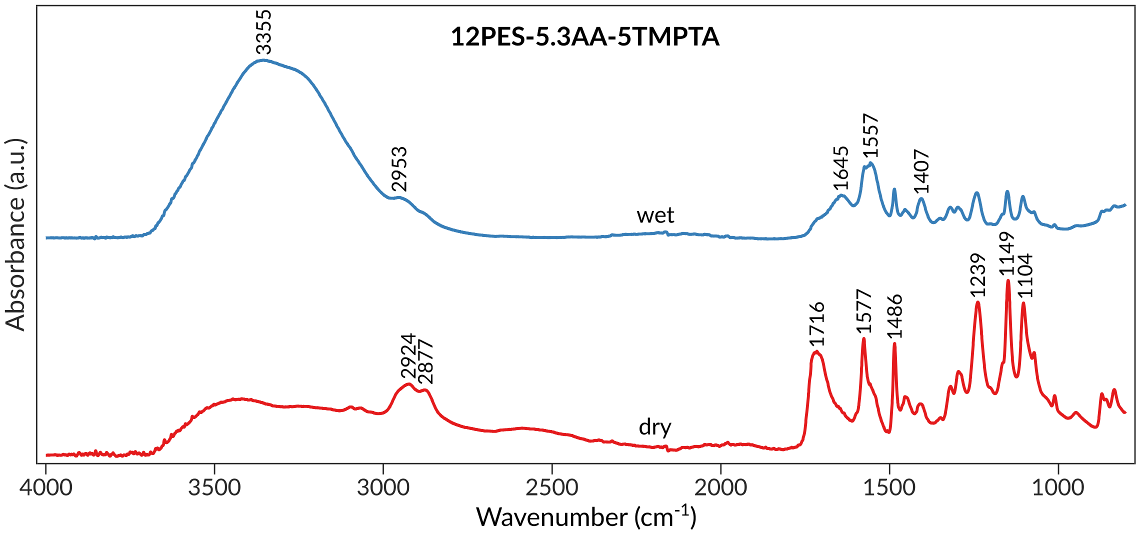

Figure 4.3. FTIR-ATR spectra of the composite PES/PAA membrane (12PES-5.3AA-5TMPTA) top surface in the wet and dry state.

FTIR-ATR spectra of composite PES/PAA membranes indicate that the distribution of the hydrogel phase within the membrane strongly depends on the CL type used during the synthesis. Homogeneity of chemical composition within the wet membrane is critical for intended applications since it determines mechanical stability and through-membrane electrical conductivity which are the important properties of drug reservoirs for iontophoresis. As we observed during our experiments, composite PES/PAA membranes synthesized with MBAA have the tendency to mechanically deform and are difficult to handle. The results of FTIR-ATR analysis also indicated compositional asymmetry. Since only the PAA hydrogel component imparts electrical conductivity to the composite membrane, we expected that its asymmetric distribution can only reduce the through-membrane conductivity. Therefore, we continued our experiments only with the membranes synthesized with TMPTA.

We used the membrane synthesized from the casting solution formulation 12PES-5.3AA-5TMPTA as the representative composite PES/PAA membrane for further investigations.

4.1.2 FTIR-ATR analysis of composite DL-PLCL/PAA implants (II)

Figure 4.4 shows the FTIR-ATR spectra of the pure hydrophobic PB (DL-PLCL), composite DL-PLCL/PAA implant dried by solvent exchange, and wet composite DL-PLCL/PAA implant. The spectrum of the pure DL-PLCL confirmed the hydrophobic nature of the polymer and contained characteristic bands of C-O-C symmetric valence vibration in the aliphatic chain at 1093 cm^{-1}, symmetric stretching of C-O-C at 1161 cm^{-1}, C=O stretching at 1732 cm^{-1}, asymmetric bending of C-H in CH_3 at 1453 cm^{-1}, and the stretching bands of CH_2 at 2867 and 2940 cm^{-1}. We observed the bands of PAA in the dried composite DL-PLCL implant corresponding to the C-O stretching at 1404 and 1560 cm^{-1}, and symmetric H-O-H stretching at 3384 cm^{-1}. In the spectrum of the wet implant, we observed the increase in H-O-H absorption band intensity and the new absorption band at 1637 cm^{-1} typical for hydrogen-bonded carboxyl groups.

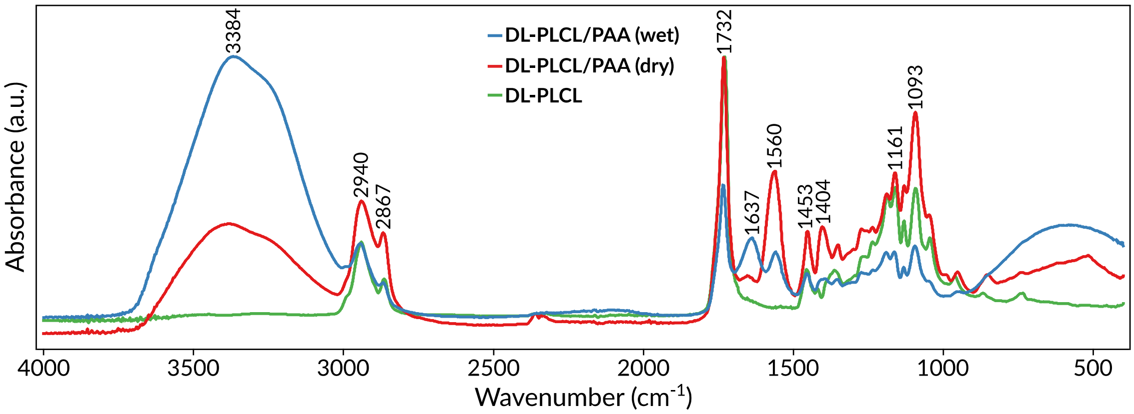

Figure 4.4. FTIR-ATR spectra of the composite DL-PLCL/PAA implant in the wet and dry state compared with the FTIR-ATR spectrum of the pure hydrophobic PB (DL-PLCL).

4.1.3 FTIR-ATR analysis of composite PLGA/PAA implants (III)

Figure 4.5 depicts the FTIR-ATR spectra of pure PLGA and UV-PLGA-PAA in the wet and dry state.

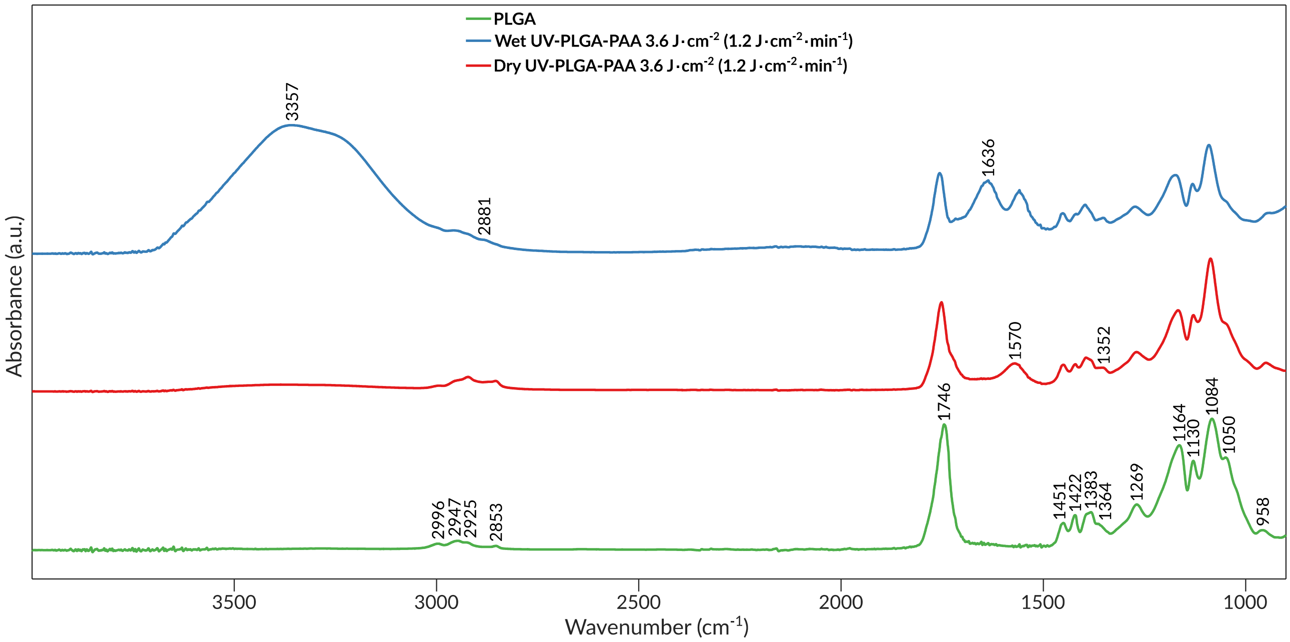

Figure 4.5. FTIR-ATR spectra of UV-PLGA-PAA in the wet and dry state compared with the FTIR-ATR spectrum of the pure hydrophobic PB (PLGA).

The spectrum of PLGA revealed the hydrophobic polymer nature and contained numerous vibration bands characteristic for lactic and glycolic units. Bands at 2947 and 2996 cm^{-1} correspond to the symmetric and anti-symmetric stretching of CH_3, respectively. The bands at 1364 and 1383 cm^{-1} correspond to symmetric bending, while the band at 1451 cm^{-1} corresponds to the anti-symmetric bending of CH_3 in lactic units. We assigned the bands at 958 and 1130 cm^{-1} to the rocking of CH_3 in lactic units. The band at 1050 cm^{-1} indicates C-CH_3 stretching in lactic units. We assigned the bands at 2853 and 2925 cm^{-1} to the symmetric and anti-symmetric stretching of CH_2, respectively. Wagging and bending bands of CH_2 in glycolic units appeared at 1394 and 1422 cm^{-1}, respectively. The band at 1269 cm^{-1} corresponds to the twisting of CH_2. We assigned the bands at 1084 and 1164 cm^{-1} to the symmetric and anti-symmetric C-O-C stretching, respectively. The intense C=O stretching band appeared at 1746 cm^{-1}.

In the spectra of UV-PLGA-PAA, some additional bands appeared due to the presence of PAA. In the dry state, the UV-PLGA-PAA spectrum contained the C-O stretching band of carboxyl groups at 1570 cm^{-1} and the weak band corresponding to C-H rocking at 1352 cm^{-1}. We also observed slight changes in band shapes within the 1500-1300 cm^{-1} and 3000-2800 cm^{-1} regions presumably due to the effects of cross-linked PAA backbone. PAA also introduced C-O stretching bands in the 1500-1300 cm^{-1} region which overlap with some bands of PLGA.

The spectrum of UV-PLGA-PAA in the wet state exhibited additional characteristic bands confirming PAA hydrogel formation. The band at 1637 cm^{-1} corresponds to the hydrogen-bonded carboxyl groups, while the band at 3357 cm^{-1} corresponds to the symmetric H-O-H stretching of hydrogen-bonded water. A very weak C-H stretching band also appeared at 2881 cm^{-1}. Extensive hydrogen bonding in the wet UV-PLGA-PAA causes minor shifts in band positions in the spectrum. The most notable shifts occurred in the positions of bands associated with carboxyl and carbonyl groups.

We observed that the FTIR-ATR spectra of UV-PLGA-PAA indicated excellent spatial homogeneity of chemical composition across the sample surface (**Figure B.1** in **Appendix B: Homogeneity of the chemical composition of UV-PLGA-PAA and G-PLGA-PAAs**). However, this was not the case for G-PLGA-PAAs. The chemical composition of G-PLGA-PAAs appeared to be spatially inhomogeneous in terms of chemical composition for all sets of applied irradiation parameters (as illustrated in the **Figures B.2**-**B.6** in **Appendix B: Homogeneity of the chemical composition of UV-PLGA-PAA and G-PLGA-PAAs**). Nevertheless, we could identify representative features of the FTIR-ATR spectra for G-PLGA-PAAs as illustrated in **Figures 4.6** and **4.7**. These features most commonly existed in G-PLGA-PAAs synthesized using a specific set of gamma irradiation parameters, but many of them can also appear locally within the same sample. We attributed such localized variability in chemical composition to the stochastic and spatially discrete nature of material interactions with gamma rays.

During the analysis of the chemical composition, we noted that the dose rate variation in the investigated range did not produce any significant systematic effects within the recorded spectra. On the other hand, the dose of gamma irradiation had a more significant impact on the features of FTIR-ATR spectra.

Spectra of G-PLGA-PAAs synthesized using the irradiation doses of 17 and 25 kGy showed band patterns similar to the spectra of UV-PLGA-PAA (**Figure 4.6**). Subtle differences existed in the spectral regions commonly corresponding to the stretching and deformation vibrations of CH_2 and CH_3 (3000-2800 cm^{-1} and 1500-1300 cm^{-1}). These pattern differences became more evident for the spectra of G-PLGA-PAA synthesized with the irradiation dose of 33 kGy (**Figure 4.7**).

In the previous research, subtle changes in chemical composition and bonding were hard to detect and quantify for poly(esters) such as PLGA using FTIR-ATR analysis even when much higher gamma irradiation doses were applied [138]. Systematic changes in FTIR-ATR spectra may also be lacking in the 3000-2800 cm^{-1} and 1500-1300 cm^{-1} spectral regions due to the random nature of chain scission which takes place during gamma irradiation of PLGA [185].

Additional changes in FTIR-ATR spectra occurred for G-PLGA-PAA synthesized with the irradiation dose of 33 kGy in the form of band splitting. The splitting was evident in the spectra recorded for dried samples when observing the overlapping C=O stretching (at 1726 and 1751 cm^{-1}) and CH_2 twisting (at 1253 and 1271 cm^{-1}) bands (**Figure 4.7**). We could explain such C-H and C=O bond changes using the concept of cage effect. The cage effect appears in the material when initially formed radicals become trapped and recombine locally before leaving the active volume of the cage via diffusion [186], [187].

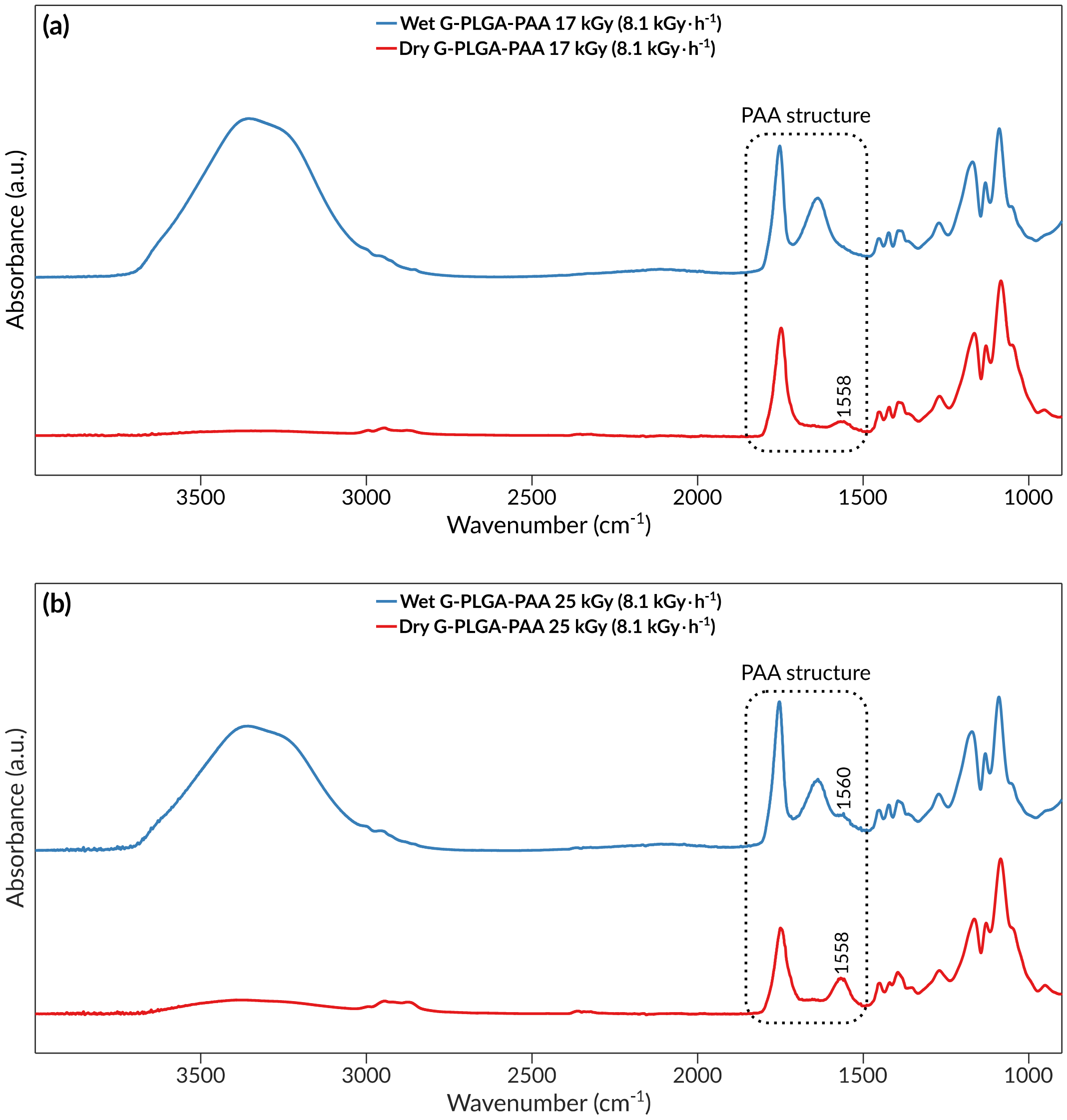

Figure 4.6. Representative FTIR-ATR spectra of G-PLGA-PAAs in the wet and dry state synthesized using the following gamma irradiation parameters (dose (kGy)/dose rate (kGy·h^{-1})): (a) 17/8.1 and (b) 25/8.1.

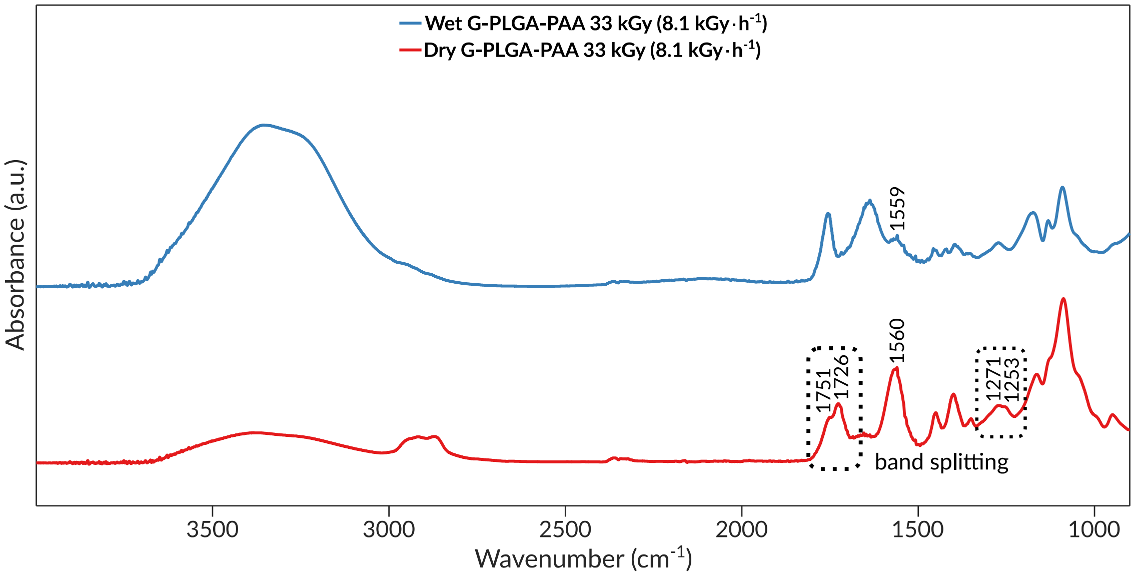

Figure 4.7. Representative FTIR-ATR spectra of G-PLGA-PAA in the wet and dry state synthesized using the dose of 33 kGy and dose rate of 8.1 kGy·h^{-1}.

In the FTIR-ATR spectra of all dry G-PLGA-PAAs, we observed the highly variable intensity ratio of the C=O stretching band and the major C-O stretching band (at about 1560 cm^{-1}). We ascribed such variation to the formation of more branched PAA hydrogel structures (resulting from the competition between inter- and intra-molecular cross-linking [188] and the process of chain scission) and possibly increased carboxyl group content in G-PLGA-PAAs due to the gamma irradiation of PLGA [189].

The major C-O stretching band of cross-linked PAA had a higher intensity and shifted toward lower wavenumbers in the spectrum of wet UV-PLGA-PAA compared to the same band in the spectrum of dry UV-PLGA-PAA (**Figure 4.5**). Such behavior indicated the involvement of the C-O group in the hydrogen bonding of carboxyl groups.

The intensity of the same C-O band in the spectra of wet G-PLGA-PAAs was much lower than in the spectrum of wet UV-PLGA-PAA or the band even became completely overlapped by the band at 1636 cm^{-1}, while the position of this C-O band practically did not change in the spectra of dry G-PLGA-PAAs (**Figures 4.6** and **4.7**). The described band properties in the spectra of wet G-PLGA-PAAs indicated significantly reduced participation of C-O groups in hydrogen bonding.

The C-O group can be less engaged in hydrogen bonding when the PAA hydrogel has a strongly branched structure. Within such a structure, the water molecules can preferentially attach to the terminal chain carboxyl groups via hydrogen bonding through C=O groups [190].

4.2 SEM analysis of composite hydrogels (I-III)

We analyzed the basic microstructure of different synthesized composite hydrogels in the dry state using acquired SEM images. SEM analysis should identify the characteristic patterns in the microstructure and provide insights about the formation of microstructural features. Based on the findings of SEM analysis and our understanding of the synthesis process we have proposed the mechanisms underlying the formation of typical microstructural features.

4.2.1 SEM analysis of composite PES/PAA membranes (I)

Figure 4.8 shows the representative microstructure of the membranes synthesized using TMPTA as the CL. Membranes exhibited a symmetric structure with the thickness of around 85 μm in the dry state.

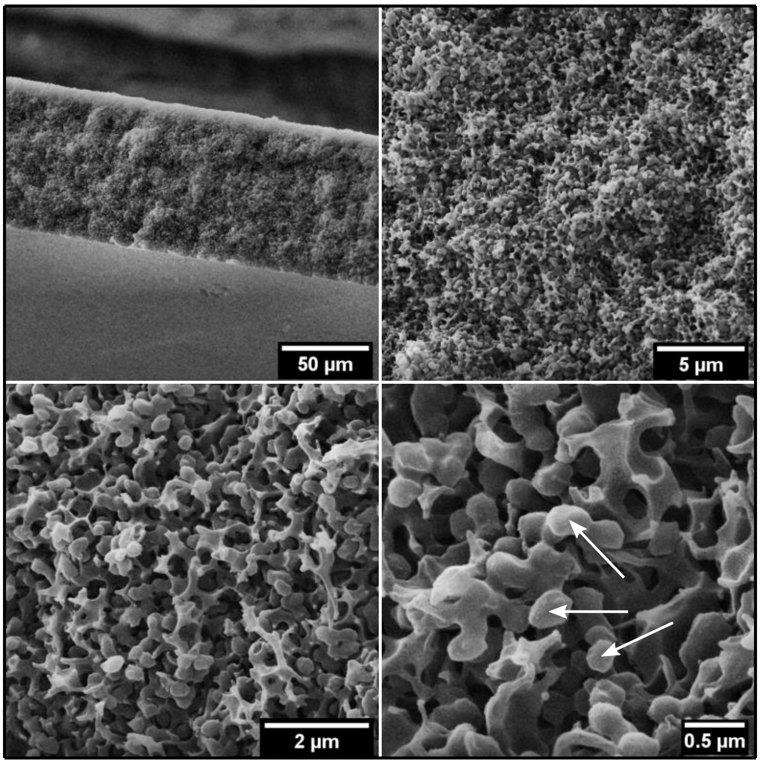

Figure 4.8. SEM images of the composite PES/PAA membrane (12PES-5.3AA-5TMPTA) in the dry state at different magnifications. White arrows indicate representative PAA-rich particles in the membrane at the highest magnification.

The heterogeneous microstructure of the membrane comprised the porous PES-rich matrix and scattered small independent clusters of PAA-rich spheroidal particles. The PAA-rich particles had an estimated mean diameter of about 280 nm and their clusters were attached to the pore walls of the PES-rich support.

4.2.2 SEM analysis of composite DL-PLCL/PAA implants (II)

Figure 4.9 illustrates the surface and cross-section of the composite DL-PLCL/PAA implant. The microstructure of the implant comprised the continuous DL-PLCL-rich matrix and PAA-rich particle inclusions distributed throughout the matrix. In the bulk of the implant, we observed almost uniformly distributed and densely packed spheroidal PAA-rich particles with a mean diameter of approximately 280 nm. On the other hand, we observed irregular sparse aggregates of PAA-rich particles with a mean cluster size of around 1.1 μm at the surface. These aggregates of PAA-rich particles protrude through the DL-PLCL-rich skin layer. All PAA-rich particles appear to be attached to the DL-PLCL-rich matrix.

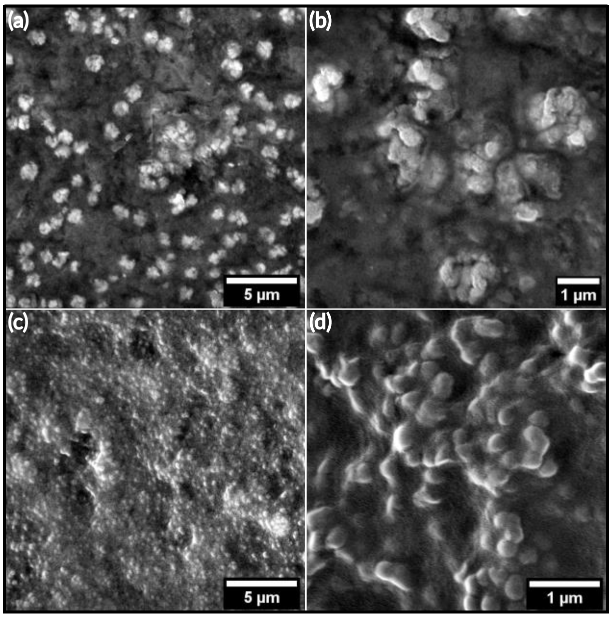

Figure 4.9. SEM images of the composite DL-PLCL/PAA implant in the dry state at different magnifications: (a, b) surface of the implant and (c, d) cross-section of the implant.

4.2.3 SEM analysis of composite PLGA/PAA implants (III)

Figure 4.10 depicts the microstructure of UV-PLGA-PAA and G-PLGA-PAAs. All samples had a microstructure which comprised the porous PLGA-rich matrix and dispersed spheroidal PAA-rich particles attached to the PLGA-rich support.

Although the overall morphology of all composite PLGA/PAA hydrogels was similar, we observed significant differences between UV-PLGA-PAA and G-PLGA-PAAs in terms of spatial uniformity and size of PAA-rich particles in the dry state. UV-PLGA-PAA exhibited a better spatial uniformity of microstructural features in comparison to G-PLGA-PAAs. The G-PLGA-PAA synthesized using the irradiation dose of 25 kGy and a dose rate of 6.1 $kGy \cdot h^{-1}$ especially stood out with even greater degrees of nonuniformity and porosity compared to the other G-PLGA-PAAs.

We also estimated the size of PAA-rich particles using **Figure 4.10** by measuring the Feret diameter of particles most clearly separated from the surrounding matrix. Size of PAA-rich particles in UV-PLGA-PAA was (0.62 ± 0.10) μm (N = 40 particles) and the size of PAA-rich particles in G-PLGA-PAA samples was (1.24 ± 0.17) μm (pooled statistics of N = 200 particles; 40 particles measured for each of 5 G-PLGA-PAAs).

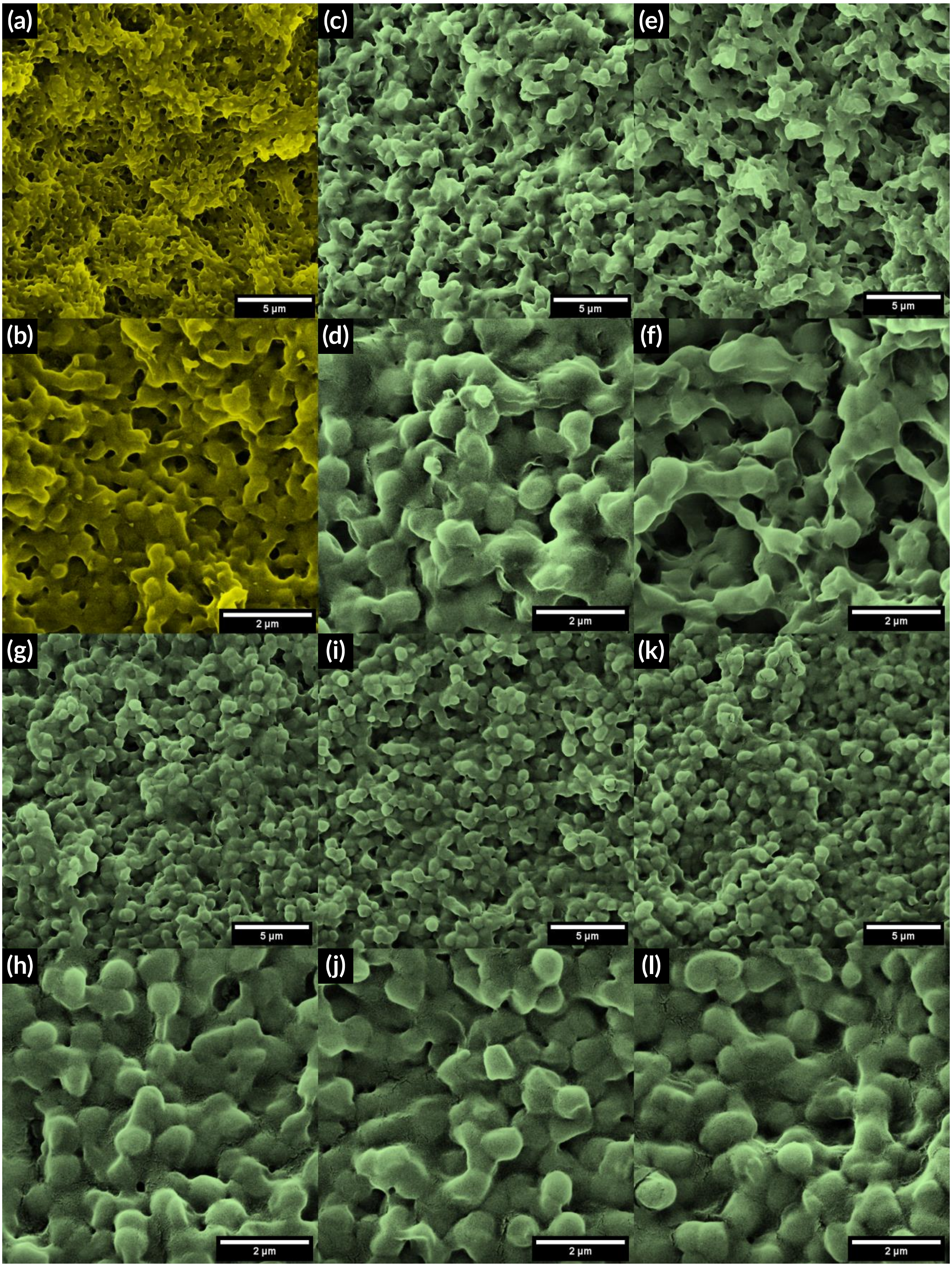

Figure 4.10. SEM images of composite PLGA/PAA implants: (a, b) UV-PLGA-PAA (dose 3.6 J·cm^{-2}; dose rate 1.2 J·cm^{-2}·min^{-1}) and (c-l) G-PLGA-PAAs synthesized using the following gamma irradiation parameters (dose (kGy)/dose rate (kGy·h^{-1})): (c, d) 17/8.1, (e, f) 25/6.1, (g, h) 25/8.1, (i, j) 25/10.1, and (k, l) 33/8.1. Images are artificially colored to improve visual clarity (yellow represents UV-PLGA-PAA and green represents different G-PLGA-PAAs).

4.2.4 Mechanisms of microstructure formation (I-III)

Specific microstructures of the composite hydrogels result from the complex interplay of several phenomena that occur during the synthesis process. Irradiation of the initial solution triggers the polymerization of AA which also involves cross-linking. The cloudy appearance of gels formed after the irradiation step in the synthesis also indicated the onset of phase separation. Immersion of the gels into the aqueous bath imposes unstable thermodynamic conditions which lead to the rapid finalization of phase separation and solidification of the composite hydrogels.

All synthesized composite hydrogels contained the aggregates of the PAA hydrogel-rich phase surrounded by the hydrophobic polymer matrix. It is important to emphasize the effects of irradiation type and each of the synthesis steps on the microstructural features within different composite hydrogels.

The first synthesis step involves the irradiation of the initial solution. The initial solution absorbs UV irradiation homogeneously due to the presence of dissolved PI. This is not the case for gamma irradiation. Gamma rays with an average energy of 1.25 MeV per photon from the ^{60}Co source can ionize the molecules of functional components (in our case AA, TMPTA, and PLGA) and form free radicals.

The formation of radicals is not a selective and efficient process since a multitude of interactions (such as inter- and intra-molecular cross-linking, and chain scission) occur at random locations within the initial solution and have different probabilities [191]. As a result, gamma-ray induced polymerization has a significantly lower rate in comparison with UV induced polymerization.

The polymerization rate by TMPTA as a trifunctional CL is higher than for monofunctional AA which leads to the formation of initial PAA-rich aggregates. These aggregates grow to become microgels after CL depletion in all composite hydrogels. A smaller number of larger PAA-rich aggregates forms under gamma irradiation compared to UV irradiation because of the slower and less efficient polymerization process. The slow process of polymerization and the stochastic nature of gamma-ray interactions with materials allow sufficient time for radical propagation and diffusion which can be important contributing factors in the evolution of the microstructure. AA polymerization starts to occur at randomly distributed confined centers within the initial solution volume mostly due to free radical formation through interactions with gamma rays. However, polymerization proceeds further in the vicinity of these centers mainly through the propagation and diffusion of free radicals. It is also common for polymer gels to exhibit local inhomogeneities in the spatial distribution of polymer network concentration and density of cross-linking [192].

Aqueous baths used in the second synthesis step served as nonsolvents during phase inversion. In the cases of composite PES/PAA membranes and PLGA/PAA implants, the resulting hydrophobic matrices became porous after finalizing phase separation and solidification in the aqueous bath. The formation of porous PES matrices typically occurs in the membrane synthesis processes where NMP is a common solvent for functional components and aqueous bath is a nonsolvent [101], [121]. Solidified porous PLGA matrix forms due to the high rate of solvent diffusion towards the aqueous nonsolvent medium which results in rapid precipitation of PLGA chains. Previous studies demonstrated the formation of porous PLGA structures through this specific dynamics of phase inversion when PLGA solutions in NMP were quenched with aqueous solutions [144], [145]. On the other hand, the immersion of the gel in the aqueous bath produced a continuous DL-PLCL-rich matrix with embedded PAA-rich particles in the case of composite DL-PLCL/PAA implants. Mechanism of surface layer formation with decreased content of the PAA-rich phase near the surface of the composite DL-PLCL/PAA implants resembles the mechanism of skin formation in membranes synthesized by immersion precipitation [193], [194]. After the rapid immersion in the PBS solution, NMP quickly diffuses out of the irradiated disk. The completion of phase separation and solidification of the reservoir initially occurs at the surface exposed to the highest nonsolvent concentration and the DL-PLCL enriched skin layer forms. This layer presents a rate-limiting barrier for further penetration of PBS solution which gradually enters the interior of the disk and drives the processes of phase separation and solidification within the bulk.

PAA-rich particles in all synthesized composite hydrogels remain attached to the hydrophobic polymer-rich support. Residual common chains resulting from incomplete polymer/polymer demixing during the phase separation stage are the cause of such attachment. The attachment of PAA-rich particles to the hydrophobic polymer-rich support due to incomplete demixing is especially pronounced for UV-PLGA-PAA.

4.3 DSC analysis of composite PLGA/PAA implants (III)

Figure 4.11 shows the DSC thermograms of synthesized composite PLGA/PAA implants. We recorded the glass transitions of PLGA which overlap with the enthalpic relaxation peaks in the thermograms. Common causes for the appearance of enthalpic relaxation peaks are the prolonged storage of the material under the glass transition temperature (T_g) and the mechanical stresses inflicted on the material during fabrication [195].

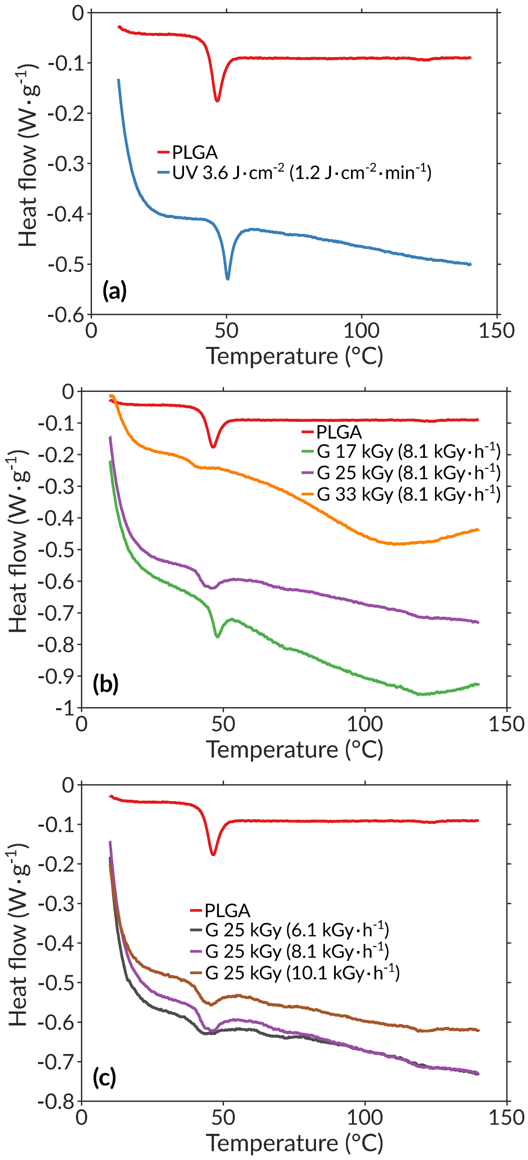

Figure 4.11. DSC thermograms of composite PLGA/PAA implants synthesized using different irradiation parameters: (a) UV-PLGA-PAA (dose 3.6 J·cm^{-2}; dose rate 1.2 J·cm^{-2}·min^{-1}), (b) G-PLGA-PAAs synthesized using the doses of 17, 25, and 33 kGy (with the constant dose rate of 8.1 kGy·h^{-1}), and (c) G-PLGA-PAAs synthesized using the dose rates of 6.1, 8.1, and 10.1 kGy·h^{-1} (with the constant dose of 25 kGy). DSC thermogram of pristine PLGA serves as a reference for comparison.

Calculated values of T_g presented in **Table 4.1** indicate shifts towards higher and lower temperatures compared to the T_g of pure PLGA.

T_g of UV-PLGA-PAA was almost 4 °C higher than that of the pure PLGA. We attributed the increase in T_g to the two main possible causes:

- polymer chain entanglement resulting from incomplete polymer/polymer demixing during the phase separation process and
- the greater mean molecular weight of PLGA in the composite.

Table 4.1. T_g values of composite PLGA/PAA implants synthesized using different irradiation parameters.

Sample type	Irradiation parameters (dose, dose rate)	T_g (°C)
PLGA	None	46.2
UV-PLGA-PAA	3.6 $J \cdot cm^{-2}$, 1.2 $J \cdot cm^{-2} \cdot min^{-1}$	50.1
G-PLGA-PAA	17 kGy, 8.1 $kGy \cdot h^{-1}$	48.2
G-PLGA-PAA	25 kGy, 6.1 $kGy \cdot h^{-1}$	44.4
G-PLGA-PAA	25 kGy, 8.1 $kGy \cdot h^{-1}$	45.3
G-PLGA-PAA	25 kGy, 10.1 $kGy \cdot h^{-1}$	46.0
G-PLGA-PAA	33 kGy, 8.1 $kGy \cdot h^{-1}$	42.3

We offered an explanation for the second possible cause that relies on the nature of polymer precipitation in the nonsolvent (that is commonly exploited for polymer fractionation [196], [197]). When the composite PLGA/PAA implants were quenched in the PBS solution, PLGA chains started to precipitate. PLGA chains of higher molecular weight precipitated more readily and quickly solidified in the PBS solution. On the other hand, oligomers of lower molecular weight may have diffused out of the composite along with NMP. The likely net result of such a precipitation process would be the increased mean molecular weight of solidified PLGA in the composite indicated by greater T_g.

The process of main chain scission in G-PLGA-PAAs which is a common consequence of gamma irradiation countered the increase in T_g arising from phase separation and solidification during the synthesis. Chain scission intensifies the motion of polymer chains due to the increase in free volume. Increased movement of polymer chains effectively lowers the value of T_g which is the temperature required to transform the polymer into a glassy state by reducing the polymer chain mobility [140]. Previous studies showed the predominant effect of chain scission on PLGA properties in the investigated dose range resulting in the dose-dependent T_g decrease [138], [140].

The influence of two opposing effects on T_g of PLGA in G-PLGA-PAA samples irradiated with the lowest dose of 17 kGy resulted in the T_g value between those for pure PLGA and UV-PLGA-PAA. We observed the gradual decrease in T_g with the increase in the irradiation dose up to the maximum irradiation dose of 33 kGy when T_g reached its minimum. The value of T_g is related to the length and mobility of polymer chains and thereby indirectly to the mechanical properties and degradation time. T_g value of the polymer which approaches the body temperature may cause the early loss of structural integrity within the material and shorten its degradation time [189].

The dose rate appeared to be a minor influence within the investigated range in our experiments. All values of T_g for G-PLGA-PAAs irradiated with 25 kGy at different dose rates differed less than 1.6 °C. We also observed the weak trend of T_g increase commensurate with the increase in the dose rate. However, this finding cannot be considered as conclusive due to the limitations in measurement accuracy.

The higher dose of gamma irradiation reduced the intensity of enthalpic relaxation peaks observed in the recorded DSC thermograms. The peak of enthalpic relaxation almost disappeared in the DSC thermogram of samples irradiated with 33 kGy. This finding indicates that chain scission can relax mechanical stresses resulting from the synthesis process in our composite PLGA/PAA implants.

We also note that additional endothermic events detected above 60 °C in the DSC thermograms indicate the release of absorbed moisture and bound water from the PAA within the composite PLGA/PAA implants.

4.4 Swelling behavior of composite hydrogels (I-III)

PAA swells extensively under physiological conditions as indicated by its high swelling degree in PBS solution reported in the literature [164]. Such behavior of PAA may lead to mechanical instability of composite hydrogels in the physiological environment. The hydrophobic polymer matrix could potentially limit the swelling of PAA within the composite material and enhance its mechanical properties. We analyzed the swelling of synthesized composite hydrogels in different media to examine the influence of the hydrophobic matrix on their swelling behavior.

4.4.1 Swelling behavior of composite PES/PAA membranes (I)

We synthesized the composite PES/PAA membranes using four different formulations of the casting solution (12PES-7AA-10MBAA, 14PES-6.5AA-10MBAA, 12PES-5.3AA-5TMPTA, and 14PES-5AA-5TMPTA). **Figure 4.12** shows the equilibrium MSDs of different membranes in distilled water. The major influences which affected the MSD were the PES content in the membrane and the type of CL used in the formulation. Hydrophobic PES support substantially limited the MSDs of all membranes. We noticed a trend of MSD reduction with the increase in PES content. We also observed improvements in the mechanical stability of membranes with higher PES content during routine handling. The use of hydrophilic CL TMPTA in the formulation yielded membranes with higher MSDs compared to the membranes synthesized with the hydrophobic MBAA. We ascribed the increased average MSDs of membranes synthesized with TMPTA to the larger size of the TMPTA molecule compared to the MBAA molecule, as well as to its hydrophilic nature. The larger size of TMPTA molecules can increase the distance between neighboring cross-links and thus facilitate the accumulation of water in the hydrogel.

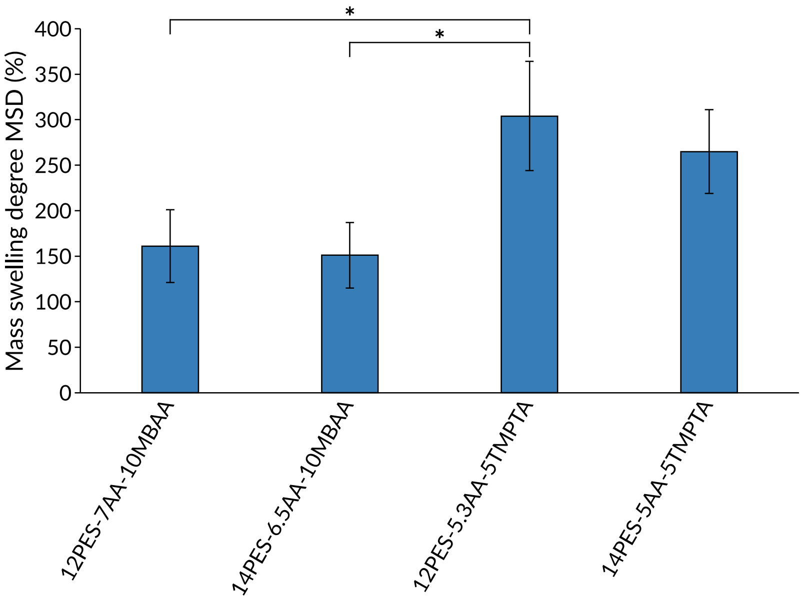

Figure 4.12. MSDs of composite PES/PAA membranes synthesized from different casting solution formulations in distilled water measured after 24 h at ambient temperature (N = 3). Significant difference (one-way ANOVA and Tukey's multiple comparisons test) is designated by $^*P < 0.05$.

Membranes synthesized with MBAA showed inferior mechanical stability in the wet state compared to the membranes synthesized using TMPTA as indicated by the tendency to curl and easily roll-up. In the case of membranes synthesized using MBAA, we also observed different surface textures at the top (plastic-like) and bottom (gel-like) sides. Conversely, we observed that the membranes synthesized with TMPTA were more resistant to mechanical deformation. The surface texture of these membranes was similar at the top and bottom sides (gel-like).

We continued the swelling experiments only with the representative membranes synthesized using TMPTA from the casting solution formulation 12PES-5.3AA-5TMPTA to examine the influence of pH and MB loading on MSD.

Figure 4.13 shows the MSDs of the membrane in the acidic CB (pH = 3 and I = 0.2 M) and slightly alkaline PBS (pH = 8 and I = 0.2 M) solutions. MSD of the membrane was significantly greater at pH = 8 in comparison with the MSD at pH = 3 indicating a pH-dependent swelling. Such swelling behavior originates from the pH sensitivity of PAA hydrogel, *i.e.* the state of charge in its carboxyl groups. At pH = 8, practically all carboxyl groups become deprotonated and negatively charged, which causes a repelling electrostatic force expanding the hydrogel network. Conversely, carboxyl groups are mainly protonated at pH = 3, which reduces the MSD.

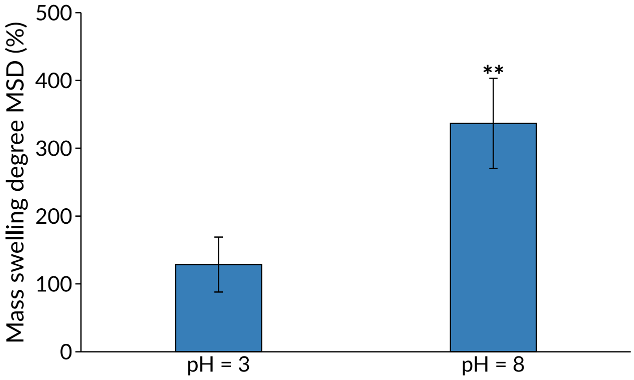

Figure 4.13. MSDs of composite PES/PAA membranes (12PES-5.3AA-5TMPTA) in CB (pH = 3 and I = 0.2 M) and PBS (pH = 8 and I = 0.2 M) measured after 24 h at ambient temperature (N = 3). Significant difference (t-test) is designated by **P < 0.01.

Figure 4.14 depicts the dependence of the membrane MSD on the molar ratio n(MB^+)/n(-COOH) after 24 h of MB loading at ambient temperature. Average MSD gradually decreased with the increase of the initial molar ratio n(MB^+)/n(-COOH). MB cations introduced into the PAA hydrogel network screened the negative charges of carboxyl groups and this process led to the stabilizing electrostatic interactions reducing the MSD.

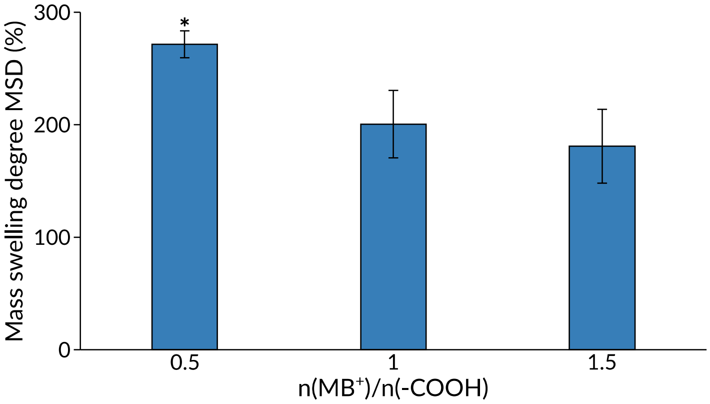

Figure 4.14. MSDs of composite PES/PAA membranes (12PES-5.3AA-5TMPTA) in MB loading solutions with different initial molar ratios n(MB^+)/n(-COOH) measured after 24 h of loading at ambient temperature (N = 3). Significant difference (one-way ANOVA and Tukey's multiple comparisons test) is designated by *P < 0.05.

4.4.2 Swelling behavior of composite DL-PLCL/PAA implants (II)

We investigated the swelling behavior of composite DL-PLCL/PAA implants in PBS (pH = 7.4 and I = 0.154 M). The equilibrium MSD of composite DL-PLCL/PAA implants before drying (MSD_e) was highly reproducible with a value of (346 ± 6) %. The value of MSD_e indicated the significant impact of the hydrophobic DL-PLCL matrix in limiting PAA hydrogel swelling.

Figure 4.15 shows the swelling kinetics of the composite DL-PLCL/PAA implants. The swelling was rapid and MSD reached its equilibrium value after approximately 6 min. We fitted the swelling kinetics using the Boltzmann sigmoid function in the following form:

$$y_{\mathrm{B}}(t) = y_{\mathrm{i}} + \frac{y_{\mathrm{f}} - y_{\mathrm{i}}}{1 + \exp\left(\frac{t_{\mathrm{ip}} - t}{s}\right)} \tag{4.1}$$

where y_{B} designates the value of the Boltzmann function at time t, y_{i} designates the initial equilibrium value, y_{f} designates the final equilibrium value, t_{ip} designates the inflection point, and s designates the slope coefficient.

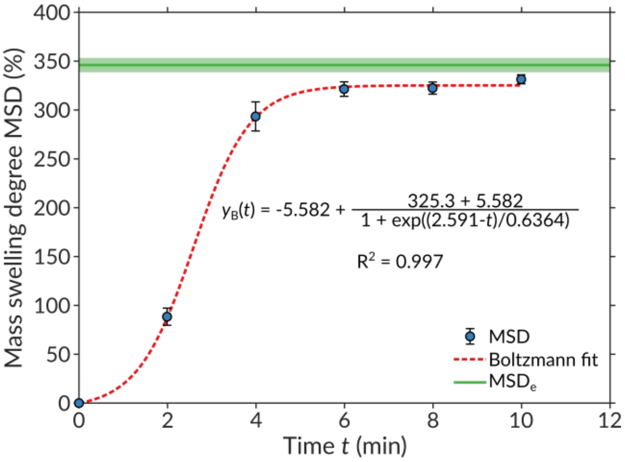

Figure 4.15. Swelling kinetics of the composite DL-PLCL/PAA implants in PBS (pH = 7.4 and I = 0.154 M) at ambient temperature fitted using the Boltzmann sigmoid function (N = 3). Error bars designate ±SD. The dark green line indicates the MSD of DL-PLCL/PAA implants in equilibrium before drying ($\mathrm{MSD_e}$) for comparison. The light green shaded area surrounding the dark green line designates the ±SD margin of $\mathrm{MSD_e}$.

The shape of the Boltzmann sigmoid function can be well correlated with the presumed stages of swelling within the implant. Initially, the swelling is slower due to the presence of a surface layer with lower PAA content functioning as an effective rate-limiting barrier to PBS penetration. When the PAA-rich aggregates at the surface become hydrated their surface expands, while their negative charges also electrostatically attract PBS cations that enter the bulk of the implant. PAA-rich microgel particles in the bulk swell rapidly due to their small size and hydrophilic surface which speeds up the macroscopic swelling. Higher content of PAA in the bulk in the form of densely packed PAA-rich particles with hydrophilic surface and high negative charge density in the swollen state further increases the rate of hydrogel formation and cation penetration. An additional increase in the macroscopic rate of swelling reflects these aspects of the implant bulk.

After one cycle of drying in air at ambient temperature, the implants reached almost the same equilibrium MSD in PBS as before, which indicates the capability of reversible swelling. While examining the swelling kinetics, we also observed that the implants retained their disk-shaped geometry during swelling and drying without bending. This observation indicated good mechanical compatibility between the PAA-rich and DL-PLCL-rich phase.

4.4.3 Swelling behavior of composite PLGA/PAA implants (III)

Figure 4.16 illustrates the equilibrium MSDs of different composite PLGA/PAA implants. The MSDs of G-PLGA-PAAs were quite similar and showed almost no dependence on the gamma irradiation parameters in the investigated range. UV-PLGA-PAA showed about 14% lower MSD on average in relative comparison with G-PLGA-PAAs. We attributed the differences in MSD to several factors such as microstructure, the spatial structure of the PAA hydrogel network, and hydrophilicity. G-PLGA-PAAs exhibited a higher degree of structural inhomogeneity and larger pore size compared to UV-PLGA-PAA, which facilitated the intake of aqueous electrolyte during swelling. PAA hydrogel formation through cross-linking induced by gamma irradiation resulted in more branched structures exposing additional hydrophilic groups to the surrounding medium. A previous study also showed that gamma irradiation of PLGA in the dose range up to 25 kGy can increase the content of carboxyl groups in PLGA [189], which could result in improved hydrophilicity of the G-PLGA-PAAs.

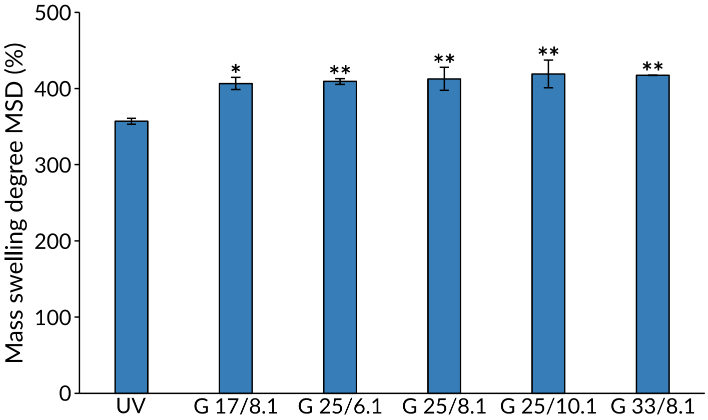

Figure 4.16. MSDs of UV-PLGA-PAA synthesized using the dose of 3.6 J·cm^{-2} and dose rate of 1.2 J·cm^{-2}·min^{-1} (designated as UV) and G-PLGA-PAAs synthesized using different irradiation parameters (designated as G dose (kGy)/dose rate (kGy·h^{-1})) measured after 24 h at ambient temperature in PBS (pH = 7.4 and I = 0.154 M) (N = 2). Significant difference (one-way ANOVA and Dunnett's multiple comparisons test) between MSDs of G-PLGA-PAAs and MSD of the control (UV-PLGA-PAA) is designated by *P < 0.05 and **P < 0.01.

PLGA matrix obviously limited the swelling of PAA hydrogel in all composite PLGA/PAA implants by providing mechanical support. Similar MSDs for all G-PLGA-PAAs also implied that the PLGA matrix retained mechanical integrity which is not compromised by the effects of gamma irradiation in the investigated range.

Figure 4.17 shows the swelling kinetics of UV-PLGA-PAA and G-PLGA-PAAs. The swelling started promptly without the initial lag unlike the swelling of composite DL-PLCL/PAA implants. We ascribed such behavior during the initial swelling stage to the porous structure in the dry state that allows for simultaneous diffusion and capillary action. Swelling later proceeded at a higher rate to approach the equilibrium MSD after approximately 30 min for UV-PLGA-PAA and about 20 min for G-PLGA-PAAs. Swelling dynamics was similar for all G-PLGA-PAAs without noticeable significant differences arising from the variation of gamma irradiation parameters within the investigated range. The swelling kinetics was faster during all swelling stages for G-PLGA-PAAs compared to UV-PLGA-PAA. We ascribed the faster kinetics mainly to the larger pore size of G-PLGA-PAAs and potentially increased content of polar and hydrophilic carboxyl groups in PLGA due to gamma irradiation as mentioned previously [189].

We measured the swelling kinetics starting from the independent set of samples of composite PLGA/PAA implants previously dried in the air under ambient conditions. The achieved MSDs after the measurements (**Figure 4.17**) were lower than equilibrium MSDs measured for composite PLGA/PAA implants that were not previously dried (**Figure 4.16**) (for about 8% in the case of UV-PLGA-PAA and for approximately 20% in the case of G-PLGA-PAAs). Such results indicated the lack of ability for reversible swelling. We attributed the observed decrease in recorded MSDs to the irreversible pore collapse that may occur during drying. The effect of irreversible pore collapse was more pronounced in G-PLGA-PAAs due to the higher degree of microstructural inhomogeneity.

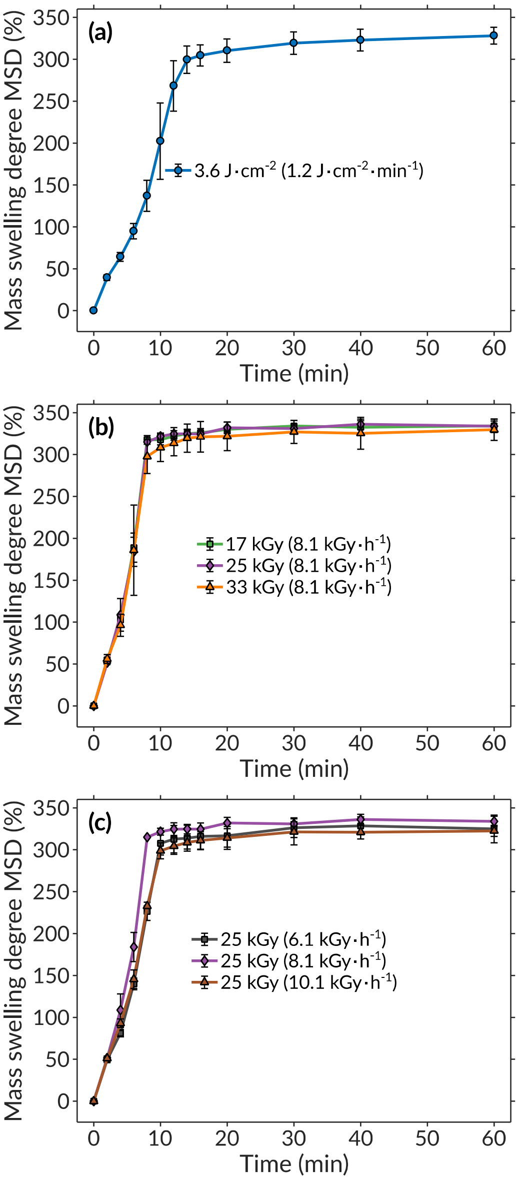

Figure 4.17. Swelling kinetics of composite PLGA/PAA implants synthesized using different UV and gamma irradiation parameters designated in the format dose (dose rate) measured in PBS (pH = 7.4 and *I* = 0.154 M) at ambient temperature (N = 3): (a) UV-PLGA-PAA, (b) G-PLGA-PAAs compared in terms of applied dose (constant dose rate of 8.1 kGy·h^{-1}), and (c) G-PLGA-PAAs compared in terms of applied dose rate (constant dose of 25 kGy).

4.5 IEC of composite hydrogels (I-III)

The ability of our composite hydrogels to store cationic drugs depends on the concentration of fixed negatively charged groups capable of cation exchange. For all composite hydrogels described in this dissertation, PAA hydrogel acts as the main drug storage component, and its abundant carboxyl groups function as weak cation exchangers. The value of IEC defines the maximum amount of cationic drugs that can be stored within a composite hydrogel by electrostatic forces.

4.5.1 IEC of composite PES/PAA membranes (I)

Figure 4.18 shows the IECs measured for membranes synthesized using different formulations of the initial casting solution. We synthesized membranes with slightly greater IEC overall when using MBAA as CL compared to TMPTA.

Figure 4.19 illustrates the RYs for membrane synthesis calculated according to the definition of RY from the section **2.2.9 Ion-exchange capacity of composite membranes and implants**. The average RY was higher in the formulations where we used TMPTA as the CL instead of the MBAA. Despite the higher RY, the lower initial concentration of AA in the casting solutions led to the reduced IEC in membranes synthesized with TMPTA.

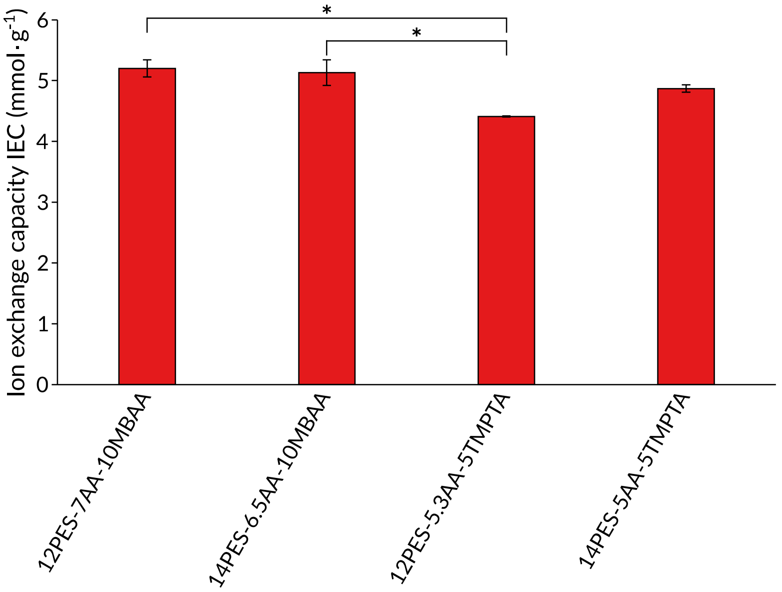

Figure 4.18. IECs of composite PES/PAA membranes synthesized using different formulations of the initial casting solution (N = 2). Significant difference (one-way ANOVA and Tukey's multiple comparisons test) is designated by *P < 0.05.

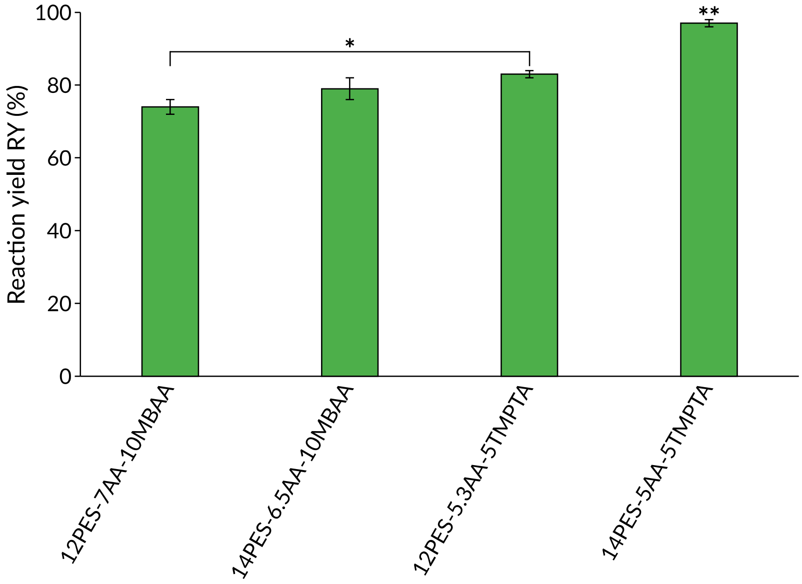

Figure 4.19. RYs of composite PES/PAA membranes synthesized using different formulations of the initial casting solution (N = 2). Significant difference (one-way ANOVA and Tukey's multiple comparisons test) is designated by *P < 0.05 and **P < 0.01.

4.5.2 IEC of composite DL-PLCL/PAA and PLGA/PAA implants (II, III)

Figure 4.20 depicts the IECs of composite DL-PLCL/PAA and PLGA/PAA implants. All materials had quite similar IECs (around 2 mmol·g^{-1}). Composite DL-PLCL/PAA implant and UV-PLGA-PAA exhibited low IEC variability, while G-PLGA-PAAs showed highly variable IEC values. Our statistical analysis demonstrated no significant influence of gamma irradiation parameters on the value of IEC. We attributed the greater IEC variability in G-PLGA-PAAs to the microstructural nonuniformities and macroscopically inhomogeneous chemical composition.

Figure 4.21 shows the RYs for composite hydrogel implant synthesis calculated according to the definition of RY from the section **2.2.9 Ion-exchange capacity of composite membranes and implants**. As was the case with IECs, the average values of RY were similar for all composite hydrogel implants (about 60%). Differences in the variability of the RY directly correspond to the variability differences between IECs of the composite hydrogel implants and the same analysis can be applied to the results obtained for RY. We note here that the average RYs of the composite hydrogel implant synthesis were lower than the average RYs of the composite PES/PAA membrane synthesis.

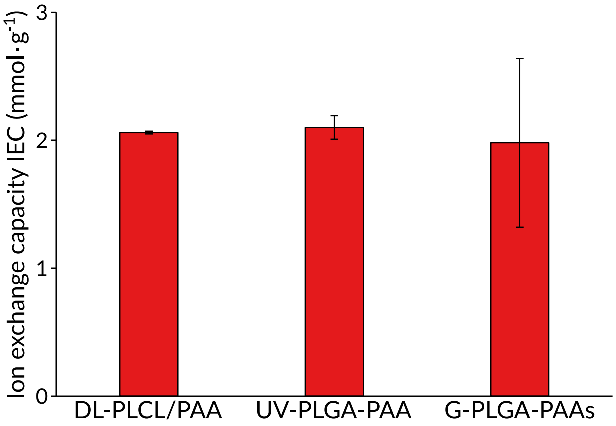

Figure 4.20. IECs of composite hydrogel implants synthesized using UV irradiation (DL-PLCL/PAA and UV-PLGA-PAA, N = 2) and gamma irradiation (G-PLGA-PAAs, pooled statistics, N = 10; N = 2 for each of the G-PLGA-PAA types).

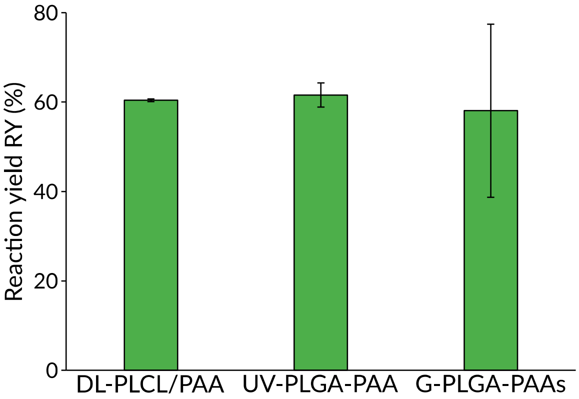

Figure 4.21. RYs of composite hydrogel implants synthesized using UV irradiation (DL-PLCL/PAA and UV-PLGA-PAA, N = 2) and gamma irradiation (G-PLGA-PAAs, pooled statistics, N = 10; N = 2 for each of the G-PLGA-PAA types).

4.6 Electrical characterization of composite PES/PAA membranes

The electrical characterization of the composite PES/PAA membranes revealed the value of bulk membrane sample resistance $R_B = (0.68 \pm 0.01)\ \Omega$ (N = 3). Using the R_B value and **Equation (2.3)**, we calculated the membrane resistance as $R_m = (2.99 \pm 0.05)\ \Omega \cdot \mathrm{cm}^2$ which is commonly listed as a property of ion-exchange membranes. The thickness of the clamped membrane determined by the vernier caliper was $d_m = (50 \pm 10)\ \mu\mathrm{m}$ (N = 3). Finally, we calculated the ionic conductivity of the membrane according to the **Equation (2.4)** as $\sigma_m = (0.17 \pm 0.04)\ \mathrm{S \cdot m^{-1}}$.

Obtained values indicated the presence of continuous electrically conductive paths through the composite PES/PAA membranes in the swollen state under physiological conditions (pH = 7.4 and I = 0.154 M). We attributed the formation of conductive paths to the swelling of ionically conductive PAA microgels within the porous PES support. Ionic conductivity of PAA hydrogels arises from the densely packed fixed carboxyl groups that mostly deprotonate at physiological pH.

4.7 Loading of composite hydrogel reservoirs with MB (I, II)

We performed the MB loading experiments on composite PES/PAA membranes and composite DL-PLCL/PAA implants. Results of the loading experiments were used to determine loading efficiencies, *i.e.* the fractions of IEC usable for cationic drug storage.

4.7.1 Loading of composite PES/PAA membranes (I)

Figure 4.22 shows the loading efficiency (as defined in section **2.2.11 Loading of composite membranes and implants with MB**) after 24 h of loading in MB solutions with different molar ratios n(MB^+)/n(-COOH). As we expected, the amount of loaded MB was commensurate with the molar ratio n(MB^+)/n(-COOH). Higher values of the molar ratio n(MB^+)/n(-COOH) correspond to the greater initial MB concentration gradient between the loading medium and the membrane. Since the concentration gradient represents the main driving force for MB loading by ion exchange, the loading efficiency at a given time increased with the molar ratio n(MB^+)/n(-COOH).

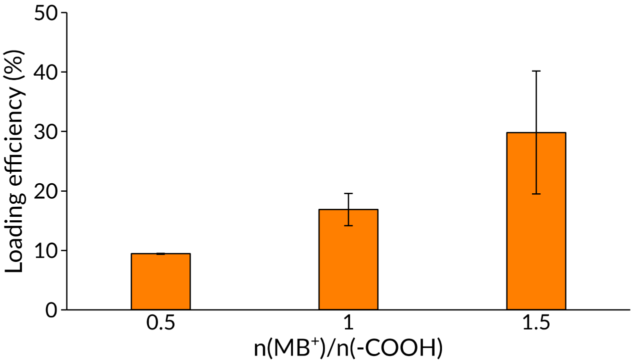

Figure 4.22. Dependence of MB loading efficiency on the initial molar ratio n(MB^+)/n(-COOH) for the composite PES/PAA membranes (12PES-5.3AA-5TMPTA) after 24 h of loading at ambient temperature (N = 3).

The maximum MB loading efficiency achieved in the experiments was about 30% of the theoretically expected maximum loading efficiency for MB (according to the definition from the section **2.2.11 Loading of composite membranes and implants with MB**). Thus, it was evident that neither of the membrane samples reached the equilibrium state at the end of MB loading experiments.

Our experiments were mostly focused on explaining the loading-dependent behavior of membranes during MB release and optimization of loading efficiency was not systematically pursued in follow-up experiments. However, we could achieve higher loading efficiency by further increasing the molar ratio n(MB^+)/n(-COOH) or prolonging the time period for loading. One can also test some of the special protocols for the loading of ion-exchange resins [198].

4.7.2 Loading of composite DL-PLCL/PAA implants (II)

We designed composite DL-PLCL/PAA implants for the prolonged release of cationic drugs. Therefore, only their maximum MB loading efficiency was of major practical interest. The results of our loading experiments conducted in 25 cm^3 of 1 $g \cdot dm^{-3}$ MB aqueous solution at ambient temperature (corresponding to the molar ratio n(MB^+)/n(-COOH) = 1) showed that the implants had an excellent loading efficiency of (95.8 ± 0.4)% after 5 days of MB loading. These results imply that an excessive amount of MB (*i.e.* the MB loading solution adjusted to achieve the molar ratio n(MB^+)/n(-COOH) > 1) is not necessary for the effective loading of composite DL-PLCL/PAA implants.

4.8 *In vitro* release of MB from composite hydrogels (I, II)

Passive release of MB from composite hydrogel reservoirs is a complex process that involves electrostatic interactions and diffusion. The passive release profile of MB depends on the properties of the composite hydrogel materials and the surrounding medium. The release of MB from the conductive composite hydrogel reservoirs can be modulated by applying electric current to initiate the process of iontophoresis. We investigated the passive release of MB from composite PES/PAA membranes and composite DL-PLCL/PAA implants in aqueous media. In addition, we examined the possibility of tuning MB release from composite PES/PAA membranes in aqueous media via iontophoresis.

4.8.1 Passive *in vitro* release of MB from composite PES/PAA membranes (I)

Figure 4.23 shows the fractional release of MB Q_t/Q_e in different buffered solutions (CB at pH = 3 and PBS at pH = 8, I = 0.2 M in both cases) as a function of time t. The value of Q_e used for the normalization corresponds to the final cumulative concentration of MB achieved after at least 48 h of equilibration that followed each of MB release experiments.

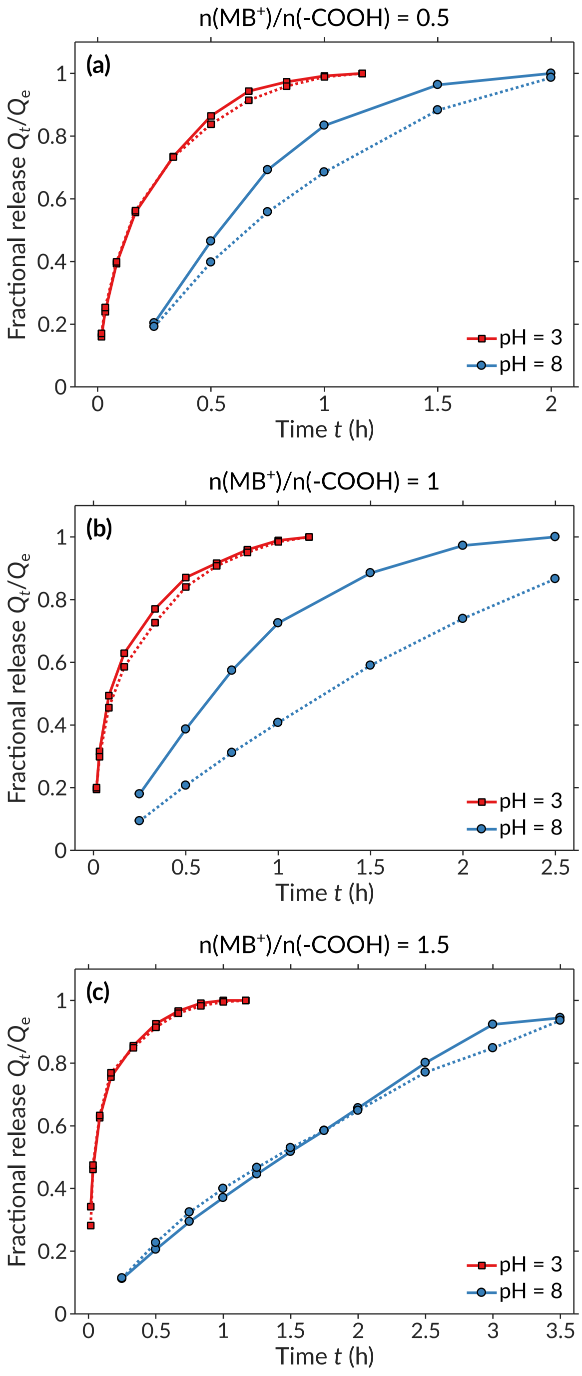

Figure 4.23. *In vitro* passive release kinetics of MB in CB (pH = 3 and I = 0.2 M) and PBS (pH = 8 and I = 0.2 M) at ambient temperature from composite PES/PAA membranes (12PES-5.3AA-5TMPTA) loaded using MB loading solutions adjusted to different values of the initial molar ratio n(MB^+)/n(-COOH). Solid and dotted lines connecting the markers designate independent measurements (N = 2).

MB release kinetics at pH = 3 exhibited a similar total release period in all of our experiments (approximately 70 minutes). The total release period was shorter compared to the experiments carried out at pH = 8, and practically independent of the molar ratio n(MB^+)/n(-COOH). The total release period at pH = 8 increased with the molar ratio n(MB^+)/n(-COOH) and was in the range from 2 h to 3.5 h.

We calculated the individual weights of MB released into different solutions normalized per dry membrane weights by utilizing the known weights of dry membrane samples and spectrophotometric calibration curves for MB in release media. **Table 4.2** shows the amounts of released MB during passive *in vitro* release experiments conducted under different experimental conditions, expressed as MB weight normalized per dry weight of the composite PES/PAA membrane (12PES-5.3AA-5TMPTA) sample (designated as m_{MB}). The comparison between the values of m_{MB} released in buffer solutions and 96% ethanol can provide the approximate ratio between the quantities of electrostatically and hydrophobically bound MB, respectively. We observed that the major amount of MB within the composite PES/PAA membrane (12PES-5.3AA-5TMPTA) sample (at least 91%) was bound by electrostatic forces. The amount of released MB was significantly smaller for experiments carried out in buffer solutions at pH = 3 (on average for 36%) in comparison with the quantity of released MB at pH = 8 when all other experimental conditions were kept equal. We ascribed the incomplete MB release at pH = 3 to the observed rapid deswelling of membrane samples that can trap a significant portion of MB molecules in collapsed PAA-rich microgels.

Table 4.2. Values of m_{MB} with corresponding SDs (N = 2) for experiments conducted under different conditions of pH and molar ratio n(MB^+)/n(-COOH) normalized per dry weight of the composite PES/PAA membrane (12PES-5.3AA-5TMPTA) sample.

pH	n(MB^+)/n(-COOH)	m_{MB} ± SD ($g \cdot g^{-1}$) (Buffer solution)	m_{MB} ± SD (× 10^{-3}) ($g \cdot g^{-1}$) (96% Ethanol)	Total m_{MB} ± SD
3	0.5	0.108 ± 0.002	5.043 ± 0.230	0.113 ± 0.002
	1	0.192 ± 0.039	6.771 ± 0.642	0.199 ± 0.039
	1.5	0.262 ± 0.078	6.760 ± 0.659	0.269 ± 0.078
8	0.5	0.127 ± 0.001	5.648 ± 0.423	0.133 ± 0.001
	1	0.223 ± 0.035	14.510 ± 10.800	0.238 ± 0.038
	1.5	0.387 ± 0.142	34.070 ± 31.869	0.421 ± 0.146

We will further analyze the release kinetics in combination with the modeling results in the section **5.2 Modeling of passive *in vitro* release of MB from composite PES/PAA membranes** in order to understand the influence of relevant parameters such as pH, molar ratio n(MB^+)/n(-COOH), and membrane thickness on the dynamics of MB release from composite PES/PAA membranes.

4.8.2 Iontophoretic *in vitro* release of MB from composite PES/PAA membranes

We conducted an *in vitro* pilot study to examine the feasibility of composite PES/PAA membrane use for iontophoretic delivery of cationic drugs. We noticed the bending of membrane samples towards the anode during preliminary experiments of iontophoretic *in vitro* release. The curvature of the membrane surface would complicate the interpretation of experimental results and to minimize this effect a mechanical support layer was introduced in direct contact with the membrane surface as shown in **Figure 2.4**. Mechanical support in the form of a porous polyester spunbond nonwoven fabric prevented the bending of the membrane sample in further experiments (used to obtain the results presented here).

Due to the specific nature of iontophoresis experiments and the required experimental setup, results obtained for active MB release via iontophoresis are not directly comparable with the results obtained for passive MB release from composite PES/PAA membranes. However, the influence of electric current on the dynamics of MB release can be investigated to obtain initial insights about the applicability of composite PES/PAA membranes for iontophoretic delivery of cationic drugs. As a representative membrane formulation, we used 12PES-5.3AA-5TMPTA.

Composite PES/PAA membranes (12PES-5.3AA-5TMPTA) prepared for iontophoresis experiments absorbed MB with a loading efficiency of (95.9 ± 1.2) % (N = 4) (as defined in the section **2.2.11 Loading**

of composite membranes and implants with MB). We calculated the individual weights of MB released from membranes into PBS solutions under different electric current regimes normalized per dry membrane weights (designated as m_{MB}) by utilizing the known weights of dry membrane samples and spectrophotometric calibration curves for MB in PBS. In the continuous electric current regime, membranes released $m_{\mathrm{MB}} = 0.029 \pm 0.011$ (or (3.01 ± 1.11) % of the loaded MB) (N = 2). Released amount of MB in the pulse electric current regime was $m_{\mathrm{MB}} = 0.026 \pm 0.007$ (or (2.74 ± 0.79) % of the loaded MB) (N = 2). For the total duration of our experiments (including the initial passive release of MB), composite PES/PAA membranes (12PES-5.3AA-5TMPTA) released only a small portion of absorbed MB (less than 5.5% in all cases). Such results indicated the potential reusability of membranes in several therapeutic sessions of iontophoretic delivery without repeating the MB loading procedure. The membranes can also be used at lower MB loadings if required, which may be beneficial for controlled release via iontophoresis as we discuss in section **6.7 Active *in vitro* release of MB from composite PES/PAA membranes via iontophoresis**.

Figure 4.24 shows a typical MB release profile during an *in vitro* iontophoretic release experiment.

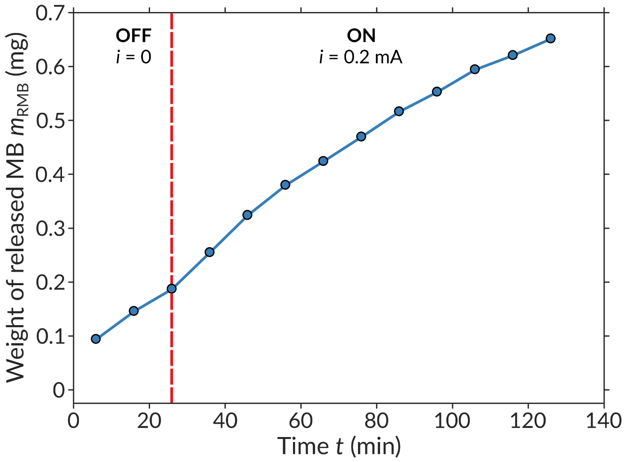

Figure 4.24. Representative profile of *in vitro* iontophoretic MB release from composite PES/PAA membranes (12PES-5.3AA-5TMPTA) in PBS (pH = 7.4 and $I = 0.154$ M) at 37 °C.

Since it was inevitable to release some amount of MB before iontophoresis was initiated, we normalized the results to the amounts of released MB during the period of 100 min when the electric excitation was applied to compare the release kinetics of different membrane samples and to compare the results for different iontophoresis regimes. **Figure 4.25** illustrates the MB release kinetics for the continuous and pulse regime of iontophoresis. It shows the fractional release of MB Q_t/Q_{ie} in PBS (pH = 7.4 and $I = 0.154$ M) as a function of time t. The value of Q_{ie} used for the normalization corresponds to the cumulative concentration of MB released during the iontophoretic MB release experiment (in the presence of electric excitation).

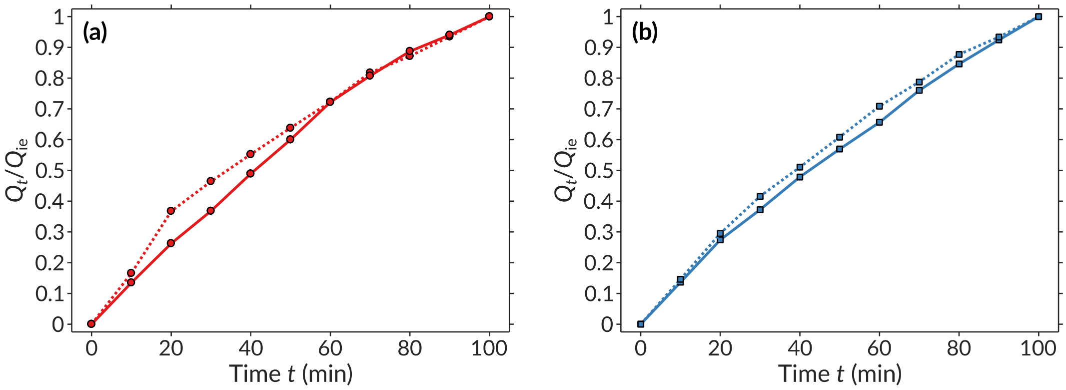

Figure 4.25. *In vitro* iontophoretic release kinetics of MB in PBS (pH = 7.4 and $I = 0.154$ M) at 37 °C under different iontophoresis regimes: (a) continuous iontophoresis regime ($i = 0.2$ mA) and (b) pulse iontophoresis regime (rectangular current pulses, $i = 0.2$ mA, $f = 1$ kHz, $DC = 50\%$). Solid and dotted lines between the markers designate two independent measurements in each regime (N = 2).

We shall present a more detailed analysis of the release kinetics in combination with the modeling results in section **5.3 Modeling of active *in vitro* release of MB from composite PES/PAA membranes via iontophoresis**.

4.8.3 Passive *in vitro* release of MB from composite DL-PLCL/PAA implants (II)

Figure 4.26 illustrates the fractional release of MB Q_t/Q_e as a function of time t. The value of Q_e used for normalization corresponds to the final cumulative concentration of released MB at the end of the *in vitro* release experiment. Release kinetics for composite DL-PLCL/PAA implants exhibited a total release period of approximately 24 days.

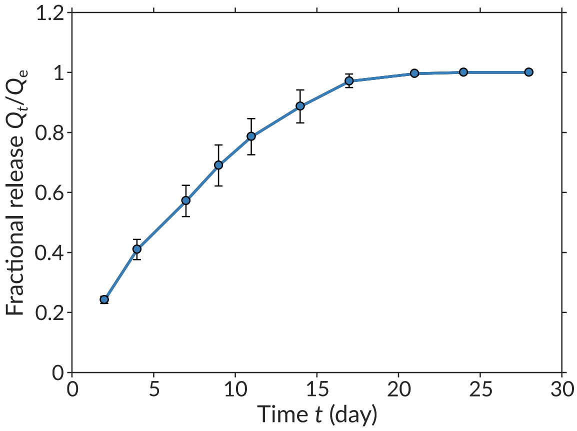

Figure 4.26. *In vitro* passive release kinetics of MB in PBS (pH = 7.4 and I = 0.154 M) at 37 °C from composite DL-PLCL/PAA implants (N = 3).

In the experiments of *in vitro* MB release from composite DL-PLCL/PAA implants into PBS (pH = 7.4 and I = 0.154 M) at 37 °C, the final released amount was (85.1 ± 1.8) % of the total absorbed amount of MB. Following similar reasoning as for composite PES/PAA membranes, such result indicated that about 85% of absorbed MB was bound by electrostatic forces (and thus susceptible to the release driven by ion exchange), while the remaining 15% was bound by hydrophobic forces.

We calculated the average weight of MB released in PBS solution normalized per dry implant weight (designated as m_{MB}) by using the known weights of dry implant samples and spectrophotometric calibration curves for MB in PBS. The obtained value was $m_{\mathrm{MB}} = 0.543 \pm 0.015$. The average m_{MB} was higher for composite DL-PLCL/PAA implants compared to composite PES/PAA membranes. Such a result can be attributed to the significantly higher initial MB loading of implants that compensates for the lower IEC and somewhat inferior capability to release MB by ion exchange.

We shall present a more detailed analysis of the release kinetics in combination with the modeling results in section **5.4.2 Determination of D_a for the composite DL-PLCL/PAA implants**.

4.9 Biocompatibility of composite DL-PLCL/PAA implants (II)

We conducted a series of *in vitro* tests and an *in vivo* pilot study to investigate the biocompatibility of unloaded composite DL-PLCL/PAA implants. Composite DL-PLCL/PAA implants caused a decrease in adhesion potential and metabolic activity of mouse fibroblast L929 cells and did not influence the viability of primary cells isolated from the spleen of male Dark Agouti rat. The composite DL-PLCL/PAA implants showed no pro-inflammatory effect and the results of *in vitro* tests also imply that the implants may have the immunosuppressive potential. Subcutaneous implantation in male Dark Agouti rats led to the normal foreign body reaction and early stages of slow fibrous capsule formation without the systemic proinflammatory response. Free carboxyl groups exposed at the surface of the composite DL-PLCL/PAA implant make the surface hydrophilic and negatively charged. These properties of the implant surface strongly influence its interactions with the biological environment. It is important to note that composite DL-PLCL/PAA implants loaded with cationic drugs can exhibit different surface properties that are time-dependent. Hence, the biocompatibility of loaded composite

DL-PLCL/PAA implants is an important topic for further research. For additional details about the studies of composite DL-PLCL/PAA implant biocompatibility refer to journal article **II**[3].

---

[3] [174] Ž. Janićijević, M. Ninkov, M. Kataranovski, and F. Radovanović, "Poly(DL-Lactide-*co*-ε-Caprolactone)/Poly(Acrylic Acid) Composite Implant for Controlled Delivery of Cationic Drugs," *Macromol. Biosci.*, vol. 19, no. 2, p. 1800322, Feb. 2019, doi: 10.1002/mabi.201800322.

Chapter 5: Modeling of composite hydrogel pore size and *in vitro* MB release behavior

5.1 Theoretical estimation of pore size in composite hydrogels (I, II)

The swelling of synthesized composite hydrogels originates from mechanically constrained swelling of PAA hydrogel within the hydrophobic polymer matrix. During the swelling, PAA hydrogel spreads to fill the pores if they exist in the surrounding polymer matrix and then further expands until the force balance is achieved in swelling equilibrium for the given medium. We can assume that the hydrophobic polymer matrix is nonporous in the swollen state. In such a case, the porosity of our composite hydrogels in the swollen state is determined by the porosity of PAA hydrogel itself (*i.e.* its mesh size).

We performed the theoretical estimation of the mean pore size using the gel correlation length model. Hu and Dickson elaborated on the theory and application of the gel correlation length model on PAA (for details refer to [199] and references therein). We provide here only a brief description of the main model concepts relevant to our estimation.

The model treats the gel confined within the pores as a semidilute polymer solution of equivalent polymer volume fraction. The semidilute polymer solution is then considered as a transient network of mean mesh size ξ defined between interchain crossings. Mean mesh size ξ is designated as the gel correlation length and assumed to be the effective pore diameter. The value of ξ can be obtained using the following expressions:

$$\xi \cong \left(L_\mathrm{B} + \frac{1}{16\pi l_\mathrm{B} A_\mathrm{C} c}\right)^{-\frac{1}{4}} (4\pi A_\mathrm{C} c)^{\frac{1}{8}} (A_\mathrm{C} c)^{-\frac{3}{4}} \tag{5.1}$$

$$c = \frac{N_\mathrm{A} \varphi}{v M_\mathrm{WMM}} \tag{5.2}$$

where L_B is the bare persistence length (12.1 nm), l_B is the Bjerrum length in water (0.713 nm), A_C is the contour distance between the two adjacent charged groups along the polymer chain, c is the concentration of the charged segments, N_A is the Avogadro constant, φ is the PAA gel volume fraction, v is the partial specific volume of the PAA gel in the composite hydrogel, and M_WMM is the MM molecular weight.

We determined the value of φ from the expression presented in Zhou et al. (for details refer to [200] and references therein):

$$\varphi = \frac{(m_\mathrm{dCH} - m_\mathrm{PB})v}{V_\mathrm{CH} - m_\mathrm{PB}/\rho_\mathrm{PB}} \tag{5.3}$$

where m_dCH is the dry weight of the composite hydrogel, m_PB is the weight of the nascent hydrophobic PB, V_CH is the composite hydrogel volume, and ρ_PB is the density of the PB. After the calculation of φ, we linearized and extended the log-log plot shown in **Figure 5.1** reprinted from the reference [199] to obtain the values of pore diameters in our samples by extrapolation.

As demonstrated by the study of Hu and Dickson [199], the use of the gel correlation length model for PAA provides results comparable with other model-fitting methods but yields systematically lower values of the pore diameter. The differences in estimated values are reasonable since the gel correlation length model intrinsically involves simplified calculations and does not account for the important effects of cross-linking in gels.

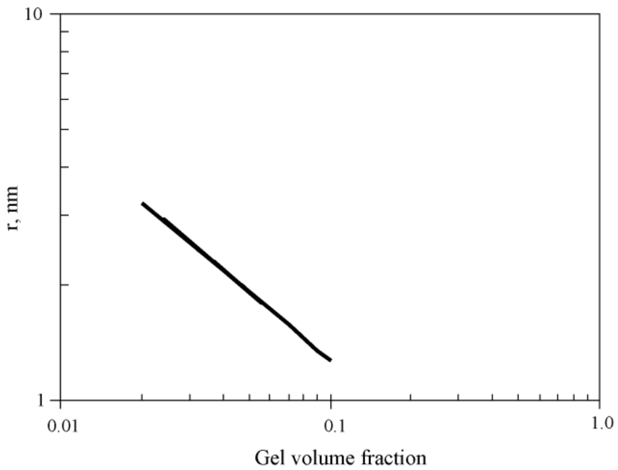

Figure 5.1. Calculated pore radius by the gel correlation length as a function of the gel volume fraction. Reprinted from the Journal of Membrane Science, vol. 321, no. 2, K. Hu and J. M. Dickson, Modelling of the pore structure variation with pH for pore-filled pH-sensitive poly(vinylidene fluoride)-poly(acrylic acid) membranes, pp. 162–171, Copyright (2008), with permission from Elsevier. Source: [199].

Our calculations indicated that the mean pore diameter decreased with the increase in MB content within the composite hydrogel reservoir. In the case of composite PES/PAA membranes (12PES-5.3AA-5TMPTA), the effective mean pore diameter was 2.28 nm without loaded MB (in PBS at pH = 8 and I = 0.2 M) and it reduced to 1.74 nm when loaded with MB (at around 30% loading efficiency). Composite DL-PLCL/PAA implants showed a similar trend where the effective mean pore diameter was 2.62 nm (in PBS at pH = 7.4 and I = 0.154 M) and lowered down to 2.22 nm after MB loading with the loading efficiency of around 96%.

5.2 Modeling of passive *in vitro* release of MB from composite PES/PAA membranes (I)

Kinetics of passive *in vitro* solute release from hydrophilic polymer matrices is commonly evaluated by fitting the experimental data to the Korsmeyer-Peppas equation [201]:

$$\frac{M_t}{M_\infty} = kt^\alpha \tag{5.4}$$

where M_t/M_∞ designates the fractional release of the solute, k designates the characteristic kinetic constant of the investigated polymer/solute system, and a designates the diffusional exponent describing the mechanism of solute release. The Korsmeyer-Peppas equation provides an adequate description of *in vitro* release up to 60% of fractional solute release, but only in systems where release occurs under perfect sink conditions (*i.e.* when there are no barriers to diffusion) [202]. The parameters of the **Equation (5.4)** are empirical and provide limited insight into the details of the solute release mechanism.

Mechanism of *in vitro* MB release from our composite PES/PAA membranes is complex since it must account for the simultaneous occurrence of several processes such as cation exchange, diffusion of cations from the membrane to the medium and vice versa, and even possible convective flow under some experimental conditions. It is evident from our results that boundary conditions are quite variable and far from the perfect sink conditions treated by common models. In order to provide the most genuine description of the MB release kinetics, we combined the analytical solution for the diffusion from thin polymer films with the empirical Weber-Morris model.

MB desorption from our composite PES/PAA membranes can be approximated as a diffusion-controlled process. Such approximation can be applied because the process of MB diffusion is much slower than electrostatic interactions related to MB desorption. We first applied the formalism of the intraparticle diffusion model introduced by Plazinski and Rudzinski [203] to the plane sheet particle geometry to form the IMD model. The basic equation of the IMD model is then given by:

$$\frac{\partial C}{\partial t} = \frac{D}{\tau}\frac{\partial^2 C}{\partial x^2} - \frac{\rho}{\varepsilon_\mathrm{p}}\frac{\partial Q}{\partial t} \tag{5.5}$$

where C designates the local MB concentration within the membrane hydrogel, Q designates the local MB concentration in the release medium, D designates the MB diffusion coefficient in the hydrogel phase, ϱ designates the membrane density, ε_p designates the membrane porosity given as the fractional volume of the hydrogel, and τ designates the tortuosity factor. Local MB concentrations C and Q are related to each other by the sorption equilibrium relationship. The tortuosity factor τ can be defined as the reciprocal of the square root of porosity for materials with interconnected porous structure [204].

We treated the problem as one-dimensional with the geometry set as symmetric about the central plane parallel to the membrane (**Figure 5.2**).

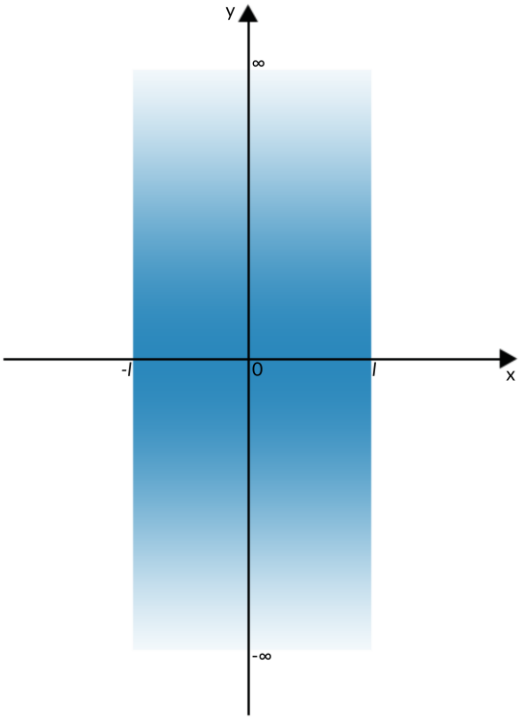

Figure 5.2. The geometry of the membrane used in the IMD model. The membrane is represented as the infinite plane sheet of finite thickness 2*l*. The vertical color gradient illustrates the infinite dimensions of the membrane along the y-axis. The thickness of the membrane is exaggerated for visualization purposes.

We then solved the **Equation (5.5)** for the following boundary condition:

$$\left.\left(\frac{\partial C}{\partial x}\right)\right|_{x=0} = 0 \tag{5.6}$$

and initial conditions at $t = 0$:

$$\begin{gathered} C(-l < x < l) = C_0 \\ C(x = \pm l) = 0 \end{gathered} \tag{5.7}$$

where C_0 designates the initial MB concentration within the membrane (assumed to be uniform) and l designates half of the membrane thickness. If we can consider the MB concentration at the membrane/medium interface as constant, regard membrane microstructure as uniform, and assume the applicability of Henry's isotherm equation, the analytical solution for fractional desorption Q_t/Q_e is given by [203]:

$$\frac{Q_t}{Q_\mathrm{e}} = 1 - \frac{8}{\pi^2}\sum_{n=0}^{\infty}\frac{1}{(2n+1)^2}\exp\left(-\frac{D_\mathrm{a}\pi^2(2n+1)^2}{4l^2}t\right) \tag{5.8}$$

where Q_t denotes the MB concentration in the release medium at time t, Q_e denotes the MB concentration in equilibrium (*i.e.* at the end of the desorption process), and D_a denotes the apparent diffusion coefficient.

Composite PES/PAA membrane parameters D and D_a are related by the expression [203], [205]:

$$D_\mathrm{a} = \frac{D}{\tau\left(1 + \rho K_\mathrm{H}/\varepsilon_\mathrm{p}\right)} \tag{5.9}$$

where K_H denotes the Henry's constant describing the equilibrium relationship between C and Q [206]. K_H can be interpreted as the membrane/medium distribution coefficient for MB.

The analytical form of the solution given by **Equation (5.8)** is equivalent to the solution obtained for the problem of non-steady state diffusion in the plane sheet for the special case when the diffusing species is initially homogeneously distributed and the surface concentrations are kept equal as explained by Crank [207]. As proposed by Crank, we also rewrote the **Equation (5.8)** in the more suitable form adequate for small times:

$$\frac{Q_t}{Q_\mathrm{e}} = 2\left(\frac{D_\mathrm{a}t}{l^2}\right)^{0.5}\left(\pi^{-0.5} + 2\sum_{n=1}^{\infty}(-1)^n ierfc\left(\frac{nl}{(D_\mathrm{a}t)^{0.5}}\right)\right) \tag{5.10}$$

The contribution of the term containing *ierfc* function can be neglected for large values of the *ierfc* function argument. Hence, for sufficiently small times, Q_t/Q_e should be proportional to the square root of time t.

If we allow for the variable boundary conditions by relaxing the assumption of perfect sink conditions, MB desorption can also be explained by the Weber-Morris equation [208]:

$$\frac{Q_t}{Q_\mathrm{e}} = At^{0.5} + B \tag{5.11}$$

where A and B are empirical parameters. A is interpreted as the rate parameter, while B is interpreted as the intercept proportional to boundary layer thickness which determines the mass transfer resistance.

Combination of **Equations (5.10)** and **(5.11)** yields the following expression for small times:

$$\frac{Q_t}{Q_\mathrm{e}} = 2\left(\frac{D_\mathrm{a}t}{\pi l^2}\right)^{0.5} + B \tag{5.12}$$

We performed the linear regression of Q_t/Q_e on $t^{0.5}$ using **Equation (5.12)** as the model. **Figure 5.3** shows the obtained linear fits.

For the fitting, we used the defined number of initial measurement points predetermined independently for each series of MB release experiments. The number of initial measurement points was chosen according to a separate analysis performed by Crank [207]. Crank estimated the maximum desorption time span during which **Equation (5.12)** retains validity and good numerical accuracy as the period while the condition $Q_t/Q_\mathrm{e} < 2/3$ holds. We then used the slope of obtained fitted lines to evaluate D_a. The expression for the slope contains parameter l which is defined as half of the wet membrane thickness. Calculation of l was carried out at the beginning of each experiment based on the wet membrane sample weight, mean MSD, measured sample area, and estimated average density of the composite membrane.

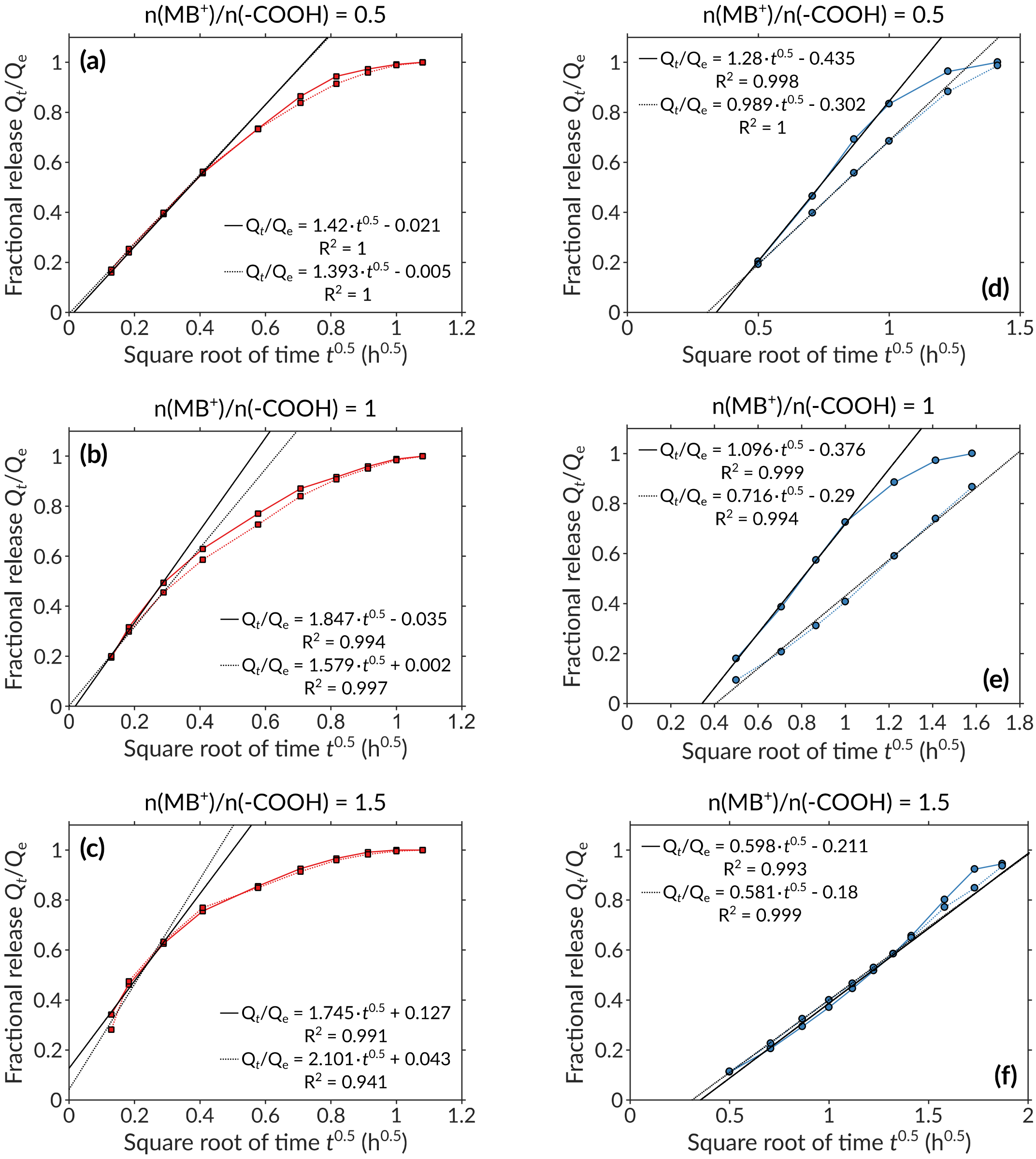

Figure 5.3. Kinetics of *in vitro* passive MB release in buffer solutions (I = 0.2 M) at pH = 3 (a-c) and pH = 8 (d-f) at ambient temperature from composite PES/PAA membranes (12PES-5.3AA-5TMPTA) loaded with MB using loading solutions with different initial molar ratios (n(MB$^+$)/n(-COOH) = 0.5, 1 or 1.5). Solid and dotted lines between the markers indicate two independent measurements carried out under the same conditions (N = 2). Solid and dotted straight lines shown in black illustrate corresponding linear fits utilized in the calculation of D_a.

We clearly observed the linear relationship between Q_t/Q_e and the square root of time t during the initial stages of MB release. This is in accordance with the assumption of the IMD model that the MB release is mainly a diffusion-controlled process which can be described using the apparent diffusion coefficient (D_a) and the intercept proportional to the boundary layer thickness related to mass transfer resistance (B).

Table 5.1 shows the summarized results of the fitting. Coefficients of determination (R^2) were greater than 0.99 in all but one case indicating statistical adequacy of the used regression model. We ascribed the nonzero values of B in the linear fits to the different boundary layer resistances. Negative values of B for experiments conducted at pH = 8 indicated the measures of present boundary layer resistances to MB desorption in our interpretation [209]. The density of uncompensated negative charges at the membrane/solution interface increased with the decrease in initial MB loading and led to the higher boundary layer resistance as indicated by the values of B for experiments carried out at pH = 8 in **Table 5.1**. Parameter B of linear fits corresponding to MB release experiments conducted at pH = 3 showed shifts towards more positive values (close to B = 0). Such a trend implied the existence of an additional effect that counteracts the effect of the boundary layer resistance to MB release. We attributed the described shifts in B values to the initial burst release of MB that was observed in all MB release experiments conducted at pH = 3. At pH = 3, protonation of carboxyl groups occurs by replacing MB cations with highly mobile hydronium ions via ion exchange. Protonation of carboxyl groups boosts MB release by forming the repulsive electrostatic force and through rapid membrane deswelling.

The values of parameter B can be also interpreted in correlation with time lag or delay in MB release from the membranes. Delay in MB release can be described using the value of the time lag parameter t_{lag} that corresponds to the intersection of the linear fit with the horizontal axis representing the square root of time t. As the values of parameter B revolved around zero for all MB release experiments performed at pH = 3, the same holds for t_{lag} indicating that there is practically no delay in MB release at pH = 3. Possible slightly negative values of t_{lag} at pH = 3 can be explained by the faster initial release compared to the release kinetics predicted by the diffusion model. Such deviation is presumably a consequence of rapid initial desorption of MB from the membrane surface. The values of t_{lag} were also similar for all MB release experiments carried out at pH = 8, but the finite delay in MB release was evident. The value of t_{lag} for experiments conducted at pH = 8 was on average about 0.12 h. All calculated values of t_{lag} are listed in **Table 5.1**. The interpretation in the context of time lag suggests that the delay in MB release mainly depends on pH as the experimental parameter dictating the state of charge in fixed carboxyl groups of PAA and indirectly their electrostatic interactions with MB cations.

Table 5.1. Values of D_a, B, and t_{lag} with their corresponding SDs (N = 2) and coefficients of determination (R^2) calculated on the basis of passive *in vitro* MB release experiments carried out under different pH and for different values of molar ratio $n(MB^+)/n(\text{-COOH})$.

pH	$n(MB^+)/n(\text{-COOH})$	D_a ± SD (× 10^{-12} $m^2 \cdot s^{-1}$)	B ± SD	t_{lag} ± SD (h)	R^2
3	0.5	1.852 ± 0.049	-0.013 ± 0.011	$(1.133 \pm 1.419) \times 10^{-4}$	1.000
	1	2.764 ± 0.607	-0.017 ± 0.026	$(1.786 \pm 2.546) \times 10^{-4}$	0.995
	1.5	3.492 ± 0.906	0.085 ± 0.060	$(-2.854 \pm 3.455) \times 10^{-3}$	0.966
8	0.5	1.870 ± 0.668	-0.368 ± 0.094	0.104 ± 0.016	0.999
	1	1.003 ± 0.607	-0.333 ± 0.061	0.141 ± 0.033	0.996
	1.5	0.384 ± 0.016	-0.196 ± 0.022	0.111 ± 0.020	0.996

D_a increased with the rise in molar ratio $n(MB^+)/n(\text{-COOH})$ at pH = 3. We associated this trend with the increase in accumulated charge comprising mainly MB cations which aid the release of MB by forming repulsive electrostatic force. The values of D_a obtained for passive *in vitro* MB release at pH = 3 were overall greater than at pH = 8. We correlated such a more general trend with the trapped water containing dissolved MB arising as a result of membrane deswelling. We presumed that a certain amount of water containing dissolved MB can become entrapped within the porous hydrophobic polymer matrix outside of the hydrogel upon the deswelling of the membrane. The diffusive transport of MB in the aqueous phase outside the hydrogel phase could potentially proceed at a faster rate than within the hydrogel and contribute to the effectively greater D_a values. One can also interpret the influence of molar ratio $n(MB^+)/n(\text{-COOH})$ on D_a in the MB release experiments carried out at pH = 8 using the analysis of mean pore size of composite PES/PAA membranes. We shall discuss this matter in section **6.6 Passive *in vitro* release of MB from composite PES/PAA membranes and DL-PLCL/PAA implants** by exploiting the results of theoretical estimation described in section **5.1 Theoretical estimation of pore size in composite hydrogels**.

MB release kinetics at pH = 3 exhibited pseudo-Fickian behavior. The release kinetics of MB at pH = 8 was overall non-Fickian but still exhibited Fickian behavior during the initial stage. We also observed more pronounced deviations from the Fickian behavior in the kinetics of MB release from composite PES/PAA membrane (12PES-5.3AA-5TMPTA) samples loaded in solutions with the molar ratios $n(MB^+)/n(\text{-COOH})$ of 1 and 1.5.

Characteristic dynamics of passive *in vitro* release of MB from composite PES/PAA membranes mainly depends on the interplay of three parameters: pH, molar ratio n(MB$^+$)/n(-COOH), and membrane thickness. Therefore, we shall explain here the influence of these parameters on the MB release kinetics in more detail.

PAA with the typical pK_a = 4.5 [163] behaves as a polyelectrolyte in aqueous solutions and exhibits pH-dependent behavior. The state of charge in fixed carboxyl groups of the PAA chain is the major driver for the pH-dependent changes in the properties of PAA hydrogel. At pH = 8, carboxyl groups are negatively charged, and conversely, at pH = 3, they are mostly protonated.

The pH-sensitivity of the PAA-rich phase of the composite PES/PAA membranes is evident from the equilibrium MSD achieved in solutions of different pH (refer to **Figure 4.13**). Initial MSD of composite PES/PAA membrane after loading with MB in the loading solution strongly depended on the molar ratio n(MB$^+$)/n(-COOH). After the same loading time of 24 h, increased molar ratio n(MB$^+$)/n(-COOH) enhanced the loading efficiency and reduced the MSD through the introduction of stabilizing electrostatic interactions as evidenced by our experiments (refer to **Figure 4.14**). Hence, depending on the molar ratio n(MB$^+$)/n(-COOH) and pH of the buffer solution in the release experiment, the membrane sample can survive different swelling transients during MB release that directly affect the release kinetics. Sufficiently rapid swelling transients may lead to the sudden release of MB from the membrane into the surrounding medium. We even visually confirmed an effect resembling MB burst release that occurred during several seconds at the beginning of MB release experiments carried out in buffer solutions at pH = 3. While quite a rapid swelling transient can occur as a consequence of a sudden change in pH of the medium, swelling degree changes caused mainly by the decrease in MB content within the composite PES/PAA membrane should be more gradual. We can thus explain the deviations from the Fickian behavior of the MB release kinetics for membrane samples with higher initial MB loading at pH = 8 through the relaxation of the PAA hydrogel chains. During the initial release stage, electrostatic interactions with abundant bound MB cations reduced the mobility of hydrogel chains, and thus the swelling also remained limited. After the initial release stage, the decreased content of electrostatically bound MB cations enabled the relaxation of hydrogel chains and MSD increased. Such changes in the configuration of hydrogel chains improved the rate of MB release. At pH = 3, deswelling caused by protonation of carboxyl groups remained a dominant factor even for membrane samples with the highest MB loading. Hence, the effect of possible hydrogel chain relaxation does not have a significant influence on the release kinetics of MB at pH = 3.

To understand the influence of composite PES/PAA membrane thickness on the MB release kinetics, we must first try to explain the mechanism of passive *in vitro* release of MB. The release of MB from composite PES/PAA membranes is a complex process involving several key steps. The release starts with the diffusion of buffer cations from the medium to the membrane interior. This process initiates the reaction of the cation exchange. After the completion of ion exchange, MB cations start diffusing through the membrane towards the surrounding medium. To enter the solution bulk and finalize the release, MB cations must also overcome the boundary layer resistance. Most of the steps introduce finite lag times which should be considered when analyzing MB release kinetics. Therefore, typical models of passive solute release from hydrogels that assume perfect sink conditions fail to provide an adequate description of MB release. We combined the analytical model of diffusion from thin films [207] with the empirical Weber-Morris model [208] to form the suitable intramembrane diffusion (IMD) model. The IMD model clearly indicates a strong dependence of the release kinetics on membrane thickness (**Equation (5.12)**). Manual laboratory-scale fabrication can lead to the casting speed variations and occasional irregularities at the membrane surface. Casting speed significantly affects the overall membrane sample thickness. In addition, surface irregularities may contribute to the local thickness variations within the membrane sample especially when coupled with swelling transients. Influence of membrane thickness variability should be more obvious at greater pH values which favor continuous swelling of membrane samples during MB release (pH = 8 in our case), and less significant at low pH values when fast and pronounced deswelling takes place (pH = 3 in our case). Our experiments corroborated this assumption. Deviations in MB release kinetics were much greater for experiments conducted at pH = 8 in comparison with the experiments conducted at pH = 3. Differences in mean thickness of membrane samples of up to about 25% (as in the worst case shown in **Figure 4.23b**) can completely explain the observed deviations by exploiting the IMD model.

5.3 Modeling of active *in vitro* release of MB from composite PES/PAA membranes via iontophoresis

We analyzed the iontophoretic *in vitro* release kinetics of MB from composite PES/PAA membranes by adopting a similar modeling approach as for passive *in vitro* release with some modifications dictated by the experimental setup and the design of iontophoretic release experiments in our pilot study.

Figure 5.4 illustrates the fitting of the representative release profile during an iontophoretic release experiment using the dependence similar to the Weber-Morris equation (for details refer to the description of **Equation (5.11)**) to indicate distinct segments of Fickian behavior in a different context. The first segment (modeled by the orange dotted line) indicates the passive MB release before the application of electric current, while the second segment (modeled by the red dotted line) indicates the iontophoretic release of MB. The MB release rate increased immediately after the electric current was turned on, as indicated by the change in slope shown in **Figure 5.4b**. Such a change in the MB release rate presumably implied the effective increase in D_a as the membrane remained in an approximately fixed position. A possible alternative to the increase in D_a is the significant membrane thickness reduction that is not likely since the additional swelling of PAA hydrogel is expected when the electric current is applied (as discussed later in section **6.7 Active *in vitro* release of MB from composite PES/PAA membranes via iontophoresis**).

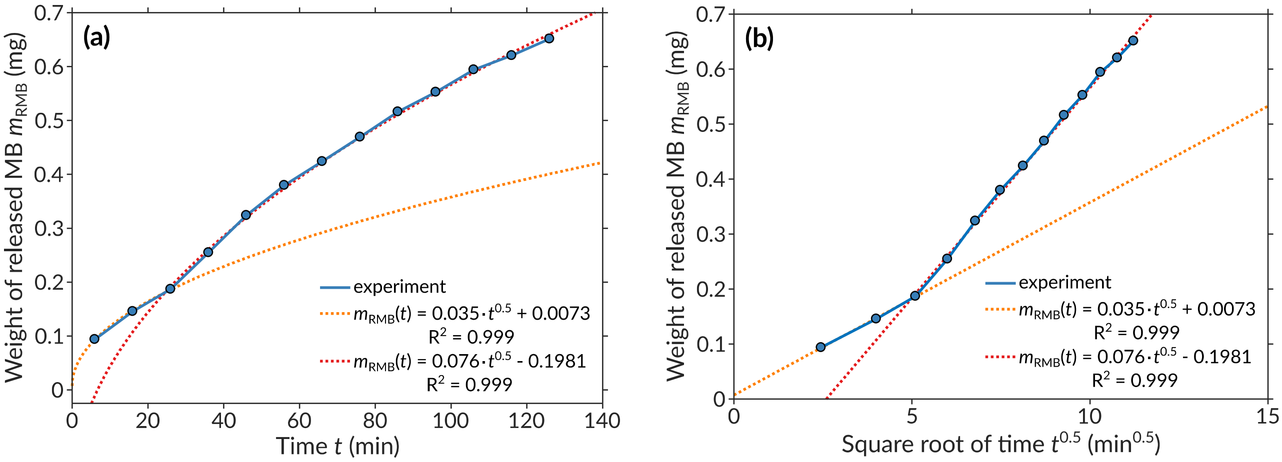

Figure 5.4. Representative profile of *in vitro* iontophoretic MB release in PBS (pH = 7.4 and I = 0.154 M) at 37 °C. Dotted lines designate fits corresponding to the passive (marked in orange) and iontophoretic (marked in red) release segments of the profile. Fitting results indicate Fickian behavior and the increase in MB release rate when the electric current is turned on.

Figures 5.5 and **5.6** illustrate the fitting of the MB release kinetics for the continuous and pulse regime of iontophoresis using the adapted form of the Weber-Morris equation. We utilized the slightly modified form of **Equation (5.11)** that is given by:

$$\frac{Q_t}{Q_{\mathrm{ie}}} = At^{0.5} + B \tag{5.13}$$

where Q_{ie} was used for normalization. Iontophoretic release behavior was almost the same for both regimes (as indicated by the values of parameters A and B that differ by only 0.42% and 1.65%, respectively). The release of MB clearly remained diffusion-controlled and its rate was almost independent of the applied electric current regime indicating the inability of the membrane release behavior to follow the changes in electric excitation. In a similar manner, as described in section **5.2 Modeling of passive *in vitro* release of MB from composite PES/PAA membranes**, the value of A can be interpreted as a measure of release rate, while the value of B can be interpreted as the measure of boundary layer resistance or time lag corresponding to MB release. Although the difference in the amount of released MB between two regimes is not statistically significant, the average amount of released MB is slightly higher in the continuous regime implying a trend that should be further investigated.

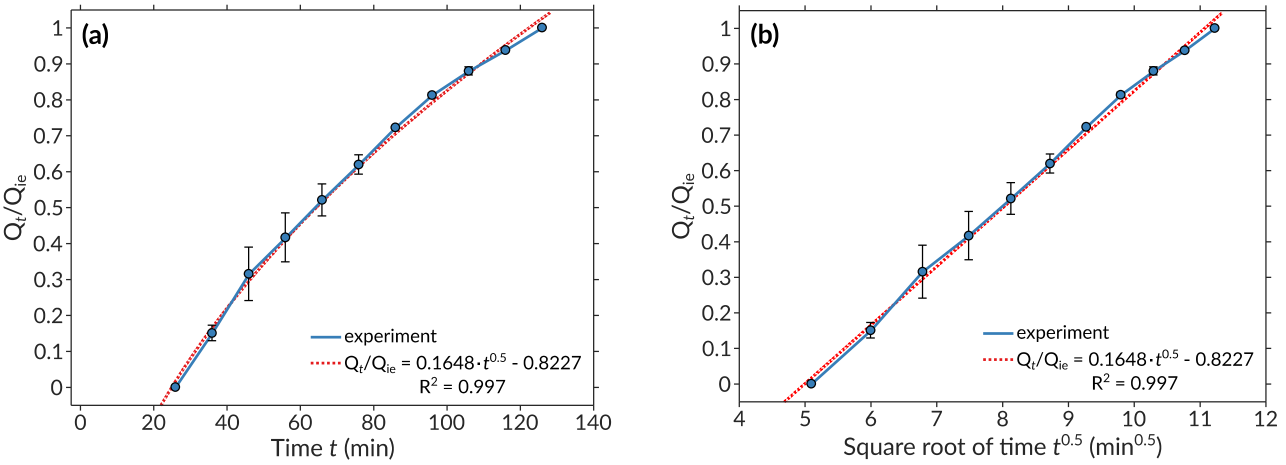

Figure 5.5. *In vitro* iontophoretic release kinetics of MB in PBS (pH = 7.4 and *I* = 0.154 M) at 37 °C under the continuous iontophoresis regime (*i* = 0.2 mA) (N = 2): (a) fitting of the release profile using **Equation (5.13)** (b) fitting of the release profile using **Equation (5.13)** plotted against the square root of time to emphasize Fickian release behavior. Dotted red lines designate the fits.

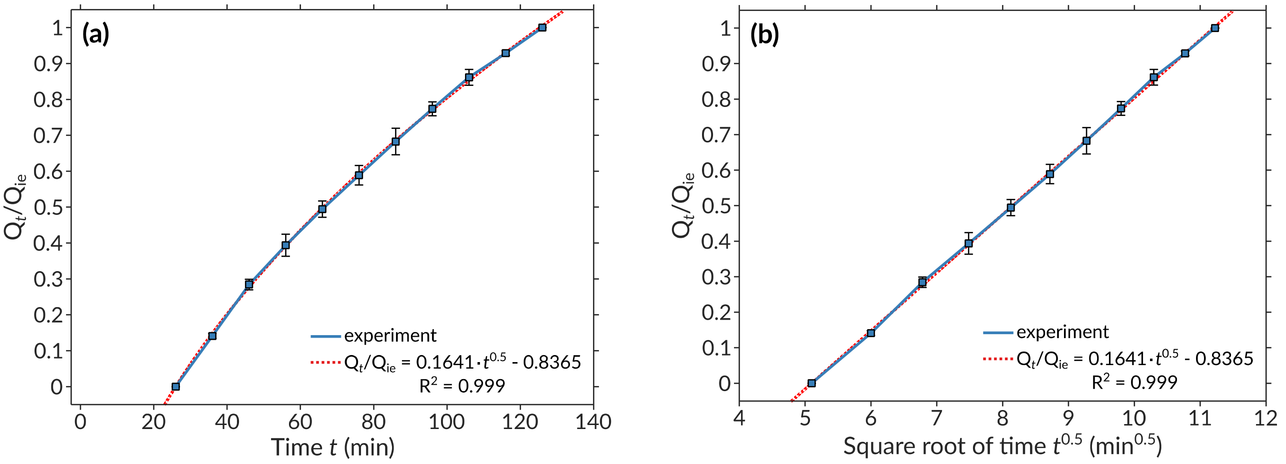

Figure 5.6. *In vitro* iontophoretic release kinetics of MB in PBS (pH = 7.4 and *I* = 0.154 M) at 37 °C under the pulse iontophoresis regime (rectangular current pulses, *i* = 0.2 mA, *f* = 1 kHz, *DC* = 50%) (N = 2): (a) fitting of the release profile using **Equation (5.13)** (b) fitting of the release profile using **Equation (5.13)** plotted against the square root of time to emphasize Fickian release behavior. Dotted red lines designate the fits.

As the release kinetics was Fickian during the iontophoretic release of MB, it should be characterized using the corresponding value of D_a. Due to experimental limitations, this value was harder to determine compared to the D_a values for passive release experiments. Therefore, we adopted some assumptions and performed empirical estimations to calculate the value of D_a.

Assuming that the effective diffusion of MB mainly occurred through the membrane surface in contact with the receptor solution during iontophoresis, we calculated the value of D_a according to the modified **Equation (5.12)** (for calculation details refer to the section **5.2 Modeling of passive *in vitro* release of MB from composite PES/PAA membranes**):

$$\frac{Q_t}{Q_\mathrm{e}} = \left(\frac{D_\mathrm{a} t}{\pi l^2}\right)^{0.5} + B \tag{5.14}$$

We determined the value of half of the membrane thickness *l* before conducting each of the iontophoresis experiments based on the wet membrane sample weight, mean MSD, measured sample area, and estimated average density of the composite PES/PAA membrane.

To calculate the D_a using **Equation (5.14)** we also needed to estimate the equilibrium amount of released MB at the end of the iontophoresis experiment. We provide a detailed explanation of this estimation in **Appendix C: Estimation of the maximum MB amount that can be released via iontophoresis**. In brief, we estimated the total amount of MB to be released by extrapolating the data corresponding to the passive *in vitro* release from composite PES/PAA membranes (at pH = 8 and $I = 0.2$ M) for different initial MB loadings. Under the assumption that the entire amount of initially electrostatically bound MB will be released in the end, we extrapolated the data on the fraction of electrostatically bound MB in the composite PES/PAA membranes at lower MB loadings by fitting a power law. We employed the extrapolated fraction of 88.4% together with the mean loading efficiency of 95.9% to predict the total amount of MB released in equilibrium.

The obtained value of D_a for the iontophoretic delivery in continuous regime was $(7.11 \pm 4.95) \times 10^{-15}$ $\mathrm{m^2 \cdot s^{-1}}$, while the D_a for the iontophoretic delivery in pulse regime was $(5.46 \pm 3.18) \times 10^{-15}$ $\mathrm{m^2 \cdot s^{-1}}$. We ascribed the high variability of D_a to the differences in average composite PES/PAA membrane thickness (using similar reasoning as the one described in section **5.2 Modeling of passive *in vitro* release of MB from composite PES/PAA membranes**) and to the possible slight membrane bending or deformation during iontophoresis. As in the case of the amount of released MB, the difference in D_a between two regimes is not statistically significant, but the average D_a remains slightly higher in the continuous regime implying a trend that warrants further investigation. The values of D_a were lower than the values obtained for passive *in vitro* release of MB from composite PES/PAA membranes and DL-PLCL/PAA implants as a consequence of different experimental conditions.

We shall discuss the effects of electrical excitation during iontophoresis on the release of MB in more detail within section **6.7 Active *in vitro* release of MB from composite PES/PAA membranes via iontophoresis**.

5.4 Modeling of passive *in vitro* release of MB from composite DL-PLCL/PAA implants (II)

Composite DL-PLCL/PAA implants described in this dissertation contain PAA hydrogel-rich regions dispersed throughout the hydrophobic polymer matrix. The distribution of PAA-rich aggregates is quite uniform within the implant bulk, while a reduced amount of PAA-rich aggregates is present near the implant surface. PAA hydrogel serves as the main storage material for dissolved cations of MB which are exchanged with PBS cations during the loading process. Passive release of MB is also initiated by ion exchange with surrounding PBS cations, but the process of release is mainly diffusion-controlled similarly as for composite PES/PAA membranes. Regions near the implant surface with lower PAA content serve as the effective diffusion barrier that determines the kinetics of MB release.

5.4.1 Drug release from monolithic cylindrical reservoirs via diffusion (II)

Composite DL-PLCL/PAA implant can be regarded as a homogeneous drug reservoir described by apparent parameters with respect to the surrounding medium that serves as the receptor solution. After MB loading, such a presumably monolithic reservoir is expected to contain uniformly distributed dissolved molecules of the MB model drug. Hence, the concentration gradient of MB between the drug reservoir and the surrounding medium drives drug release by diffusion. The rate of drug release via diffusion from monolithic drug reservoirs is affected by reservoir geometry [210]. Kinetics of diffusion-controlled drug release for the monolithic cylindrical reservoir is given by the complex analytical expression [211]:

$$\begin{aligned} \frac{M_t}{M_\infty} &= 1 - \frac{32}{\pi^2} \sum_{n=1}^{\infty} \frac{1}{q_n^2} \exp\left(-\frac{q_n^2}{R^2} D_\mathrm{a} t\right) \\ &\times \sum_{p=0}^{\infty} \frac{1}{(2p+1)^2} \exp\left(-\frac{(2p+1)^2 \pi^2}{H^2} D_\mathrm{a} t\right) \end{aligned} \tag{5.15}$$

where M_t is the cumulative amount of released drug after time t, M_∞ is the cumulative amount of released drug in equilibrium (*i.e.* after an infinite period of time in theory), R is the radius of the cylinder, H is the height of the cylinder, and D_a represents the apparent diffusion coefficient. In **Equation (5.15)**, the dummy variables for summation are designated as n and p, while the roots of the Bessel function of the first kind and zero order are designated as q_n ($J_0(q_n) = 0$). The expression on the right-hand side of **Equation (5.15)** is characterized by slow convergence for small times and a large number of series terms must be included for its accurate numerical evaluation. This expression can be approximately evaluated for small times using the expansion [212]:

$$\frac{M_t}{M_\infty} = \left(\frac{D_\mathrm{a}t}{L^2}\right)^{0.5}\left[\frac{2}{\pi^{0.5}} + \frac{4}{\pi^{0.5}}\left(\frac{L}{R}\right)\right] - \frac{D_\mathrm{a}t}{L^2}\left[\frac{8}{\pi}\left(\frac{L}{R}\right) + \left(\frac{L}{R}\right)^2\right] + \left(\frac{D_\mathrm{a}t}{L^2}\right)^{1.5}\left[\frac{2}{\pi^{0.5}}\left(\frac{L}{R}\right)^2 - \frac{1}{6\pi^{0.5}}\left(\frac{L}{R}\right)^3\right] + \left(\frac{D_\mathrm{a}t}{L^2}\right)^2\left[\frac{1}{3\pi}\left(\frac{L}{R}\right)^3 - \frac{1}{8}\left(\frac{L}{R}\right)^4\right] + \cdots \tag{5.16}$$

where $L = H/2$. When the ratio L/R is small (as in the case of disk-shaped reservoirs) the first four terms of the expansion can be used as a sufficiently accurate approximation. For $L/R = 0$, expansion becomes a single term equivalent to the approximation for small times in the case of plane sheet reservoirs (as used in section **5.2 Modeling of passive *in vitro* release of MB from composite PES/PAA membranes**). Numerical evaluation of the truncated expansion is computationally a significantly less demanding task which is easy to implement. We shall use the first four terms on the right-hand side of **Equation (5.16)** to calculate the value of D_a in the next section.

5.4.2 Determination of D_a for the composite DL-PLCL/PAA implants (II)

The most important parameter which determines the drug release kinetics from composite DL-PLCL/PAA implants is D_a. We used the experimental data from MB release experiments to evaluate D_a via nonlinear regression. The regression model we applied is given by the following expression (based on **Equation (5.16)**):

$$\frac{M_t}{M_\infty} = \left(\frac{D_\mathrm{a}t}{L^2}\right)^{0.5}\left[\frac{2}{\pi^{0.5}} + \frac{4}{\pi^{0.5}}\left(\frac{L}{R}\right)\right] - \frac{D_\mathrm{a}t}{L^2}\left[\frac{8}{\pi}\left(\frac{L}{R}\right) + \left(\frac{L}{R}\right)^2\right] + \left(\frac{D_\mathrm{a}t}{L^2}\right)^{1.5}\left[\frac{2}{\pi^{0.5}}\left(\frac{L}{R}\right)^2 - \frac{1}{6\pi^{0.5}}\left(\frac{L}{R}\right)^3\right] + \left(\frac{D_\mathrm{a}t}{L^2}\right)^2\left[\frac{1}{3\pi}\left(\frac{L}{R}\right)^3 - \frac{1}{8}\left(\frac{L}{R}\right)^4\right] + b \tag{5.17}$$

where b is the added ordinate intercept accounting for the barrier to diffusion interpreted in a similar manner as B in **Equation (5.11)**. We employed this model to fit the release kinetics in the region of the first six experimental time points.

We performed the nonlinear regression by minimizing the sum of squared errors (SSE) using the simplified form of the gradient descent optimization algorithm with two variable parameters:

- D_a (assumed to be constant) and
- constant ordinate intercept b (to describe imperfect sink conditions).

In our algorithm, we independently varied one of the parameters during each iteration for a fixed small step in the direction which reduced the SSE up to the point of reaching a steady minimum value of SSE.

Using the initial weights of wet implants loaded with MB and measurements by a liner we determined the average values of $L = 0.629$ mm and $R = 6.5$ mm. Variable parameters had the initial values $D_\mathrm{a} = 2.815 \times 10^{-13}\ \mathrm{m^2 \cdot s^{-1}}$ and $b = 0$. We extracted the initial value of D_a from the slope of linear fit displayed in **Figure 5.7** assuming the very thin disk implant geometry ($L \ll R$) which allows the use of approximation for plane sheet reservoirs. We assigned the initial value of $b = 0$ assuming no additional barriers to diffusion.

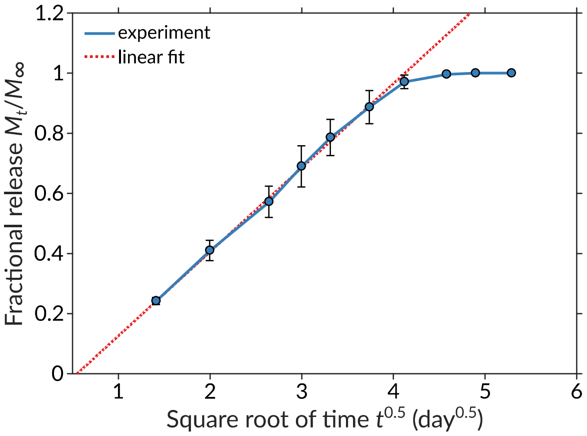

Figure 5.7. Kinetics of MB release in PBS (pH = 7.4 and I = 0.154 M) at 37 °C from composite DL-PLCL/PAA implants shown as the fractional amount of released MB versus square root of time (solid blue line) (N = 3). Linear fit (dotted red line) indicates the diffusion-controlled kinetics.

Using the MATLAB programming package we implemented the algorithm in the form of a script (**Appendix D: Script for the determination of D_a for the composite DL-PLCL/PAA implants**). The algorithm converged successfully to yield the output values $D_a = 3.54 \times 10^{-13}$ m$^2\cdot$s^{-1} and $b = -0.259$ (adjusted coefficient of determination R^2 = 0.9971). **Figure 5.8** depicts the comparison between the regression model and the experimental data.

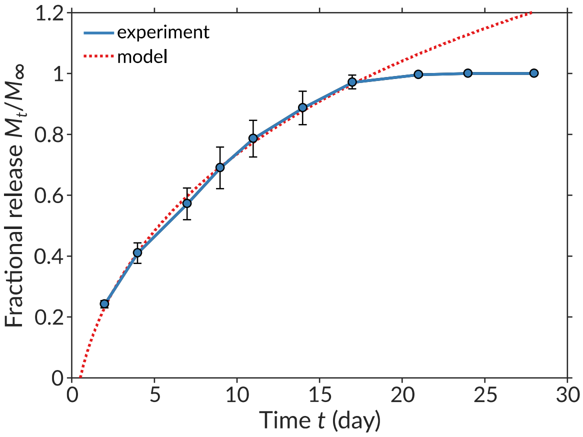

Figure 5.8. Measured kinetics of MB release in PBS (pH = 7.4 and I = 0.154 M) at 37 °C from composite DL-PLCL/PAA implants (solid blue line) and MB release kinetics predicted by the model of solute release via diffusion from monolithic cylinders (dotted red line) (N = 3). Values of parameters extracted from the applied model via nonlinear regression are D_a = 3.54 × 10^{-13} m$^2\cdot$s^{-1} and b = -0.2587. Displayed error bars correspond to the ±3SD.

We also illustrate the convergence curve of the algorithm in **Figure 5.9**.

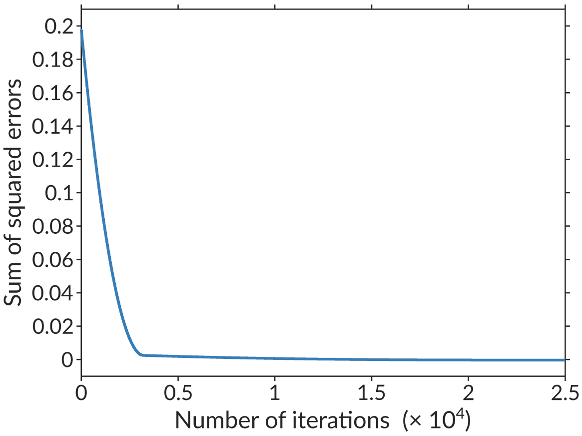

Figure 5.9. Convergence curve of the simplified gradient descent algorithm used to calculate the parameters D_a and b of the composite DL-PLCL/PAA implants.

Release kinetics of MB clearly indicated Fickian behavior that extended to long times (to about 97% of fractional release). The release of MB was obviously diffusion-controlled and the described regression model successfully predicts the amount of released MB during the first 17 days of the experiment. The model relies on the assumption that the implant effectively behaves as a homogeneous disk-shaped drug reservoir relative to the surrounding medium (as elaborated in section **5.4.1 Drug release from monolithic cylindrical reservoirs via diffusion**). Using the model we calculated the value of D_a for the composite DL-PLCL/PAA implants to be 3.54×10^{-13} $m^2 \cdot s^{-1}$. As we can conclude from **Figure 5.8** and confirm by the calculated value of b, the model predicts a negative intercept for the release curve which may indicate the presence of boundary layer resistance to diffusion (similar to the case of MB release from composite PES/PAA membranes at pH = 8).

The value of D_a and characteristic release kinetics for composite DL-PLCL/PAA implants mainly stem from the implant microstructure and porosity of the hydrogel phase as we shall discuss in section **6.6 Passive *in vitro* release of MB from composite PES/PAA membranes and DL-PLCL/PAA implants**.

Chapter 6: Discussion

6.1 Characterization of composite hydrogel materials (I-III)

FTIR-ATR analysis of composite hydrogels revealed bands characteristic for PAA and the corresponding hydrophobic polymer matrix (PES, DL-PLCL, or PLGA). Bands typical of different PAA structures can be found in [190]. The bands of widely studied hydrophobic polymer matrices such as PES and PLGA are described in detail in [213] and [214], respectively. FTIR-ATR spectra of the synthesized composite hydrogels did not show significant shifts in the absorption bands compared to the spectra of pure components (cross-linked PAA hydrogel and used hydrophobic polymers). Such findings indicated mainly the physical blending of the separated phases without additional chemical bonding. Chemical composition was mostly uniform in all composite hydrogels synthesized using UV irradiation, while G-PLGA-PAAs exhibited a rather inhomogeneous chemical composition. According to the FTIR-ATR spectra, all cross-linked PAA hydrogels obtained using UV irradiation and TMPTA as a CL showed mutually similar and less branched structure, while cross-linked PAA hydrogels within G-PLGA-PAAs seemed to exhibit a more branched structure. We also showed that the hydrophilic nature of the TMPTA CL was crucial for obtaining composite PES/PAA membranes of uniform chemical composition over the membrane cross-sections.

All composite hydrogels synthesized in this dissertation exhibited heterogeneous microstructure comprising distinct hydrogel-rich and hydrophobic polymer-rich regions. SEM analysis of the composite hydrogels revealed the microstructure comprising PAA-rich particles supported by the surrounding matrix dominantly composed of the hydrophobic polymer. In composite PES/PAA membranes and DL-PLCL/PAA implants, the average size of the PAA-rich particles in the dry state was similar and smaller than average particle size in composite PLGA/PAA implants. We shall discuss the impact of microstructural properties on the relevant behaviors and other parameters of composite hydrogels separately in appropriate sections. Here, we shall summarize some more general findings and observations.

In section **4.2.4 Mechanisms of microstructure formation**, we proposed qualitative mechanisms of microstructure formation based on our findings and available data. It is important to note that the process of microstructure formation in composite hydrogels during the synthesis is highly complex and difficult to model or monitor *in situ* using experimental techniques. In fact, even the theoretical description of the phase inversion process in simpler membrane forming polymeric solutions known as ternary systems (nonsolvent/solvent/polymer) remains the subject of ongoing research [215]–[217]. Boom et al. made notable attempts to study thermodynamics and kinetics of liquid-liquid phase separation in quaternary membrane-forming systems comprising two polymers [218]–[220]. Using the model system PES/poly(vinylpyrrolidone)/NMP/water they found that at longer time scales PES forms a porous membrane and the hydrophilic polymeric additive fills the pores [218]. Our synthesis process includes the irradiation step before immersion precipitation and involves the PAA hydrogel formation. Consideration of these aspects further increases the complexity of required calculations and the theoretical description of such systems should be the subject of further research. However, we can extract some useful qualitative information from our experimental observations that can serve as guidelines for future experiments.

The process of phase separation starts already during the irradiation phase of the synthesis process as a consequence of AA cross-linking. Regions of cross-linked PAA in such case already serve as an initial template for the phase separation and solidification within the aqueous bath in the next step. After immersion in the aqueous bath, liquid-liquid demixing occurs. During this process, the hydrophobic matrix solidifies while the PAA hydrogel simultaneously forms by rapidly absorbing water. As explained by Wienk et al. in [221], phase separation of membrane-forming ternary systems in the metastable region occurs via nucleation and growth of the polymer-lean phase within the continuous polymer-rich phase which solidifies. The outcome of such phase separation is a porous membrane. In our composite hydrogels, regions commonly corresponding to the polymer-lean phase are filled by the swollen PAA hydrogel in the wet state. The spatial distribution of PAA hydrogel appears to be qualitatively similar to the distribution of hydrophilic polymeric additive in the quaternary model system studied by Boom et al. [218]. During solidification in the aqueous bath, hydrophobic polymer matrix reaches a certain level of rigidity which defines the final morphology visualized in the dry state. Our analysis suggests that the porosity of the hydrophobic polymer matrix in the obtained composite hydrogel correlates with the T_g of the hydrophobic polymer used for the synthesis. As the entire synthesis process takes place at ambient temperature, the polymers with lower T_g (such as DL-PLCL) exhibit different behavior compared to the polymers with T_g above the ambient temperature (such as PLGA and PES). After solidification, DL-PLCL within the composite DL-PLCL/PAA implants remains in its rubbery state with increased chain mobility. Conversely, PES and PLGA reach the glassy state after solidification, which results in a porous rigid matrix structure. Hence, the mobile chains of DL-PLCL are able to follow the swelling dynamics of PAA hydrogel, while the PES and PLGA matrices retain fixed morphology obtained during the synthesis. Such an explanation is in good agreement with the microstructure observed in the SEM images of composite hydrogels in the dry state (refer to **Figures 4.8**-**4.10**).

DSC analysis of the composite PLGA/PAA implants showed that synthesis using UV irradiation led to the increase in T_g of PLGA in the composite PLGA/PAA implants, while the use of gamma irradiation during the synthesis reduced the T_g in a dose-dependent manner mainly through the process of chain scission. As the absorbed dose of gamma irradiation can be adjusted in the synthesis process, this parameter can be used to modulate the mechanical properties and degradation rate of the composite PLGA/PAA implants in the physiological media. As an alternative for future experiments, the gamma-irradiated PLGA matrix can be replaced by a suitable polyphosphoester chemically tailored to exhibit desired degradation behavior as proposed by Bauer et al. [222].

6.2 Swelling behavior of composite hydrogels (I-III)

The swelling behavior of different synthesized composite hydrogels can be intercompared in terms of equilibrium MSD and swelling kinetics (only for composite hydrogel implants).

All composite hydrogels synthesized by using UV irradiation exhibited similar MSDs in a mildly alkaline environment similar to the physiological pH that were independent of composite geometry and hydrophobic polymer matrix. The MSD of composite PES/PAA membranes was less reproducible compared to the swelling degree of disk-shaped implants due to the highly porous PES-rich support and thickness inhomogeneities arising from the synthesis process. The composite PES/PAA membranes exhibited MB loading-dependent equilibrium MSD. Obtained composite PES/PAA membranes also clearly showed pH-dependent MSD in equilibrium, while the MSDs of synthesized composite hydrogel implants were not tested in acidic media to avoid the rapid degradation of the hydrophobic polymer matrix.

G-PLGA-PAAs exhibited higher equilibrium MSDs compared to other composite hydrogels as a consequence of differences in microstructure and hydrophilicity. In comparison with the other composite hydrogels, the microstructure was more inhomogeneous with greater pore size. PAA hydrogels cross-linked using gamma irradiation may have a more branched network that increases hydrophilicity, while the hydrophilicity of PLGA could also be increased through the interaction with gamma irradiation.

All values of equilibrium MSDs for composite hydrogels were significantly lower than almost all values for different cross-linked PAA hydrogels that can be found in the literature [164], [223]. Mechanical support provided by different hydrophobic polymers efficiently reduced and stabilized the MSDs of the composite hydrogels. The value of MSD can be also controlled by the fraction of hydrophobic polymer within the initial solution used for the synthesis as evidenced by the MSDs of composite PES/PAA membranes in distilled water (refer to the **Figure 4.12**).

We investigated the swelling kinetics of disk-shaped composite DL-PLCL/PAA and PLGA/PAA implants after one cycle of air-drying at ambient temperature. The swelling kinetics was much faster for composite DL-PLCL/PAA implants in comparison with the swelling kinetics of UV-PLGA-PAA and

G-PLGA-PAAs, and the MSD stabilized within minutes. Such rapid swelling kinetics is comparable with the swelling kinetics of superporous hydrogels (SPHs). To the best of our knowledge, a similar rate of swelling was not previously reported for other material classes except for SPHs [224]. It is important to note that SPHs are hydrophilic polymeric networks comprising numerous interconnected microscopic pores that enable intense capillary action and rapid absorption of large water amounts [225]. The microstructure of composite DL-PLCL/PAA implants was fundamentally different and exhibited practically no porosity. Hence, a more detailed analysis of the swelling mechanism may be an interesting area for further research using techniques such as super-resolution microscopy. We presumed that the swelling kinetics of composite DL-PLCL/PAA implants was faster compared to the swelling kinetics of all composite PLGA/PAA implants due to the reduced disk thickness, smaller size of PAA-rich particles, and the dense packing of PAA-rich particles within the hydrophobic matrix in the dry state.

Composite PLGA/PAA implants were not capable of reversible swelling after air-drying due to the porous PLGA support. UV-PLGA-PAA and G-PLGA-PAAs may have suffered from pore collapse during drying, while such an effect was more evident in G-PLGA-PAAs with quite nonuniform structure. During reswelling, the swelling rate was spatially inhomogeneous in G-PLGA-PAAs which was reflected by disk bending especially in the initial stage of the process. Conversely, composite DL-PLCL/PAA implants were capable of reversible swelling with minimal changes in the equilibrium MSD. During the process of reswelling, composite DL-PLCL/PAA implants continuously retained their initial geometry. Such findings indicated that the absence of porosity in our composite hydrogels was beneficial for mechanical stability during drying and reswelling. Therefore, composite DL-PLCL/PAA implants can be stored in the dry state after loading the drug. Their use at the point of care would then only require quick rehydration for several minutes which is especially convenient in the clinical setting. Our findings also showed that the absence of porosity led to the initial lag in swelling until the medium penetrated into the bulk of the composite hydrogel, while the lag was not observed when the hydrophobic polymeric matrix was porous allowing for easier medium penetration in the dry state.

Our synthesized composite hydrogels exhibited much faster and commonly qualitatively different swelling kinetics in comparison with data reported in the literature for bulk PAA hydrogels [226]. The main reasons for such differences in swelling behavior were the significantly smaller size of the PAA-rich hydrogel (practically to the level of microgel particles) and mechanical barrier formed by the hydrophobic polymer matrix. PAA-rich submicron-sized particles in the dry state swell more rapidly than the bulk sample of PAA hydrogel due to enhanced medium penetration. The hydrophobic polymer matrix introduces an early plateau in the swelling kinetics by exerting the additional elastic force acting in opposition to the osmotic force driving the swelling. The swelling stops when the osmotic and elastic forces are balanced and the composite hydrogel reaches the swelling equilibrium [227].

As we illustrated here, the hydrophobic polymer matrix can effectively limit the swelling of PAA within the composite hydrogel materials and improve the overall mechanical stability. Owing to the specific composition and microstructure, our synthesized composite hydrogels showed relatively fast swelling kinetics.

6.3 IEC analysis of composite hydrogels (I-III)

IEC of synthesized composite hydrogels mainly depended on the composition of the initial solution used for the synthesis and the applied synthesis method. Synthesized composite PES/PAA membranes had IECs above 4.4 $\mathrm{mmol \cdot g^{-1}}$ of dry weight, while the IECs of all disk-shaped composite hydrogel implants were about 2 $\mathrm{mmol \cdot g^{-1}}$ of dry weight. Formulation of the initial solution for composite hydrogel implant synthesis had higher amounts of the hydrophobic polymer and a greater amount of the CL relative to the MM to obtain adequate mechanical properties. Hence, the amount of the MM had to be reduced in the initial solution, which resulted in the expected overall lower IECs.

We easily obtained the RY of above 80% for the synthesis of composite PES/PAA membranes using TMPTA as a CL, while it did not decrease below 70% for the synthesis with MBAA as a CL (**Figure 4.19**). On the other hand, RY for the synthesis of disk-shaped composite hydrogel implants was always lower and revolved around the average of 60% in all cases (**Figure 4.21**). Our experimental findings indicated that such lower values of RY were not caused by the differences in the thickness of the irradiated solution layer, irradiation type, or hydrophobic polymer. We presumed that the reduced RY may mainly be a consequence of the residual oxygen dissolved in the initial solution for the synthesis of composite hydrogel implants. It is well known that oxygen can act as a temporary or permanent inhibitor in radical polymerization reactions [228]. We significantly decreased the effect of oxygen presence during the synthesis of composite PES/PAA membranes by nitrogen purging.

IECs of all synthesized composite PES/PAA membranes were higher than IECs of previously reported mechanically stable weakly acidic cation-exchange membranes (1 mmol·g^{-1} [117] and 3.7 mmol·g^{-1} [118]). We note that pore-filled membranes at the highest mass gain were reported to reach the IEC value of 5 mmol·g^{-1}, but such composite membranes exhibited fragility due to large pressures caused by swelling that are exerted on the matrix of poly(1,1-difluoroethylene) [112].

IECs of all synthesized composite hydrogels are lower but still comparable with the commercially available pharmaceutical-grade weakly acidic cation-exchange materials in the form of resins (AMBERLITE™ IRP64, ~10 mmol·g^{-1} [229]) or fibers (Smopex®-102, 6.4 mmol·g^{-1} [78]). Although the IECs of synthesized composite hydrogels are lower, they still offer the advantage of using a compact material with adjustable properties such as IEC and D_a already during the synthesis stage.

6.4 Electrical properties of composite PES/PAA membranes

Synthesized composite PES/PAA membranes exhibited effective ionic conductivity in the wet state when equilibrated in alkaline media which simulated physiological conditions. The ionic conductivity originates from the presence of PAA hydrogel which behaves as a weak anionic polyelectrolyte. Many PAA-rich microgel particles swelled to form a continuous conductive pathway within a porous PES-rich matrix enabling the flow of electric current.

We can compare the electrical properties of composite PES/PAA membranes with the relevant electrical properties of polyelectrolyte hydrogels, commercial ion-exchange membranes, and electrode gels used for biomedical applications. **Table 6.1** lists the types, thicknesses, and resistances of representative commercially available cation-exchange membranes to facilitate comparison with the data obtained for composite PES/PAA membranes.

Table 6.1. Comparison of electrical properties of our composite PES/PAA membrane (12PES-5.3AA-5TMPTA) and commercially available cation-exchange membranes (based on [182], [230], and references therein).

Membrane	Type	Thickness (µm)	Resistance (Ω·cm^2)
12PES-5.3AA-5TMPTA	heterogeneous	50	2.99[a]
Ionac MC3470	heterogeneous	500–520	5[b]
Ralex CMH-PES	heterogeneous	764	11.33[c]
Qianqiu CEM	heterogeneous	480	≤ 13
Fumasep FKE	homogeneous	34	2.46[c]
Nafion 117	homogeneous	200	1.5[c]
Neosepta CM-1	homogeneous	133	1.67[c]
Neosepta CMX	homogeneous	164	2.68[d]

[a] Measured in PBS (pH = 7.4 and I = 0.154 M) at 22 °C; [b] Measured in 1 M NaCl; [c] Measured in 0.5 M NaCl at 25 °C; [d] Measured in 0.2 M NaCl at 25 °C.

Effective through-membrane ionic conductivity of composite PES/PAA membranes (12PES-5.3AA-5TMPTA) of (0.17 ± 0.04) S·m^{-1} was about one order of magnitude lower than the ionic conductivity of anionic polyelectrolyte hydrogels in PBS solution reported in the literature [63]. The value was also significantly smaller than those determined for free PAA hydrogels synthesized under various conditions [162]. Such results were expected due to the tortuosity in conductive pathways imposed by the porous nonconductive PES matrix.

However, the through-membrane ionic conductivity is comparable with the electrical conductivity of commercially available universal electrode gels and conductive adhesive pastes [231]. The value of membrane resistance is also similar to the values obtained for commercial cation-exchange membranes under comparable experimental conditions (**Table 6.1**).

Although the presence of hydrophobic and nonconductive PES matrix limits through-membrane electrical conductivity, the obtained value remains adequate and comparable with the values of other conductive materials used in electrotherapy. We do not expect any limitations imposed by electrical properties of composite PES/PAA membranes in practical applications where they should act as reservoirs for iontophoretic drug delivery.

6.5 Loading of composite PES/PAA membranes and DL-PLCL/PAA implants (I, II)

Although the optimization of MB loading into composite drug reservoirs was not systematically pursued in this dissertation, we briefly discuss here the properties of composite PES/PAA membranes and composite DL-PLCL/PAA implants in terms of cationic drug loading.

Results regarding the MB loading efficiency for composite PES/PAA membranes indicated an expected dependence on the molar ratio $n(MB^+)/n(\text{-}COOH)$ which practically corresponds to the concentration gradient of MB cations between the surrounding medium and the membrane. Membrane samples absorbed the largest amount of MB cations from the MB loading solution with the highest initial molar ratio $n(MB^+)/n(\text{-}COOH)$ after the same time period of loading (refer to the **Figure 4.22** in the section **4.7.1 Loading of composite PES/PAA membranes**). Hence, it is possible to adjust the MB loading within the membrane by modulating the molar ratio $n(MB^+)/n(\text{-}COOH)$.

Depending on the used cationic drug, it may not be cost-effective to increase the molar ratio $n(MB^+)/n(\text{-}COOH)$ in order to achieve higher loading during a shorter time period. Our results suggested that an increase in the molar ratio $n(MB^+)/n(\text{-}COOH)$ above 1 was not necessarily required to achieve excellent loading efficiencies. Loading of composite PES/PAA membranes for iontophoresis experiments and the loading of composite DL-PLCL/PAA implants during 120 h in the 1 $g \cdot dm^{-3}$ MB solutions adjusted to attain the molar ratio $n(MB^+)/n(\text{-}COOH) = 1$ showed that MB loading efficiencies of around 96% (compared to the theoretical maximum loading efficiency of drug reservoirs as defined in **2.2.11 Loading of composite membranes and implants with MB**) can be reached without using the excessive amount of MB in the loading solution. Loading procedure lasting several days may not be an issue for composite DL-PLCL/PAA implants that may be further stored in the dry state after MB loading. However, such a relatively long loading procedure may not be suitable for composite PES/PAA membranes which need to be stored in the wet state. The loading rate can be improved by different strategies as explained by Jeong and Park [198]. We also note that high loading efficiency is not always required and the loading protocol should be adapted to specific applications.

6.6 Passive *in vitro* release of MB from composite PES/PAA membranes and DL-PLCL/PAA implants (I, II)

The largest amount of loaded MB was electrostatically bound to the composite PES/PAA membranes or composite DL-PLCL/PAA implants and could be efficiently released in buffered alkaline media resembling the typical physiological environment as demonstrated by our *in vitro* release experiments. In all cases, above 85% of the initially loaded MB ends up released during the *in vitro* release experiments in buffered alkaline media. In buffered acidic media, pH-sensitive PAA hydrogel collapses and presumably traps a significant portion of loaded MB thereby preventing its release.

We observed that diffusion is the rate-limiting step that governs the MB release kinetics in synthesized composite PES/PAA membranes and composite DL-PLCL/PAA implants. Consequently, the release of MB from composite hydrogel membranes and implants proceeds at significantly different timescales that are mainly determined by the reservoir geometry and microstructural properties.

The most important parameter of the composite hydrogel defining the passive *in vitro* release kinetics of MB is D_a. As a reference point, the diffusion coefficient of MB in water is $\sim 10^{-10}$ $m^2 \cdot s^{-1}$ [232]. Values of calculated D_a varied for composite PES/PAA membranes under different experimental conditions of passive *in vitro* MB release, but all revolved around the value of 10^{-12} $m^2 \cdot s^{-1}$. The D_a of the composite DL-PLCL/PAA implant was approximately one order of magnitude lower (3.54×10^{-13} $m^2 \cdot s^{-1}$). Calculated values of D_a for MB were significantly lower than the diffusion coefficients of MB in pure UV cross-linked poly(ethylene glycol) diacrylate hydrogels ($\sim 10^{-11}$ $m^2 \cdot s^{-1}$) determined in a previous study [233].

We can attempt to explain such discrepancy from the perspectives of effective pore size and microstructure of composite PES/PAA membranes and composite DL-PLCL/PAA implants. In the wet state, swollen cross-linked PAA hydrogel fills all voids in the structure of the hydrophobic matrix within composite hydrogels. Hence, we can estimate the effective mean pore diameter theoretically as explained in section **5.1 Theoretical estimation of pore size in composite hydrogels**. Calculated values of the mean pore diameter for composite PES/PAA membranes were in the approximate range from 1.7 nm to 2.3 nm, while the same values for composite DL-PLCL/PAA implants were in the approximate range from 2.2 nm to 2.6 nm. The results of our calculations showed that the mean pore diameter depends on the MB content within the composite hydrogel reservoir. There is a trend of decrease in mean pore diameter with the increase in MB content. We attributed the shrinking of the pores related to the rise in the MB content to the increased probability of electrostatic association between positively charged MB cations and negatively charged groups along PAA hydrogel chains. Evans et al. reported calculated poly(ethylene glycol) diacrylate hydrogel mesh sizes in the range between 2.1 nm and 2.3 nm [233]. Sizes of MB molecule reported in the literature (0.591 nm × 1.382 nm [234] and 0.61 nm × 1.43 nm × 0.4 nm [235]) are comparable with the aforementioned effective pore diameters which indicates the possible influence of pore size on D_a. In the case of composite PES/PAA membranes, we ascribed the reduced value of D_a compared to the poly(ethylene glycol) diacrylate hydrogel to the combined effects of the smaller pore size after MB loading and the presence of porous hydrophobic PES matrix further limiting the diffusion of MB. It is important to notice that the effective pore diameter in composite PES/PAA membranes would have increased during the release experiment as MB cations exited the membrane. At sufficiently high initial MB loading, this could have led to a significant acceleration of MB release resulting in kinetics that strongly deviates from the Fickian behavior. Such change in release kinetics was detected during our passive *in vitro* MB release experiments conducted for higher MB loadings (about 17% and 30% of loading efficiency in PBS at pH = 8 and $I = 0.2$ M). The pore size of composite DL-PLCL/PAA implants was quite similar to the pore size of poly(ethylene glycol) diacrylate hydrogel (and it can even become greater after some period of MB release). In this case, the specific microstructure of the implant played the most important role in reducing the value of D_a. DL-PLCL-rich surface layer with a significantly reduced content of PAA hydrogel acted as an effective rate-limiting barrier to MB diffusion and dominantly determined the passive MB release kinetics.

6.7 Active *in vitro* release of MB from composite PES/PAA membranes via iontophoresis

Within composite PES/PAA membranes, mainly PAA hydrogel regions serve for the storage of MB cations. PAA hydrogel in PBS medium becomes a network with immobile and densely packed negatively charged groups comprising carboxylate anions. Because of the network electroneutrality requirement, osmotic pressure forms within the anionic polyelectrolyte forcing network expansion and hydrogel swelling in order to minimize charge density [236]. The application of the direct-current electric field causes the movement of mobile cations within the hydrogel towards the cathode. The directed motion of mobile charges causes additional charge disbalance leading to further volume changes in polyelectrolyte gels [237]. Jabbari et al. have extensively studied the swelling behavior of a PAA hydrogel in PBS under the influence of direct-current electric fields [164]. According to their findings, PAA hydrogel additionally swells when placed in the direct-current electric field to decrease the density of fixed negative charges and thereby compensate for the removal of mobile ions from the hydrogel network and satisfy the electroneutrality requirement. Their results also indicate that the swelling extent of PAA hydrogel depends mainly on the electric field intensity, cross-linking density of the hydrogel, and the geometry of the experimental setup which may lead to mechanical deformations of the measured sample (such as expansion, shrinking, and bending). Chansai et al. reported the increase in mesh size of the PAA hydrogel loaded with sulfosalicylic acid caused by the applied direct-current electric field [238]. They attributed the observed electrically induced swelling of PAA hydrogel to the ionization of carboxyl groups of PAA during the penetration of mobile cations from the medium through the PAA hydrogel network as explained in more detail by Murdan [239].

Our results coincided with the general findings of previous studies. The applied electric current in continuous and pulse regimes caused an increase in D_a after the current source was turned on. It seemed that the effect of electric current was slightly reduced in the pulse regime at the frequency of 1 kHz without changing the MB release kinetics. Such preliminary results indicated that the motion of charged groups within the PAA hydrogel network could not follow the changes in electrical excitation. As a result, the composite PES/PAA membrane behaved as if it was stimulated by a continuous electric current of slightly lower amplitude. Hence, the external electrical modulation of D_a using PWM may be an interesting option for further research.

We also observed the bending of membrane samples towards the anode during preliminary tests. Porous polyester membrane support in our experiments minimized this effect and enabled the more accurate determination of D_a values. The values of D_a during iontophoretic *in vitro* MB release were lower than in our passive *in vitro* MB release experiments, but the iontophoretic MB release rate was higher than the passive MB release rate before iontophoresis was initiated. We presumed that the increase in the MB release rate during iontophoresis was mainly caused by the additional expansion of the PAA hydrogel network and effectively increased pore size. The presence of a porous PES matrix in the composite PES/PAA membranes limited the extent of additional PAA hydrogel swelling.

Our iontophoretic release experiments were conducted in the experimental setup comparable to the one used by Chansai et al. to study the iontophoretic release of sulfosalicylic acid (M_w = 254 Da) from pure cross-linked PAA hydrogel films [238]. The pure cross-linked PAA hydrogels in their study typically exhibited the values of D_a ~10^{-12} $m^2 \cdot s^{-1}$. These PAA hydrogel films had a significantly lower cross-linking ratio and about an order of magnitude higher average mesh size (greater than 14 nm in all cases) compared to the PAA hydrogel in our composite PES/PAA membranes (12PES-5.3AA-5TMPTA). A decrease in the average pore diameter of the PAA hydrogel combined with the presence of the PES matrix contributed to the lower D_a values that were observed during our experiments of iontophoretic MB release. As the average pore diameter of the PAA hydrogel showed the tendency to decrease with the rise in MB loading, its effect on the value of D_a may have been even more pronounced due to the comparable size of the average pore diameter and the MB molecule.

It is important to note the effect of MB loading on the kinetics of iontophoretic MB release. When the loading efficiency is very high, a strong electrostatic association exists between mobile MB cations and fixed negatively charged carboxyl groups of PAA. In such cases, applied electric current can mainly facilitate ion exchange and induce network expansion of PAA hydrogel. Hence, the net result is the greater value of D_a as mobile MB cations can participate more readily in charge transport through the composite PES/PAA membrane and carry a significant portion of the electric current. Conversely, when MB loading is low, the electrostatic association between MB cations and dissociated groups of PAA becomes weaker. Applied electric current can then be the dominant driving force for the movement of mobile cations within the membrane while also increasing the mean pore size of the PAA hydrogel network. The amount of released MB is expected to increase linearly with time in proportion to the electric current intensity. This is corroborated by our demonstration experiment conducted under comparable conditions as the experiments in our pilot study, but using significantly lower MB loading of the membrane (for details refer to **Appendix E: Demonstration of iontophoretic MB release from composite PES/PAA membranes**) [173]. However, we must note that the efficiency of MB release is reduced in these cases. Cations in the PBS medium have much higher mobilities and lower weight compared to MB cations. As the mobile cations from PBS also comprise the majority of the mobile cations within the membrane at low MB loadings, they will carry most of the current and significantly decrease the capability for MB transport through the composite PES/PAA membrane.

At the end of this section, we must refer to the expected amount of the drug to be released using a transdermal delivery system in practice. This depends on multiple factors, including the physicochemical properties and potency of the used drug. Taking into account the economic, practical, and cosmetic considerations, the expected maximum dose is 50 mg per day through the patch having the surface not larger than 50 cm^2 [240]. Composite PES/PAA membranes can store and release more than 4 mg of MB as a cationic model drug per 1 cm^2 of surface area if the maximum loading efficiency of about 96% is achieved. Hence, the composite PES/PAA membrane can meet the expectations of practical transdermal drug delivery systems for cationic drugs of low molecular weight.

6.8 Composite hydrogel synthesis approaches (I-III)

We utilized the innovative synthesis approach comprising the modification of the traditional liquid phase inversion process. We mixed the functional PAA hydrogel components (MM and CL) within the initial solution containing the hydrophobic PB and copolymerized them by irradiation before the immersion in a nonsolvent bath. Hence, the synthesis approach comprised two distinct steps that should be sequentially applied:

1) polymerization by (UV or gamma) irradiation and
2) phase separation and solidification in the aqueous bath.

As a result of the described approach, we obtained different composite hydrogels comprising microgels of PAA supported by hydrophobic polymer matrices in the shapes of membranes and disks.

Irradiation type had a significant influence on the properties of obtained disk-shaped composite hydrogels. UV irradiation contributed to the reproducible homogeneous products with smaller PAA microgel particles but required the use of a potentially toxic PI. Synthesis with gamma irradiation did not require the use of a PI, improved the water content of composite hydrogels, and introduced the possibility to adjust the degradation behavior of the hydrophobic matrix. However, gamma irradiation also contributed to the inhomogeneous products with larger PAA microgel particles. None of the irradiation methods was sufficient to achieve appropriate sterilization of the end products due to the nature of the synthesis method. Therefore, aseptic conditions during fabrication may be considered as an option to reduce bioburden. Low bioburden can provide the possibility for sterilization of the end products under mild conditions that prevent degradation of material properties. Another option is to use electron-beam irradiation for the synthesis and sterilization of the composite hydrogels. Electron-beam irradiation proved to be an effective alternative to UV irradiation in the synthesis of hydrogels that enables rapid polymerization without the use of photoinitiators while providing the control of the degree of cross-linking as well as the simultaneous sterilization of the products [241]. Electron-beam irradiation is also an efficient sterilization method in biomedical applications offering many advantages such as high dose rate, well-controlled dose range, reduced polymer degradation, and rapid processing [44], [242]. As the risks associated with sterilization by gamma irradiation become more evident [243], electron-beam irradiation may have a promising future as a safer alternative for terminal sterilization of medical devices and pharmaceutical products [242].

The employed synthesis approach enables a relatively simple and rapid fabrication of composite hydrogels. The fabrication protocol involving UV irradiation is easy to scale up and automate. It is important to note that the properties of the fabricated composite hydrogel can be tuned already during the synthesis stage by adjusting the formulations of the initial solution and the nonsolvent bath.

This dissertation only deals with the delivery of small hydrophilic cationic drugs with M_w below 300 Da. In terms of drug delivery, formulation adjustments may lead to the modulation of PAA hydrogel mean pore diameter and D_a values. Peppas and Wright showed that PAA hydrogels with greater mesh size can be synthesized and used to deliver drugs of much larger M_w [244]. We can expand the applicability of synthesized composite hydrogel reservoirs by aiming to fabricate supported PAA microgels with similar drug release properties.

Chapter 7: Conclusions and outlook

In this dissertation, we successfully synthesized composite hydrogel membranes and implants based on the cross-linked PAA hydrogel and different support matrices composed of hydrophobic polymers using the sequential application of 1) irradiation triggered polymerization and cross-linking and 2) immersion precipitation in an aqueous bath. The synthesis methods involving UV irradiation are relatively simple, robust, scalable, easy to automate, and compatible with some of the existing industrial processes in membrane technology. The application of UV irradiation led to reproducible composite reservoirs with an overall homogeneous chemical composition. Even though gamma irradiation can increase the water content of composite hydrogel implants and tune the degradation behavior of the hydrophobic polymer matrix, this method requires further optimization to achieve more reproducible material properties.

Composite hydrogels obtained using these synthesis procedures comprise a hydrophobic polymer-rich matrix as a mechanical support and dispersed PAA-rich particles. All of these composite hydrogels exhibited good IEC suitable for storing the commonly required amounts of low molecular weight cationic drugs.

We found that the nature of the CL used for the synthesis plays an important role in determining the composite PES/PAA membrane microstructure, symmetry, and electrical conductivity. The use of the hydrophilic CL TMPTA led to the formation of symmetric membranes with improved water content and adequate electrical conductivity for iontophoresis.

In the case of composite hydrogel implants, properties of the hydrophobic polymer-rich matrix influence the final implant microstructure and overall distribution of PAA-rich aggregates. Our findings suggest the correlation between the porosity of the hydrophobic polymer-rich matrix and the T_g of the hydrophobic polymer used for the synthesis. We obtained composite PLGA/PAA implants with the rigid porous PLGA-rich matrix and the composite DL-PLCL/PAA implants with the soft continuous DL-PLCL-rich matrix. In composite DL-PLCL/PAA implants, the DL-PLCL-rich phase builds a characteristic continuous matrix with a dense PAA hydrogel-sparse surface layer which serves as a rate-limiting diffusion barrier. A combination of such a DL-PLCL-rich matrix structure and the densely packed PAA-rich particles in the composite DL-PLCL/PAA implants led to the highly reproducible release behavior, rapid swelling kinetics, and capability of almost reversible swelling.

In vitro MB release investigations showed that composite PES/PAA membranes have suitable properties for passive as well as iontophoretic delivery of small cationic drugs at short time scales (order of hours), while the composite DL-PLCL/PAA implants are suitable for sustained passive delivery in the longer term (order of weeks). Release kinetics for both types of composite cationic drug reservoirs is diffusion-controlled (even during iontophoretic delivery) which was adequately described by using the value of D_a as a parameter. A modeling approach was developed that combines the analytical solution for the diffusion from polymer sheets or cylinders with the empirical Weber-Morris model to calculate the value of D_a and predict the MB *in vitro* release kinetics.

Electric excitation of composite PES/PAA membranes intended for iontophoretic transdermal drug delivery caused the effective increase in the MB release rate for high initial MB loading. We ascribed this behavior to the swelling of PAA hydrogel under applied direct-current electric fields, which leads to the increase in PAA hydrogel pore size and consequently the value of D_a. The through-membrane ionic conductivity of composite PES/PAA membranes used in iontophoresis experiments was comparable to the electrical conductivity of materials that are typically used in electrotherapy.

To evaluate the properties of composite PES/PAA membranes relevant for iontophoresis, we engineered custom electronic devices suitable for *in vitro* iontophoresis experiments and electrical characterization based on four-terminal impedance sensing. The use of these electronic devices is not limited to the analysis of conductive membranes, and they can be valuable experimental tools in various research laboratories with limited resources.

Electron-beam irradiation should be considered in further research as an alternative to UV and gamma irradiation during the synthesis as it can possibly retain the beneficial properties of UV irradiation without the use of initiators and match the sterilization efficiency of gamma irradiation. The composition of the initial solution for the synthesis should be optimized to aim at the controlled delivery of cationic drugs of larger sizes and higher molecular weights.

While the composite hydrogel implants are mainly tailored for biomedical applications, composite hydrogel membranes synthesized in this dissertation are versatile and promising materials for use in various fields. Composite PES/PAA membranes could be further investigated for different applications such as:

- flexible soft electrodes,
- reactors, templates, or reservoirs in nanoparticle synthesis, and
- membrane supported catalysts.

Similar composite hydrogel membranes can be also developed in the future to serve as important tools in the emerging interdisciplinary field of iontronics.

Bibliography

[1] O. S. Fenton, K. N. Olafson, P. S. Pillai, M. J. Mitchell, and R. Langer, “Advances in Biomaterials for Drug Delivery,” *Adv. Mater.*, vol. 30, no. 29, p. 1705328, Jul. 2018, doi: 10.1002/adma.201705328.

[2] I. S. Vizirianakis, Ed., *Handbook of Personalized Medicine: Advances in Nanotechnology, Drug Delivery and Therapy*. Boca Raton: CRC Press, 2013.

[3] H. Zhong, G. Chan, Y. Hu, H. Hu, and D. Ouyang, “A Comprehensive Map of FDA-Approved Pharmaceutical Products,” *Pharmaceutics*, vol. 10, no. 4, p. 263, Dec. 2018, doi: 10.3390/pharmaceutics10040263.

[4] J. Li and D. J. Mooney, “Designing hydrogels for controlled drug delivery,” *Nat. Rev. Mater.*, vol. 1, no. 12, pp. 1–18, 2016, doi: 10.1038/natrevmats.2016.71.

[5] BCC Research, “Global Markets and Technologies for Advanced Drug Delivery Systems,” 2016. [Online]. Available: https://www.bccresearch.com/market-research/pharmaceuticals/advanced-drug-delivery-systems-tech-markets-report.html. [Accessed: 29-Oct-2019].

[6] R. Langer, “Drug delivery and targeting.,” *Nature*, vol. 392, no. 6679 Suppl, pp. 5–10, Apr. 1998.

[7] M. E. Ruiz and S. Scioli Montoto, “Routes of Drug Administration,” in *ADME Processes in Pharmaceutical Sciences*, A. Talevi and P. A. Quiroga, Eds. Cham: Springer International Publishing, 2018, pp. 97–133.

[8] A. T. Florence and P. U. Jani, “Novel Oral Drug Formulations,” *Drug Saf.*, vol. 10, no. 3, pp. 233–266, Mar. 1994, doi: 10.2165/00002018-199410030-00005.

[9] G. J. Tortora and B. Derrickson, “The Integumentary System,” in *Principles of Anatomy and Physiology*, 13th ed., John Wiley & Sons, 2012, pp. 153–181.

[10] S. Mehdipour-Ataei and M. Oroujzadeh, “Membranes, Polymeric: Biomedical Devices,” in *Concise Encyclopedia of Biomedical Polymers and Polymeric Biomaterials*, vol. 2, M. K. Mishra, Ed. CRC Press, 2018, p. 874.

[11] D. F. Stamatialis, “Drug Delivery through Skin: Overcoming the Ultimate Biological Membrane,” in *Membranes for the Life Sciences*, Weinheim, Germany: Wiley-VCH Verlag GmbH & Co. KGaA, 2008, pp. 191–226.

[12] A. K. Banga, “Percutaneous Absorption and Enhancement Strategies,” in *Transdermal and Intradermal Delivery of Therapeutic Agents: Application of Physical Technologies*, 1st ed., CRC Press, 2011, pp. 1–26.

[13] A. Alexander *et al.*, “Approaches for breaking the barriers of drug permeation through transdermal drug delivery,” *J. Control. Release*, vol. 164, no. 1, pp. 26–40, 2012, doi: 10.1016/j.jconrel.2012.09.017.

[14] S. Singh and J. Singh, “Transdermal drug delivery by passive diffusion and iontophoresis: A review,” *Med. Res. Rev.*, vol. 13, no. 5, pp. 569–621, Sep. 1993, doi: 10.1002/med.2610130504.

[15] M. B. Brown, G. P. Martin, S. A. Jones, and F. K. Akomeah, “Dermal and Transdermal Drug Delivery Systems: Current and Future Prospects,” *Drug Deliv.*, vol. 13, no. 3, pp. 175–187, Jan. 2006, doi: 10.1080/10717540500455975.

[16] M. R. Prausnitz, S. Mitragotri, and R. Langer, “Current status and future potential of transdermal drug delivery,” *Nat. Rev. Drug Discov.*, vol. 3, no. 2, pp. 115–124, Feb. 2004, doi: 10.1038/nrd1304.

[17] N. Dixit, V. Bali, S. Baboota, A. Ahuja, and J. Ali, “Iontophoresis - An Approach for Controlled Drug Delivery: A Review,” *Curr. Drug Deliv.*, vol. 4, no. 1, pp. 1–10, Jan. 2007, doi: 10.2174/156720107704010001.

[18] V. Dhote, P. Bhatnagar, P. K. Mishra, S. C. Mahajan, and D. K. Mishra, "Iontophoresis: A Potential Emergence of a Transdermal Drug Delivery System," *Sci. Pharm.*, vol. 80, no. 1, pp. 1–28, Dec. 2012, doi: 10.3797/scipharm.1108-20.

[19] Y. Y. Huang, S. M. Wu, and C. Y. Wang, "Response surface method: a novel strategy to optimize iontophoretic transdermal delivery of thyrotropin-releasing hormone.," *Pharm. Res.*, vol. 13, no. 4, pp. 547–52, Apr. 1996, doi: 10.1023/a:1016089819967.

[20] M. Clemessy, G. Couarraze, B. Bevan, and F. Puisieux, "Preservation of skin permeability during in vitro iontophoretic experiments," *Int. J. Pharm.*, vol. 101, no. 3, pp. 219–226, Jan. 1994, doi: 10.1016/0378-5173(94)90217-8.

[21] Y. N. Kalia, A. Naik, J. Garrison, and R. H. Guy, "Iontophoretic drug delivery," *Adv. Drug Deliv. Rev.*, vol. 56, no. 5, pp. 619–658, 2004, doi: 10.1016/j.addr.2003.10.026.

[22] P. W. Ledger, "Skin biological issues in electrically enhanced transdermal delivery," *Adv. Drug Deliv. Rev.*, vol. 9, no. 2–3, pp. 289–307, Sep. 1992, doi: 10.1016/0169-409X(92)90027-N.

[23] P. Tyle, "lontophoretic Devices for Drug Delivery," *Pharm. Res.*, vol. 3, no. 6, pp. 318–326, 1986, doi: 10.1023/A:1016327822325.

[24] L. F. Santos, I. J. Correia, A. S. Silva, and J. F. Mano, "Biomaterials for drug delivery patches," *Eur. J. Pharm. Sci.*, vol. 118, pp. 49–66, Jun. 2018, doi: 10.1016/j.ejps.2018.03.020.

[25] T. Tanner and R. Marks, "Delivering drugs by the transdermal route: review and comment," *Ski. Res. Technol.*, vol. 14, no. 3, pp. 249–260, Aug. 2008, doi: 10.1111/j.1600-0846.2008.00316.x.

[26] A. M. Wokovich, S. Prodduturi, W. H. Doub, A. S. Hussain, and L. F. Buhse, "Transdermal drug delivery system (TDDS) adhesion as a critical safety, efficacy and quality attribute," *Eur. J. Pharm. Biopharm.*, vol. 64, no. 1, pp. 1–8, Aug. 2006, doi: 10.1016/j.ejpb.2006.03.009.

[27] S. Prodduturi, N. Sadrieh, A. M. Wokovich, W. H. Doub, B. J. Westenberger, and L. Buhse, "Transdermal delivery of fentanyl from matrix and reservoir systems: Effect of heat and compromised skin," *J. Pharm. Sci.*, vol. 99, no. 5, pp. 2357–2366, May 2010, doi: 10.1002/jps.22004.

[28] D. F. Stamatialis, B. J. Papenburg, M. Girones, S. N. M. Bettahalli, S. Schmitmeier, and M. Wessling, "Medical applications of membranes : Drug delivery , artificial organs and tissue engineering," *J. Memb. Sci.*, vol. 308, pp. 1–34, 2008, doi: 10.1016/j.memsci.2007.09.059.

[29] A. Naik, Y. N. Kalia, and R. H. Guy, "Transdermal drug delivery: overcoming the skin's barrier function," *Pharm. Sci. Technolo. Today*, vol. 3, no. 9, pp. 318–326, Sep. 2000, doi: 10.1016/S1461-5347(00)00295-9.

[30] N. A. Peppas, K. M. Wood, and J. B. Thomas, "Membranes in Controlled Release," in *Membranes for the Life Sciences*, K. Peinemann and S. Pereira Nunes, Eds. Weinheim, Germany: Wiley-VCH Verlag GmbH & Co. KGaA, 2008, pp. 175–190.

[31] D. Stamatialis, H. Rolevink, and G. Koops, "Passive and Iontophoretic Controlled Delivery of Salmon Calcitonin Through Artificial Membranes," *Curr. Drug Deliv.*, vol. 1, no. 2, pp. 137–143, Apr. 2004, doi: 10.2174/1567201043479911.

[32] M. Mabrouk *et al.*, "Nanoparticle- and Nanoporous-Membrane-Mediated Delivery of Therapeutics," *Pharmaceutics*, vol. 11, no. 6, p. 294, Jun. 2019, doi: 10.3390/pharmaceutics11060294.

[33] Y. Fumimoto *et al.*, "Creation of a Rich Subcutaneous Vascular Network with Implanted Adipose Tissue–Derived Stromal Cells and Adipose Tissue Enhances Subcutaneous Grafting of Islets in Diabetic Mice," *Tissue Eng. Part C Methods*, vol. 15, no. 3, pp. 437–444, 2009, doi: 10.1089/ten.tec.2008.0555.

[34] N. Rajgor, M. Patel, and V. H. Bhaskar, "Implantable drug delivery systems: An overview," *Syst.*

Rev. Pharm., vol. 2, no. 2, pp. 91–95, 2011, doi: 10.4103/0975-8453.86297.

[35] K. Ronak, K. Yatin, L. Baldaniya, and D. Tusharbindu R, "Implant - Controlled Release Medicated Formulation," *Int. J. Pharm. Chem. Sci.*, vol. 1, no. 1, pp. 59–66, 2012.

[36] A. Kumar and J. Pillai, "Implantable drug delivery systems: An overview," in *Nanostructures for the Engineering of Cells, Tissues and Organs: From Design to Applications*, 1st ed., A. M. Grumezescu, Ed. Elsevier Science, 2018, pp. 473–511.

[37] A. Santos, M. Sinn Aw, M. Bariana, T. Kumeria, Y. Wang, and D. Losic, "Drug-releasing implants: current progress, challenges and perspectives," *J. Mater. Chem. B*, vol. 2, no. 37, pp. 6157–6182, Aug. 2014, doi: 10.1039/C4TB00548A.

[38] S. Stewart, J. Domínguez-Robles, R. Donnelly, and E. Larrañeta, "Implantable Polymeric Drug Delivery Devices: Classification, Manufacture, Materials, and Clinical Applications," *Polymers (Basel).*, vol. 10, no. 12, p. 1379, Dec. 2018, doi: 10.3390/polym10121379.

[39] K. Gulati, M. Kogawa, M. Prideaux, D. M. Findlay, G. J. Atkins, and D. Losic, "Drug-releasing nano-engineered titanium implants: therapeutic efficacy in 3D cell culture model, controlled release and stability," *Mater. Sci. Eng. C*, vol. 69, pp. 831–840, Dec. 2016, doi: 10.1016/j.msec.2016.07.047.

[40] K. D. Lance *et al.*, "In Vitro and In Vivo Sustained Zero-Order Delivery of Rapamycin (Sirolimus) From a Biodegradable Intraocular Device," *Investig. Opthalmology Vis. Sci.*, vol. 56, no. 12, pp. 7331–7337, Nov. 2015, doi: 10.1167/iovs.15-17757.

[41] M. Rahimi, H. Mobedi, and A. Behnamghader, "*In situ*-forming PLGA implants loaded with leuprolide acetate/β-cyclodextrin complexes: mathematical modelling and degradation," *J. Microencapsul.*, vol. 33, no. 4, pp. 355–364, May 2016, doi: 10.1080/02652048.2016.1194905.

[42] D. King and S. McGinty, "Assessing the potential of mathematical modelling in designing drug-releasing orthopaedic implants," *J. Control. Release*, vol. 239, pp. 49–61, Oct. 2016, doi: 10.1016/j.jconrel.2016.08.009.

[43] J. M. Anderson, A. Rodriguez, and D. T. Chang, "Foreign body reaction to biomaterials," *Semin. Immunol.*, vol. 20, no. 2, pp. 86–100, Apr. 2008, doi: 10.1016/j.smim.2007.11.004.

[44] Z. Dai, J. Ronholm, Y. Tian, B. Sethi, and X. Cao, "Sterilization techniques for biodegradable scaffolds in tissue engineering applications," *J. Tissue Eng.*, vol. 7, pp. 1–13, 2016, doi: 10.1177/2041731416648810.

[45] K. A. da Silva Aquino, "Sterilization by Gamma Irradiation," in *Gamma Radiation*, F. Adrovic, Ed. InTech, 2012, pp. 171–206.

[46] F. Hasanain, K. Guenther, W. M. Mullett, and E. Craven, "Gamma Sterilization of Pharmaceuticals--A Review of the Irradiation of Excipients, Active Pharmaceutical Ingredients, and Final Drug Product Formulations," *PDA J. Pharm. Sci. Technol.*, vol. 68, no. 2, pp. 113–137, Mar. 2014, doi: 10.5731/pdajpst.2014.00955.

[47] M. B. Sintzel, A. Merkli, C. Tabatabay, and R. Gurny, "Influence of Irradiation Sterilization on Polymers Used as Drug Carriers—A Review," *Drug Dev. Ind. Pharm.*, vol. 23, no. 9, pp. 857–878, Jan. 1997, doi: 10.3109/03639049709148693.

[48] W. B. Liechty, D. R. Kryscio, B. V. Slaughter, and N. A. Peppas, "Polymers for Drug Delivery Systems," *Annu. Rev. Chem. Biomol. Eng.*, vol. 1, no. 1, pp. 149–173, Jun. 2010, doi: 10.1146/annurev-chembioeng-073009-100847.

[49] R. Langer, "Polymer-controlled drug delivery systems," *Acc. Chem. Res.*, vol. 26, no. 10, pp. 537–542, Oct. 1993, doi: 10.1021/ar00034a004.

[50] H. Tian, Z. Tang, X. Zhuang, X. Chen, and X. Jing, "Biodegradable synthetic polymers: Preparation, functionalization and biomedical application," *Prog. Polym. Sci.*, vol. 37, no. 2, pp. 237–

280, Feb. 2012, doi: 10.1016/j.progpolymsci.2011.06.004.

[51] S. Fredenberg, M. Wahlgren, M. Reslow, and A. Axelsson, "The mechanisms of drug release in poly(lactic-co-glycolic acid)-based drug delivery systems—A review," *Int. J. Pharm.*, vol. 415, no. 1–2, pp. 34–52, Aug. 2011, doi: 10.1016/j.ijpharm.2011.05.049.

[52] L. Claes and A. Ignatius, "Development of new, biodegradable implants," *Chirurg*, vol. 73, no. 10, pp. 990–996, 2002, doi: 10.1007/s00104-002-0543-0.

[53] N. Kamaly, B. Yameen, J. Wu, and O. C. Farokhzad, "Degradable Controlled-Release Polymers and Polymeric Nanoparticles: Mechanisms of Controlling Drug Release," *Chem. Rev.*, vol. 116, no. 4, pp. 2602–2663, Feb. 2016, doi: 10.1021/acs.chemrev.5b00346.

[54] Y. Lu, A. A. Aimetti, R. Langer, and Z. Gu, "Bioresponsive materials," *Nat. Rev. Mater.*, vol. 2, no. 1, p. 16075, Jan. 2017, doi: 10.1038/natrevmats.2016.75.

[55] D. Schmaljohann, "Thermo- and pH-responsive polymers in drug delivery," *Adv. Drug Deliv. Rev.*, vol. 58, no. 15, pp. 1655–1670, Dec. 2006, doi: 10.1016/j.addr.2006.09.020.

[56] S. Mura, J. Nicolas, and P. Couvreur, "Stimuli-responsive nanocarriers for drug delivery," *Nat. Mater.*, vol. 12, no. 11, pp. 991–1003, Nov. 2013, doi: 10.1038/nmat3776.

[57] T. H. Qazi, R. Rai, and A. R. Boccaccini, "Tissue engineering of electrically responsive tissues using polyaniline based polymers: A review," *Biomaterials*, vol. 35, no. 33, pp. 9068–9086, Nov. 2014, doi: 10.1016/j.biomaterials.2014.07.020.

[58] J. Ge, E. Neofytou, T. J. Cahill, R. E. Beygui, and R. N. Zare, "Drug Release from Electric-Field-Responsive Nanoparticles," *ACS Nano*, vol. 6, no. 1, pp. 227–233, Jan. 2012, doi: 10.1021/nn203430m.

[59] D. Svirskis, J. Travas-Sejdic, A. Rodgers, and S. Garg, "Electrochemically controlled drug delivery based on intrinsically conducting polymers," *J. Control. Release*, vol. 146, no. 1, pp. 6–15, Aug. 2010, doi: 10.1016/j.jconrel.2010.03.023.

[60] F. Wang, Y.-H. Lai, and M.-Y. Han, "Stimuli-Responsive Conjugated Copolymers Having Electro-Active Azulene and Bithiophene Units in the Polymer Skeleton: Effect of Protonation and p-Doping on Conducting Properties," *Macromolecules*, vol. 37, no. 9, pp. 3222–3230, 2004, doi: 10.1021/ma035335q.

[61] A. Izumi, R. Nomura, and T. Masuda, "Design and Synthesis of Stimuli-Responsive Conjugated Polymers Having Azobenzene Units in the Main Chain," *Macromolecules*, vol. 34, no. 13, pp. 4342–4347, 2001, doi: 10.1021/ma002101n.

[62] M. Hess *et al.*, "Terminology of polymers containing ionizable or ionic groups and of polymers containing ions (IUPAC Recommendations 2006)," *Pure Appl. Chem.*, vol. 78, no. 11, pp. 2067–2074, 2006, doi: 10.1351/pac200678112067.

[63] C.-J. Lee *et al.*, "Ionic Conductivity of Polyelectrolyte Hydrogels," *ACS Appl. Mater. Interfaces*, vol. 10, no. 6, pp. 5845–5852, Feb. 2018, doi: 10.1021/acsami.7b15934.

[64] A. B. Scranton, B. Rangarajan, and J. Klier, "Biomedical applications of polyelectrolytes," in *Biopolymers II. Advances in Polymer Science, vol. 122*, N. A. Peppas and R. S. Langer, Eds. Springer, Berlin, Heidelberg, 1995, pp. 1–54.

[65] S. Gupta, P. Benien, and P. K. Sahoo, "Ion exchange resins transforming drug delivery systems," *Curr. Drug Deliv.*, vol. 7, no. 3, pp. 252–262, 2010, doi: 10.2174/156720110791560955.

[66] D. P. Elder, "Pharmaceutical Applications of Ion-Exchange Resins," *J. Chem. Educ.*, vol. 82, no. 4, pp. 575–587, 2005.

[67] J. Hirvonen, "Topical Iontophoretic Delivery," *Am. J. Drug Deliv.*, vol. 3, no. 2, pp. 67–81, 2005, doi: 10.2165/00137696-200503020-00001.

[68] F. G. Helfferich, *Ion Exchange*. New York: Dover Publications, 1995.

[69] M. Vuorio, J. A. Manzanares, L. Murtomäki, J. Hirvonen, T. Kankkunen, and K. Kontturi, "Ion-exchange fibers and drugs: a transient study," *J. Control. Release*, vol. 91, no. 3, pp. 439–448, 2003, doi: 10.1016/S0168-3659(03)00270-0.

[70] I. Singh, A. K. Rehni, R. Kalra, G. Joshi, M. Kumar, and H. Y. Aboul-Enein, "Ion exchange resins: Drug delivery and therapeutic applications," *Fabad J. Pharm. Sci.*, vol. 32, no. 2, pp. 91–100, 2007.

[71] T. Jaskari, M. Vuorio, K. Kontturi, J. A. Manzanares, and J. Hirvonen, "Ion-exchange fibers and drugs: an equilibrium study," *J. Control. Release*, vol. 70, no. 1–2, pp. 219–229, Jan. 2001, doi: 10.1016/S0168-3659(00)00359-X.

[72] K. Hänninen, A. Marie Kaukonen, T. Kankkunen, and J. Hirvonen, "Rate and extent of ion-exchange process: the effect of physico-chemical characteristics of salicylate anions," *J. Control. Release*, vol. 91, no. 3, pp. 449–463, Sep. 2003, doi: 10.1016/S0168-3659(03)00276-1.

[73] O. M. Conaghey, J. Corish, and O. I. Corrigan, "Iontophoretically assisted in vitro membrane transport of nicotine from a hydrogel containing ion exchange resins," *Int. J. Pharm.*, vol. 170, no. 2, pp. 225–237, Aug. 1998, doi: 10.1016/S0378-5173(98)00145-8.

[74] S. Åkerman *et al.*, "Transport of drugs across porous ion exchange membranes," *J. Control. Release*, vol. 50, no. 1–3, pp. 153–166, Jan. 1998, doi: 10.1016/S0168-3659(97)00131-4.

[75] T. Jaskari, M. Vuorio, K. Kontturi, A. Urtti, J. A. Manzanares, and J. Hirvonen, "Controlled transdermal iontophoresis by ion-exchange fiber.," *J. Control. Release*, vol. 67, no. 2–3, pp. 179–90, 2000, doi: 10.1016/S0168-3659(00)00204-2.

[76] V. Anand, R. Kandarapu, and S. Garg, "Ion-exchange resins: carrying drug delivery forward," *Drug Discov. Today*, vol. 6, no. 17, pp. 905–914, Sep. 2001, doi: 10.1016/S1359-6446(01)01922-5.

[77] T. Kankkunen *et al.*, "Improved stability and release control of levodopa and metaraminol using ion-exchange fibers and transdermal iontophoresis," *Eur. J. Pharm. Sci.*, vol. 16, no. 4–5, pp. 273–280, Sep. 2002, doi: 10.1016/S0928-0987(02)00113-6.

[78] K. Malinovskaja, T. Laaksonen, K. Kontturi, and J. Hirvonen, "Ion-exchange and iontophoresis-controlled delivery of apomorphine," *Eur. J. Pharm. Biopharm.*, vol. 83, no. 3, pp. 477–484, 2013, doi: 10.1016/j.ejpb.2012.11.014.

[79] K. Malinovskaja, T. Laaksonen, and J. Hirvonen, "Controlled transdermal delivery of leuprorelin by pulsed iontophoresis and ion-exchange fiber.," *Eur. J. Pharm. Biopharm.*, vol. 88, no. 3, pp. 594–601, 2014, doi: 10.1016/j.ejpb.2014.08.010.

[80] Y. Gao, J. Yuan, H. Liu, Y. Yang, Y. Hou, and S. Li, "Tramadol loading, release and iontophoretic characteristics of ion-exchange fiber," *Int. J. Pharm.*, vol. 465, no. 1–2, pp. 102–111, 2014, doi: 10.1016/j.ijpharm.2014.02.017.

[81] O. Wichterle and D. Lím, "Hydrophilic Gels for Biological Use," *Nature*, vol. 185, no. 4706, pp. 117–118, Jan. 1960, doi: 10.1038/185117a0.

[82] E. Caló and V. V. Khutoryanskiy, "Biomedical applications of hydrogels: A review of patents and commercial products," *Eur. Polym. J.*, vol. 65, pp. 252–267, 2015, doi: 10.1016/j.eurpolymj.2014.11.024.

[83] N. A. Peppas, P. Bures, W. Leobandung, and H. Ichikawa, "Hydrogels in pharmaceutical formulations," *Eur. J. Pharm. Biopharm.*, vol. 50, no. 1, pp. 27–46, Jul. 2000, doi: 10.1016/S0939-6411(00)00090-4.

[84] A. S. Hoffman, "Hydrogels for biomedical applications," *Adv. Drug Deliv. Rev.*, vol. 64, pp. 18–23, Dec. 2012, doi: 10.1016/j.addr.2012.09.010.

[85] P. I. Lee and C.-J. Kim, "Probing the mechanisms of drug release from hydrogels," *J. Control. Release*, vol. 16, no. 1–2, pp. 229–236, Jun. 1991, doi: 10.1016/0168-3659(91)90046-G.

[86] T. R. Hoare and D. S. Kohane, “Hydrogels in drug delivery: Progress and challenges,” *Polymer (Guildf).*, vol. 49, no. 8, pp. 1993–2007, 2008, doi: 10.1016/j.polymer.2008.01.027.

[87] O. Okay, “General Properties of Hydrogels,” in *Hydrogel Sensors and Actuators. Springer Series on Chemical Sensors and Biosensors (Methods and Applications), vol 6*, G. Gerlach and K.-F. Arndt, Eds. Springer, Berlin, Heidelberg, 2009, pp. 1–14.

[88] Y. S. Zhang and A. Khademhosseini, “Advances in engineering hydrogels.,” *Science*, vol. 356, no. 6337, May 2017, doi: 10.1126/science.aaf3627.

[89] A. M. S. Costa and J. F. Mano, “Extremely strong and tough hydrogels as prospective candidates for tissue repair – A review,” *Eur. Polym. J.*, vol. 72, pp. 344–364, Nov. 2015, doi: 10.1016/j.eurpolymj.2015.07.053.

[90] H. Yao, J. Wang, and S. Mi, “Photo Processing for Biomedical Hydrogels Design and Functionality: A Review,” *Polymers (Basel).*, vol. 10, no. 1, p. 11, Dec. 2017, doi: 10.3390/polym10010011.

[91] E. Suljovrujic, Z. R. Miladinovic, M. Micic, D. Suljovrujic, and D. Milicevic, “The influence of monomer/solvent feed ratio on POEGDMA thermoresponsive hydrogels: Radiation-induced synthesis, swelling properties and VPTT,” *Radiat. Phys. Chem.*, vol. 158, pp. 37–45, May 2019, doi: 10.1016/j.radphyschem.2018.12.034.

[92] H. L. Abd El-Mohdy, E. A. Hegazy, E. M. El-Nesr, and M. A. El-Wahab, “Synthesis, characterization and properties of radiation-induced Starch/(EG-co-MAA) hydrogels,” *Arab. J. Chem.*, vol. 9, pp. S1627–S1635, Nov. 2016, doi: 10.1016/j.arabjc.2012.04.022.

[93] S. Kadlubowski, M. Matusiak, J. Jenczyk, M. N. Olejniczak, M. Kozanecki, and L. Okrasa, “Radiation-induced synthesis of thermo-sensitive, gradient hydrogels based on 2-(2-methoxyethoxy)ethyl methacrylate,” *Radiat. Phys. Chem.*, vol. 100, pp. 23–31, Jul. 2014, doi: 10.1016/j.radphyschem.2014.03.014.

[94] A. E.-H. Ali and E.-S. A. Hegazy, “Radiation synthesis of poly(ethylene glycol)/acrylic acid hydrogel as carrier for site specific drug delivery,” *J. Biomed. Mater. Res. Part B Appl. Biomater.*, vol. 81B, no. 1, pp. 168–174, Apr. 2007, doi: 10.1002/jbm.b.30650.

[95] X. Coqueret, “Obtaining high performance polymeric materials by irradiation,” in *Radiation Chemistry – From basic science to applications in biology and material science*, M. Spotheim-Maurizot, M. Mostafavi, T. Douki, and J. Belloni, Eds. EDP Sciences, France, 2008, pp. 131–149.

[96] T. D. Callinan, “Polymer Synthesis by Gamma Radiation,” *J. Electrochem. Soc.*, vol. 103, no. 5, p. 292, May 1956, doi: 10.1149/1.2430313.

[97] F. Liu, N. A. Hashim, Y. Liu, M. R. M. Abed, and K. Li, “Progress in the production and modification of PVDF membranes,” *J. Memb. Sci.*, vol. 375, no. 1–2, pp. 1–27, Jun. 2011, doi: 10.1016/j.memsci.2011.03.014.

[98] S. Loeb and S. Sourirajan, “Sea Water Demineralization by Means of an Osmotic Membrane,” in *Saline Water Conversion—II, Advances in Chemistry, Vol. 38*, American Chemical Society, 1963, pp. 117–132.

[99] A. K. Hołda and I. F. J. Vankelecom, “Understanding and guiding the phase inversion process for synthesis of solvent resistant nanofiltration membranes,” *J. Appl. Polym. Sci.*, vol. 132, no. 27, p. 42130, Jul. 2015, doi: 10.1002/app.42130.

[100] M. Mulder, “Preparation techniques for immersion precipitation,” in *Basic Principles of Membrane Technology*, 2nd ed., Dordrecht: Kluwer Academic Publishers, 1996, pp. 77–81.

[101] X. Tan and D. Rodrigue, “A Review on Porous Polymeric Membrane Preparation. Part I: Production Techniques with Polysulfone and Poly (Vinylidene Fluoride),” *Polymers (Basel).*, vol. 11, no. 7, p. 1160, Jul. 2019, doi: 10.3390/polym11071160.

[102] E. E. Abdel-Hady, M. M. El-Toony, and M. O. Abdel-Hamed, "Casting Membrane of Acrylamide/Polymethacrylic acid and Reinforced by PAC for Application in Fuel Cell Unit," *J. Membr. Sci. Technol.*, vol. 2, no. 1, pp. 1–8, 2012, doi: 10.4172/2155-9589.1000111.

[103] P. Aerts, I. Genné, R. Leysen, P. A. Jacobs, and I. F. J. Vankelecom, "The role of the nature of the casting substrate on the properties of membranes prepared via immersion precipitation," *J. Memb. Sci.*, vol. 283, no. 1–2, pp. 320–327, Oct. 2006, doi: 10.1016/j.memsci.2006.06.039.

[104] M. Ulbricht, "Advanced functional polymer membranes," *Polymer (Guildf).*, vol. 47, no. 7, pp. 2217–2262, Mar. 2006, doi: 10.1016/j.polymer.2006.01.084.

[105] Q. Yang, N. Adrus, F. Tomicki, and M. Ulbricht, "Composites of functional polymeric hydrogels and porous membranes," *J. Mater. Chem.*, vol. 21, no. 9, pp. 2783–2811, 2011, doi: 10.1039/c0jm02234a.

[106] R. V. Kulkarni and S. Biswanath, "Electrically responsive smart hydrogels in drug delivery: A review," *J. Appl. Biomater. Biomech.*, vol. 5, no. 3, pp. 125–139, 2007, doi: 10.1177/228080000700500301.

[107] H. Chen, A. M. Rahmathullah, G. R. Palmese, and Y. A. Elabd, "Polymer-Polymer Nanocomposite Membranes as Breathable Barriers with Electro-Sensitive Permeability," in *Nanoscience and Nanotechnology for Chemical and Biological Defense, ACS Symposium Series, vol. 1016*, American Chemical Society, 2009, pp. 307–322.

[108] H. Chen, G. R. Palmese, and Y. A. Elabd, "Electrosensitive Permeability of Membranes with Oriented Polyelectrolyte Nanodomains," *Macromolecules*, vol. 40, no. 4, pp. 781–782, 2007, doi: 10.1021/ma062678q.

[109] H. Chen, G. R. Palmese, and Y. A. Elabd, "Membranes with Oriented Polyelectrolyte Nanodomains," *Chem. Mater.*, vol. 18, no. 20, pp. 4875–4881, Oct. 2006, doi: 10.1021/cm061422w.

[110] E. Kokufuta, T. Yamauchi, and Y. Osada, "Electrically controlled separation of maleic acid and fumaric acid through a poly(vinyl alcohol)/poly(acrylic acid) composite membrane," *Polym. Gels Networks*, vol. 3, no. 4, pp. 397–406, Jan. 1995, doi: 10.1016/0966-7822(94)00010-7.

[111] T. Yamauchi, E. Kokufuta, and Y. Osada, "Electrically controlled protein permeation through a poly(vinyl alcohol)/poly(acrylic acid) composite membrane," *Polym. Gels Networks*, vol. 1, no. 4, pp. 247–255, Jan. 1993, doi: 10.1016/0966-7822(93)90003-Z.

[112] K. Hu and J. M. Dickson, "Development and characterization of poly(vinylidene fluoride)-poly(acrylic acid) pore-filled pH-sensitive membranes," *J. Memb. Sci.*, vol. 301, no. 1–2, pp. 19–28, 2007, doi: 10.1016/j.memsci.2007.05.031.

[113] C. Song, W. Shi, H. Jiang, J. Tu, and D. Ge, "pH-sensitive characteristics of poly(acrylic acid)-functionalized anodic aluminum oxide (AAO) membranes," *J. Memb. Sci.*, vol. 372, no. 1–2, pp. 340–345, Apr. 2011, doi: 10.1016/j.memsci.2011.02.017.

[114] T. Luo *et al.*, "pH-responsive poly(ether sulfone) composite membranes blended with amphiphilic polystyrene-block-poly(acrylic acid) copolymers," *J. Memb. Sci.*, vol. 450, pp. 162–173, Jan. 2014, doi: 10.1016/j.memsci.2013.09.002.

[115] W. Shi, J. Deng, H. Qin, D. Wang, and C. Zhao, "Poly(ether sulfone) membranes with photo-responsive permeability," *J. Memb. Sci.*, vol. 455, pp. 357–367, Apr. 2014, doi: 10.1016/j.memsci.2014.01.005.

[116] X. Niu, D. Li, Y. Chen, and F. Ran, "Modification of a polyethersulfone membrane with a block copolymer brush of poly(2-methacryloyloxyethyl phosphorylcholine-*co*-glycidyl methacrylate) and a branched polypeptide chain of Arg–Glu–Asp–Val," *RSC Adv.*, vol. 9, no. 44, pp. 25274–25284, 2019, doi: 10.1039/c9ra04234b.

[117] C. O. M'Bareck, Q. T. Nguyen, S. Alexandre, and I. Zimmerlin, "Fabrication of ion-exchange ultrafiltration membranes for water treatment. I. Semi-interpenetrating polymer networks of

polysulfone and poly(acrylic acid)," *J. Memb. Sci.*, vol. 278, no. 1–2, pp. 10–18, 2006, doi: 10.1016/j.memsci.2005.10.058.

[118] Q. Wei, J. Li, B. Qian, B. Fang, and C. Zhao, "Preparation, characterization and application of functional polyethersulfone membranes blended with poly (acrylic acid) gels," *J. Memb. Sci.*, vol. 337, no. 1–2, pp. 266–273, 2009, doi: 10.1016/j.memsci.2009.03.055.

[119] C. Sun, H. Ji, H. Qin, S. Nie, W. Zhao, and C. Zhao, "A facile approach toward multifunctional polyethersulfone membranes via *in situ* cross-linked copolymerization," *J. Biomater. Sci. Polym. Ed.*, vol. 26, no. 15, pp. 1013–1034, 2015, doi: 10.1080/09205063.2015.1071929.

[120] P. Radovanovic, M. Kellner, J. Matovic, R. Liska, and T. Koch, "Asymmetric membranes with interpenetrating proton-conducting morphology made by a combination of immersion precipitation and photopolymerization," *J. Memb. Sci.*, vol. 401–402, pp. 254–261, 2012, doi: 10.1016/j.memsci.2012.02.012.

[121] A. Stajčić, A. Nastasović, J. Stajić-Trošić, J. Marković, A. Onjia, and F. Radovanović, "Novel membrane-supported hydrogel for removal of heavy metals," *J. Environ. Chem. Eng.*, vol. 3, no. 1, pp. 453–461, 2015, doi: 10.1016/j.jece.2015.01.005.

[122] S. H. Yuk, S. H. Cho, and H. B. Lee, "Electric Current-Sensitive Drug Delivery Systems Using Sodium Alginate/Polyacrylic Acid Composites," *Pharm. Res.*, vol. 9, no. 7, pp. 955–957, 1992, doi: 10.1023/A:1015821504229.

[123] S. Y. Kim and Y. M. Lee, "Drug release behavior of electrical responsive poly(vinyl alcohol)/poly(acrylic acid) IPN hydrogels under an electric stimulus," *J. Appl. Polym. Sci.*, vol. 74, no. 7, pp. 1752–1761, Nov. 1999, doi: 10.1002/(SICI)1097-4628(19991114)74:7<1752::AID-APP18>3.0.CO;2-H.

[124] P. D. Vispute, M. P. Wagh, and N. N. Inamdar, "Comparative Evaluation Of Ion Exchange Resins And Fibers In Iontophoretic Transdermal Delivery Of Sumatriptan Succinate," *Adv. Mater. Lett.*, vol. 7, no. 9, pp. 754–759, 2016, doi: 10.5185/amlett.2016.6158.

[125] S. Kamath, D. Bhattacharyya, C. Padukudru, R. B. Timmons, and L. Tang, "Surface chemistry influences implant-mediated host tissue responses," *J. Biomed. Mater. Res. Part A*, vol. 86A, no. 3, pp. 617–626, Sep. 2008, doi: 10.1002/jbm.a.31649.

[126] L. Guo, G. Liu, R. Y. Hong, and H. Z. Li, "Preparation and Characterization of Chitosan Poly(acrylic acid) Magnetic Microspheres," *Mar. Drugs*, vol. 8, no. 7, pp. 2212–2222, 2010, doi: 10.3390/md8072212.

[127] Abdel-Mohdy, A. Abou-Okeil, S. El-Sabagh, and S. M. El-Sawy, "Preparation and Characterization of Chitosan / Polyacrylic Acid / Ag-Nanoparticles Composite Membranes," *Int. J. Chem. Mol. Eng.*, vol. 9, no. 9, pp. 1149–1154, 2015.

[128] K. S. Stankevich, N. V. Danilenko, R. M. Gadirov, S. I. Goreninskii, S. I. Tverdokhlebov, and V. D. Filimonov, "A new approach for the immobilization of poly(acrylic) acid as a chemically reactive cross-linker on the surface of poly(lactic) acid-based biomaterials," *Mater. Sci. Eng. C*, vol. 71, pp. 862–869, 2017, doi: 10.1016/j.msec.2016.10.078.

[129] H. A. Abd El-Rehim, E.-S. A. Hegazy, A. A. Hamed, and A. E. Swilem, "Controlling the size and swellability of stimuli-responsive polyvinylpyrrolidone–poly(acrylic acid) nanogels synthesized by gamma radiation-induced template polymerization," *Eur. Polym. J.*, vol. 49, no. 3, pp. 601–612, Mar. 2013, doi: 10.1016/j.eurpolymj.2012.12.002.

[130] S. D. Sütekin and O. Güven, "Radiation-induced controlled polymerization of acrylic acid by RAFT and RAFT-MADIX methods in protic solvents," *Radiat. Phys. Chem.*, vol. 142, pp. 82–87, Jan. 2018, doi: 10.1016/j.radphyschem.2017.01.046.

[131] M. Matusiak, S. Kadlubowski, and P. Ulanski, "Radiation-induced synthesis of poly(acrylic acid) nanogels," *Radiat. Phys. Chem.*, vol. 142, pp. 125–129, Jan. 2018, doi:

10.1016/j.radphyschem.2017.01.037.

[132] H. K. Makadia and S. J. Siegel, “Poly Lactic-co-Glycolic Acid (PLGA) as biodegradable controlled drug delivery carrier,” *Polymers (Basel).*, vol. 3, no. 3, pp. 1377–1397, 2011, doi: 10.3390/polym3031377.

[133] H. Kimura and Y. Ogura, “Biodegradable Polymers for Ocular Drug Delivery,” *Ophthalmologica*, vol. 215, no. 3, pp. 143–155, 2001, doi: 10.1159/000050849.

[134] L. Montanari *et al.*, “Gamma irradiation effects on poly(DL-lactictide-co-glycolide) microspheres,” *J. Control. Release*, vol. 56, no. 1–3, pp. 219–229, 1998, doi: 10.1016/S0168-3659(98)00082-0.

[135] T. H. Lee, J. Wang, and C. H. Wang, “Double-walled microspheres for the sustained release of a highly water soluble drug: Characterization and irradiation studies,” *J. Control. Release*, vol. 83, no. 3, pp. 437–452, 2002, doi: 10.1016/S0168-3659(02)00235-3.

[136] J. S. Lee, G. S. Chae, G. Khang, M. S. Kim, S. H. Cho, and H. B. Lee, “The effect of gamma irradiation on PLGA and release behavior of BCNU from PLGA wafer,” *Macromol. Res.*, vol. 11, no. 5, pp. 352–356, Oct. 2003, doi: 10.1007/BF03218376.

[137] C. Carrascosa, L. Espejo, S. Torrado, and J. J. Torrado, “Effect of γ-sterilization process on PLGA microspheres loaded with insulin-like growth factor - I (IGF-I),” *J. Biomater. Appl.*, vol. 18, no. 2, pp. 95–108, 2003, doi: 10.1177/088532803038026.

[138] S. Y. Jo *et al.*, “Degradation behavior of poly (L-lactide-co-glycolide) films through gamma-ray irradiation,” *Radiat. Phys. Chem.*, vol. 81, no. 7, pp. 846–850, 2012, doi: 10.1016/j.radphyschem.2012.03.013.

[139] H. Keles, A. Naylor, F. Clegg, and C. Sammon, “Investigation of factors influencing the hydrolytic degradation of single PLGA microparticles,” *Polym. Degrad. Stab.*, vol. 119, pp. 228–241, 2015, doi: 10.1016/j.polymdegradstab.2015.04.025.

[140] L. Davison, E. Themistou, F. Buchanan, and E. Cunningham, “Low temperature gamma sterilization of a bioresorbable polymer, PLGA,” *Radiat. Phys. Chem.*, vol. 143, pp. 27–32, 2018, doi: 10.1016/j.radphyschem.2017.09.009.

[141] M. Rafienia, H. Mirzadeh, H. Mobedi, and A. Jamshidi, “*In Vitro* Evaluation of Drug Solubility and Gamma Irradiation on the Release of Betamethasone under Simulated *In Vivo* Conditions,” *J. Bioact. Compat. Polym.*, vol. 22, no. 4, pp. 443–459, 2007, doi: 10.1177/0883911507080110.

[142] M. Rafienia, S. H. Emami, H. Mirzadeh, H. Mobedi, and S. Karbasi, “Influence of Poly (Lactide-Co-Glycolide) Type and Gamma Irradiation on the Betamethasone Acetate Release from the *In Situ* Forming Systems,” *Curr. Drug Deliv.*, vol. 6, no. 2, pp. 184–191, 2009, doi: 10.2174/156720109787846243.

[143] S. R. Benhabbour *et al.*, “Ultra-long-acting tunable biodegradable and removable controlled release implants for drug delivery,” *Nat. Commun.*, vol. 10, no. 1, p. 4324, Dec. 2019, doi: 10.1038/s41467-019-12141-5.

[144] K. J. J. Brodbeck, J. R. R. Desnoyer, and A. J. J. McHugh, “Phase inversion dynamics of PLGA solutions related to drug delivery. Part II. The role of solution thermodynamics and bath-side mass transfer.,” *J. Control. Release*, vol. 62, no. 3, pp. 333–344, 1999, doi: 10.1016/S0168-3659(99)00159-5.

[145] P. D. Graham, K. J. Brodbeck, and A. J. McHugh, “Phase inversion dynamics of PLGA solutions related to drug delivery,” *J. Control. Release*, vol. 58, no. 2, pp. 233–245, 1999, doi: 10.1016/S0168-3659(98)00158-8.

[146] M. Parent, C. Nouvel, M. Koerber, A. Sapin, P. Maincent, and A. Boudier, “PLGA *in situ* implants formed by phase inversion: Critical physicochemical parameters to modulate drug release,” *J. Control. Release*, vol. 172, no. 1, pp. 292–304, Nov. 2013, doi: 10.1016/j.jconrel.2013.08.024.

[147] D. Klose, F. Siepmann, K. Elkharraz, and S. Krenzlin, "How porosity and size affect the drug release mechanisms from PLGA-based microparticles," *Int. J. Pharm.*, vol. 314, no. 2, pp. 198–206, May 2006, doi: 10.1016/j.ijpharm.2005.07.031.

[148] H. Keles, A. Naylor, F. Clegg, and C. Sammon, "Studying the release of hGH from gamma-irradiated PLGA microparticles using ATR-FTIR imaging," *Vib. Spectrosc.*, vol. 71, pp. 76–84, Mar. 2014, doi: 10.1016/j.vibspec.2014.01.012.

[149] A. Jouyban, M. A. A. Fakhree, and A. Shayanfar, "Review of Pharmaceutical Applications of N-Methyl-2-Pyrrolidone," *J. Pharm. Pharm. Sci.*, vol. 13, no. 4, pp. 524–535, 2010, doi: 10.18433/J3P306.

[150] Jü, "N-Methylpyrrolidone_Structural_Formulae," *Own work, Public Domain*, 2010. [Online]. Available: https://commons.wikimedia.org/w/index.php?curid=9276220. [Accessed: 19-Mar-2020].

[151] N. A. Alenazi, M. A. Hussein, K. A. Alamry, and A. M. Asiri, "Modified polyether-sulfone membrane: a mini review," *Des. Monomers Polym.*, vol. 20, no. 1, pp. 532–546, Jan. 2017, doi: 10.1080/15685551.2017.1398208.

[152] S. H. Teoh, Z. G. Tang, and G. W. Hastings, "Thermoplastic Polymers In Biomedical Applications: Structures, Properties and Processing," in *Handbook of Biomaterial Properties*, 2nd ed., W. Murphy, J. Black, and G. Hastings, Eds. New York, NY: Springer New York, 2016, pp. 272–273.

[153] J. Drobny, "Properties of polyethersulfone," in *Specialty Thermoplastics. Landolt-Börnstein - Group VIII Advanced Materials and Technologies (Numerical Data and Functional Relationships in Science and Technology), vol 13.*, J. Drobny, Ed. Berlin, Heidelberg: Springer Berlin Heidelberg, 2015, pp. 98–101.

[154] C. Zhou *et al.*, "Effect of Polyethersulfone Molecular Weight on Structure and Performance of Ultrafiltration Membranes," *Ind. Eng. Chem. Res.*, vol. 49, no. 20, pp. 9988–9997, Oct. 2010, doi: 10.1021/ie100199h.

[155] Jü, "Polyethersulfones," *Own work, CC0*, 2012. [Online]. Available: https://commons.wikimedia.org/w/index.php?curid=19216919. [Accessed: 19-Mar-2020].

[156] Durect Corporation, "LACTEL® 25:75 DL-PLCL(B6015-1) Technical Datasheet." .

[157] P. In Pyo Park and S. Jonnalagadda, "Predictors of glass transition in the biodegradable poly-lactide and poly-lactide-*co* -glycolide polymers," *J. Appl. Polym. Sci.*, vol. 100, no. 3, pp. 1983–1987, May 2006, doi: 10.1002/app.22135.

[158] Sigma-Aldrich, "Poly(D,L-lactide-*co*-caprolactone)." [Online]. Available: https://www.sigmaaldrich.com/catalog/product/aldrich/457647?lang=en&region=SX. [Accessed: 19-Mar-2020].

[159] Fvasconcellos, "Skeletal formula of poly(lactic-*co*-glycolic acid) (PLGA)," *Public Domain*, 2008. [Online]. Available: https://commons.wikimedia.org/w/index.php?curid=4596206. [Accessed: 19-Mar-2020].

[160] N. J. Shah *et al.*, "Adaptive growth factor delivery from a polyelectrolyte coating promotes synergistic bone tissue repair and reconstruction.," *Proc. Natl. Acad. Sci. U. S. A.*, vol. 111, no. 35, pp. 12847–52, Sep. 2014, doi: 10.1073/pnas.1408035111.

[161] M. L. Macdonald, R. E. Samuel, N. J. Shah, R. F. Padera, Y. M. Beben, and P. T. Hammond, "Tissue integration of growth factor-eluting layer-by-layer polyelectrolyte multilayer coated implants," *Biomaterials*, vol. 32, no. 5, pp. 1446–1453, Feb. 2011, doi: 10.1016/j.biomaterials.2010.10.052.

[162] J. V. Stamenković, P. I. Premović, and S. V. Mentus, "Electrical conductivity of poly(acrylic acid) gels," *Journal of the Serbian Chemical Society*, vol. 62, no. 10. pp. 945–950, 1997.

[163] T. Swift, L. Swanson, M. Geoghegan, and S. Rimmer, "The pH-responsive behaviour of poly(acrylic acid) in aqueous solution is dependent on molar mass," *Soft Matter*, vol. 12, no. 9, pp. 2542–2549, Feb. 2016, doi: 10.1039/C5SM02693H.

[164] E. Jabbari, J. Tavakoli, and A. S. Sarvestani, "Swelling characteristics of acrylic acid polyelectrolyte hydrogel in a dc electric field," *Smart Mater. Struct.*, vol. 16, no. 5, pp. 1614–1620, 2007, doi: 10.1088/0964-1726/16/5/015.

[165] OmenBreeze, "Chemical structure of poly(acrylic acid), or polyacrylic acid," *Own work based on: Polyacrylic acid.png by Edgar181., CC0*, 2019. [Online]. Available: https://commons.wikimedia.org/w/index.php?curid=84857828. [Accessed: 19-Mar-2020].

[166] World Health Organization, "World Health Organization Model List of Essential Medicines, 21st List." Geneva, p. 4, 2019.

[167] L. A. Elnahas, M. A. Elblbesy, Y. S. Youssef, T. E. Shalaby, and M. A. Yehia, "Drug Delivery Stimulation by Alternating Current Using Methylene Blue Dye Absorption by Pig's Skin as a Model," *Am. J. Biomed. Sci.*, vol. 5, no. 1, pp. 14–24, Jan. 2013, doi: 10.5099/aj130100014.

[168] J.-H. Lee and E.-Y. Choi, "Iontophoresis Enhances Transdermal Delivery of Methylene Blue in Rat Skin (I): The Effect of Current Application Duration," *J. Korean Phys. Ther.*, vol. 23, no. 6, pp. 77–84, Dec. 2011.

[169] P. G. Johnson, S. A. Gallo, S. W. Hui, and A. R. Oseroff, "A Pulsed Electric Field Enhances Cutaneous Delivery of Methylene Blue in Excised Full-Thickness Porcine Skin," *J. Invest. Dermatol.*, vol. 111, no. 3, pp. 457–463, Sep. 1998, doi: 10.1046/j.1523-1747.1998.00301.x.

[170] K. Edwards, "New Twist on an Old Favorite: Gentian Violet and Methylene Blue Antibacterial Foams," *Adv. Wound Care*, vol. 5, no. 1, pp. 11–18, 2016, doi: 10.1089/wound.2014.0593.

[171] K. Y. Woo and J. Heil, "A prospective evaluation of methylene blue and gentian violet dressing for management of chronic wounds with local infection," *Int. Wound J.*, vol. 14, no. 6, pp. 1029–1035, 2017, doi: 10.1111/iwj.12753.

[172] Harbinary, "2D-structure of dichloropane methylene blue," *Own work, Public Domain*, 2018. [Online]. Available: https://commons.wikimedia.org/w/index.php?curid=8525246. [Accessed: 19-Mar-2020].

[173] Ž. Janićijević and F. Radovanović, "Polyethersulfone/poly(acrylic acid) composite hydrogel membrane reservoirs for controlled delivery of cationic drug formulations," *Polymer (Guildf).*, vol. 147, pp. 56–66, Jul. 2018, doi: 10.1016/j.polymer.2018.05.065.

[174] Ž. Janićijević, M. Ninkov, M. Kataranovski, and F. Radovanović, "Poly(DL-Lactide-*co*-ε-Caprolactone)/Poly(Acrylic Acid) Composite Implant for Controlled Delivery of Cationic Drugs," *Macromol. Biosci.*, vol. 19, no. 2, p. 1800322, Feb. 2019, doi: 10.1002/mabi.201800322.

[175] Ž. Janićijević, I. Vujčić, Đ. Veljović, M. Vujisić, and F. Radovanović, "Composite poly(DL-lactide-co-glycolide)/poly(acrylic acid) hydrogels synthesized using UV and gamma irradiation: comparison of material properties," *Radiat. Phys. Chem.*, vol. 166, p. 108466, Jan. 2020, doi: 10.1016/j.radphyschem.2019.108466.

[176] P. Atanasijević and Ž. Janićijević, "Programabilni pulsni strujni izvor za *in vitro* ispitivanja jontoforeze [Programmable pulse current source for *in vitro* investigations of iontophoresis]," u *Zborniku 61. Konferencije za elektroniku, telekomunikacije, računarstvo, automatiku i nuklearnu tehniku, ETRAN 2017*, 2017, pp. BT1.2.1-5.

[177] "Practice for use of the ethanol-chlorobenzene dosimetry system," ISO/ASTM 51538:2017, 2017.

[178] D. Razem and I. Dvornik, "Application of the ethanol-chlorobenzene dosimeter to electron-beam and gamma-radiation dosimetry: II Cobalt-60 grama rays," in *IAEA Symposium on Dosimetry in Agriculture, Industry, Biology, and Medicine*, 1972, pp. 405–419.

[179] A. Kovács, V. Stenger, and G. Fóldiák, "Evaluation methods of the ethanol-monochlorobenzene dosimeter system," in *6th Tihany Symposium on Radiation Chemistry*, 1987, pp. 701–709.

[180] C. A. Schneider, W. S. Rasband, and K. W. Eliceiri, "NIH Image to ImageJ: 25 years of image analysis," *Nat. Methods*, vol. 9, no. 7, pp. 671–675, Jul. 2012, doi: 10.1038/nmeth.2089.

[181] K. S. Ngai, S. Ramesh, K. Ramesh, and J. C. Juan, "Electrical, dielectric and electrochemical characterization of novel poly(acrylic acid)-based polymer electrolytes complexed with lithium tetrafluoroborate," *Chem. Phys. Lett.*, vol. 692, pp. 19–27, Jan. 2018, doi: 10.1016/j.cplett.2017.11.042.

[182] A. H. Galama, N. A. Hoog, and D. R. Yntema, "Method for determining ion exchange membrane resistance for electrodialysis systems," *Desalination*, vol. 380, pp. 1–11, Feb. 2016, doi: 10.1016/j.desal.2015.11.018.

[183] Microchip Technology, "Rail-to-Rail Input/Output, 10 MHz Op Amps," MCP6021/1R/2/3/4 datasheet, Nov. 2001 [Revised Jan. 2017].

[184] P. Horowitz and W. Hill, "FETs as variable resistors," in *The Art of Electronics*, 3rd ed., Cambridge University Press, 2015, pp. 161–163.

[185] L. M. Oliveira, P. L. B. Araujo, and E. S. Araujo, "The effect of gamma radiation on mechanical properties of biodegradable polymers poly(3-hydroxybutyrate) and poly(3-hydroxybutyrate-co-3-hydroxyvalerate)," *Mater. Res.*, vol. 16, no. 1, pp. 195–203, Dec. 2012, doi: 10.1590/S1516-14392012005000173.

[186] C. C. Chu and N. D. Campbell, "Scanning electron microscopic study of the hydrolytic degradation of poly(glycolic acid) suture," *J. Biomed. Mater. Res.*, vol. 16, no. 4, pp. 417–430, Jul. 1982, doi: 10.1002/jbm.820160410.

[187] J. S. C. Loo, C. P. Ooi, and F. Y. C. Boey, "Degradation of poly(lactide-*co*-glycolide) (PLGA) and poly(L-lactide) (PLLA) by electron beam radiation.," *Biomaterials*, vol. 26, no. 12, pp. 1359–67, Apr. 2005, doi: 10.1016/j.biomaterials.2004.05.001.

[188] M. M. Ghobashy, "Ionizing Radiation-Induced Polymerization," in *Ionizing Radiation Effects and Applications*, B. Djezzar, Ed. InTech, 2018, pp. 113–134.

[189] S. Yoshioka, Y. Aso, T. Otsuka, and S. Kojima, "The effect of γ-irradiation on drug release from poly(lactide) microspheres," *Radiat. Phys. Chem.*, vol. 46, no. 2, pp. 281–285, Aug. 1995, doi: 10.1016/0969-806X(95)00025-S.

[190] M. Todica, R. Stefan, C. V. Pop, and L. Olar, "IR and Raman investigation of some poly(acrylic) acid gels in aqueous and neutralized state," *Acta Phys. Pol. A*, vol. 128, no. 1, pp. 128–135, 2015, doi: 10.12693/APhysPolA.128.128.

[191] M. Ferry *et al.*, "Ionizing Radiation Effects in Polymers," *Ref. Modul. Mater. Sci. Mater. Eng.*, Jan. 2016, doi: 10.1016/B978-0-12-803581-8.02095-6.

[192] E. S. Matsuo, M. Orkisz, S. T. Sun, Y. Li, and T. Tanaka, "Origin of Structural Inhomogeneities in Polymer Gels," *Macromolecules*, vol. 27, no. 23, pp. 6791–6796, 1994, doi: 10.1021/ma00101a018.

[193] J. G. Wijmans, J. P. B. Baaij, and C. A. Smolders, "The mechanism of formation of microporous or skinned membranes produced by immersion precipitation," *J. Memb. Sci.*, vol. 14, no. 3, pp. 263–274, Jan. 1983, doi: 10.1016/0376-7388(83)80005-2.

[194] H. Strathmann and K. Kock, "The formation mechanism of phase inversion membranes," *Desalination*, vol. 21, no. 3, pp. 241–255, Sep. 1977, doi: 10.1016/S0011-9164(00)88244-2.

[195] P. Gabbott, "A Practical Introduction to Differential Scanning Calorimetry," in *Principles and Applications of Thermal Analysis*, P. Gabbott, Ed. Oxford, UK: Blackwell Publishing Ltd, 2008, pp. 1–50.

[196] D. R. Morey and J. W. Tamblyn, "The Fractional Precipitation of Molecular-weight Species from

High Polymers: Theories of the Process and Some Experimental Evidence," *J. Phys. Colloid Chem.*, vol. 51, no. 3, pp. 721–746, 1947, doi: 10.1021/j150453a012.

[197] F. Francuskiewicz, "Precipitation Fractionation," in *Polymer Fractionation*, Springer, Berlin, Heidelberg, 1994, pp. 39–63.

[198] S. H. Jeong and K. Park, "Drug loading and release properties of ion-exchange resin complexes as a drug delivery matrix," *Int. J. Pharm.*, vol. 361, no. 1–2, pp. 26–32, 2008, doi: 10.1016/j.ijpharm.2008.05.006.

[199] K. Hu and J. M. Dickson, "Modelling of the pore structure variation with pH for pore-filled pH-sensitive poly(vinylidene fluoride)-poly(acrylic acid) membranes," *J. Memb. Sci.*, vol. 321, no. 2, pp. 162–171, 2008, doi: 10.1016/j.memsci.2008.04.046.

[200] J. Zhou, R. F. Childs, and A. M. Mika, "Calculation of the salt separation by negatively charged gel-filled membranes," *J. Memb. Sci.*, vol. 260, no. 1–2, pp. 164–173, 2005, doi: 10.1016/j.memsci.2005.03.028.

[201] R. W. Korsmeyer, R. Gurny, E. Doelker, P. Buri, and N. A. Peppas, "Mechanisms of solute release from porous hydrophilic polymers," *Int. J. Pharm.*, vol. 15, no. 1, pp. 25–35, 1983, doi: 10.1016/0378-5173(83)90064-9.

[202] P. L. Ritger and N. A. Peppas, "A simple equation for description of solute release I. Fickian and non-fickian release from non-swellable devices in the form of slabs, spheres, cylinders or discs," *J. Control. Release*, vol. 5, no. 1, pp. 23–36, 1987, doi: 10.1016/0168-3659(87)90034-4.

[203] W. Plazinski and W. Rudzinski, "A novel two-resistance model for description of the adsorption kinetics onto porous particles," *Langmuir*, vol. 26, no. 2, pp. 802–808, 2010, doi: 10.1021/la902211c.

[204] L. Pisani, "Simple Expression for the Tortuosity of Porous Media," *Transp. Porous Media*, vol. 88, no. 2, pp. 193–203, 2011, doi: 10.1007/s11242-011-9734-9.

[205] M. Suzuki, "Diffusion in Porous Particles," in *Adsorption Engineering*, Tokyo: Kodansha Ltd., 1990, pp. 63–93.

[206] N. Ayawei, A. N. Ebelegi, and D. Wankasi, "Modelling and Interpretation of Adsorption Isotherms," *J. Chem.*, vol. 2017, pp. 1–11, 2017, doi: 10.1155/2017/3039817.

[207] J. Crank, *The Mathematics of Diffusion*, 2nd ed. London: Oxford University Press, 1975.

[208] W. J. Weber and J. C. Morris, "Advances in water pollution research: removal of biologically resistant pollutant from waste water by adsorption," *Proc. Int. Conf. Water Pollut. Symp.*, vol. 2, pp. 231–266, 1962.

[209] G. McKay, M. S. Otterburn, and A. G. Sweeney, "The removal of colour from effluent using various adsorbents-III. Silica: Rate processes," *Water Res.*, vol. 14, no. 1, pp. 15–20, 1980, doi: 10.1016/0043-1354(80)90037-8.

[210] J. Siepmann and F. Siepmann, "Mathematical modeling of drug delivery," *Int. J. Pharm.*, vol. 364, no. 2, pp. 328–343, 2008, doi: 10.1016/j.ijpharm.2008.09.004.

[211] J. M. Vergnaud, "Mathematical treatment of diffusion in cylinders," in *Controlled Drug Release of Oral Dosage Forms*, Chichester, England: Ellis Horwood Limited, 1993, pp. 75–104.

[212] C. W. Nestor, Jr., "Diffusion from Solid Cylinders," Oak Ridge National Lab., TN, USA, Tech. Rep. ORNL/CSD/TM-84, Jan. 1980.

[213] K. Nishikida and J. Coates, "Infrared and Raman Analysis of Polymers," in *Handbook of plastics analysis*, 1st ed., H. Lobo and J. V. Bonilla, Eds. New York: Marcel Dekker, 2003, pp. 247–248.

[214] E. Vey, C. Rodger, J. Booth, M. Claybourn, A. F. Miller, and A. Saiani, "Degradation kinetics of poly(lactic-co-glycolic) acid block copolymer cast films in phosphate buffer solution as revealed

by infrared and Raman spectroscopies," *Polym. Degrad. Stab.*, vol. 96, no. 10, pp. 1882–1889, 2011, doi: 10.1016/j.polymdegradstab.2011.07.011.

[215] L. Keshavarz, M. A. Khansary, and S. Shirazian, "Phase diagram of ternary polymeric solutions containing nonsolvent/solvent/polymer: Theoretical calculation and experimental validation," *Polymer (Guildf).*, vol. 73, pp. 1–8, Sep. 2015, doi: 10.1016/j.polymer.2015.07.027.

[216] A. Ghasemi, M. Asgarpour Khansary, and M. A. Aroon, "A comparative theoretical and experimental study on liquid-liquid equilibria of membrane forming polymeric solutions," *Fluid Phase Equilib.*, vol. 435, pp. 60–72, Mar. 2017, doi: 10.1016/j.fluid.2016.12.005.

[217] M. A. Khansary, A. Marjani, and S. Shirazian, "On the search of rigorous thermo-kinetic model for wet phase inversion technique," *J. Memb. Sci.*, vol. 538, pp. 18–33, Sep. 2017, doi: 10.1016/j.memsci.2017.05.050.

[218] R. M. Boom, T. van den Boomgaard, and C. A. Smolders, "Mass transfer and thermodynamics during immersion precipitation for a two-polymer system: Evaluation with the system PES—PVP—NMP—water," *J. Memb. Sci.*, vol. 90, no. 3, pp. 231–249, May 1994, doi: 10.1016/0376-7388(94)80074-X.

[219] R. M. Boom, T. van den Boomgaard, and C. A. Smolders, "Equilibrium Thermodynamics of a Quaternary Membrane-Forming System with Two Polymers. 1. Calculations," *Macromolecules*, vol. 27, no. 8, pp. 2034–2040, Apr. 1994, doi: 10.1021/ma00086a009.

[220] R. M. Boom, H. W. Reinders, H. H. W. Rolevink, T. van den Boomgaard, and C. A. Smolders, "Equilibrium Thermodynamics of a Quaternary Membrane-Forming System with Two Polymers. 2. Experiments," *Macromolecules*, vol. 27, no. 8, pp. 2041–2044, Apr. 1994, doi: 10.1021/ma00086a010.

[221] I. M. Wienk, R. M. Boom, M. A. M. Beerlage, A. M. W. Bulte, C. A. Smolders, and H. Strathmann, "Recent advances in the formation of phase inversion membranes made from amorphous or semi-crystalline polymers," *J. Memb. Sci.*, vol. 113, no. 2, pp. 361–371, May 1996, doi: 10.1016/0376-7388(95)00256-1.

[222] K. N. Bauer, L. Liu, M. Wagner, D. Andrienko, and F. R. Wurm, "Mechanistic study on the hydrolytic degradation of polyphosphates," *Eur. Polym. J.*, vol. 108, pp. 286–294, Nov. 2018, doi: 10.1016/j.eurpolymj.2018.08.058.

[223] N. Sheikh, L. Jalili, and F. Anvari, "A study on the swelling behavior of poly(acrylic acid) hydrogels obtained by electron beam crosslinking," *Radiat. Phys. Chem.*, vol. 79, no. 6, pp. 735–739, Jun. 2010, doi: 10.1016/j.radphyschem.2009.12.013.

[224] R. A. Gemeinhart and C. Guo, "Fast Swelling Hydrogel Systems," in *Reflexive polymers and hydrogels : understanding and designing fast responsive polymeric systems*, N. Yui, R. J. Mrsny, and K. Park, Eds. CRC Press, 2004, pp. 245–257.

[225] N. Vishal Gupta and H. G. Shivakumar, "Preparation and characterization of superporous hydrogels as gastroretentive drug delivery system for rosiglitazone maleate," *DARU, J. Pharm. Sci.*, vol. 18, no. 3, pp. 200–210, 2010, doi: 10.2174/156720109789941722.

[226] A. Kostić, B. Adnadjević, A. Popović, and J. Jovanović, "Comparison of the swelling kinetics of a partially neutralized poly(acrylic acid) hydrogel in distilled water and physiological solution," *J. Serbian Chem. Soc.*, vol. 72, no. 11, pp. 1139–1153, 2007, doi: 10.2298/JSC0711139K.

[227] F. Ganji, S. Vasheghani-Farahani, and E. Vasheghani-Farahani, "Theoretical Description of Hydrogel Swelling: A Review," *Iran. Polym. J.*, vol. 19, no. 5, pp. 375–398, 2010, doi: 10.1007/s12303-009-0004-6.

[228] V. A. Bhanu and K. Kishore, "Role of oxygen in polymerization reactions," *Chem. Rev.*, vol. 91, no. 2, pp. 99–117, Mar. 1991, doi: 10.1021/cr00002a001.

[229] "AMBERLITE™ IRP64 Pharmaceutical Grade Cation Exchange Resin (Polacrilex Resin),"

Technical Data Sheet, 2006. [Online]. Available: https://www.dow.com/assets/attachments/business/process_chemicals/amberlite_and_duolite_pharmaceutical_grade_resins/amberlite_irp64/tds/amberlite_irp64.pdf.

[230] D. Ariono, Khoiruddin, Subagjo, and I. G. Wenten, "Heterogeneous structure and its effect on properties and electrochemical behavior of ion-exchange membrane," *Mater. Res. Express*, vol. 4, no. 2, p. 024006, Feb. 2017, doi: 10.1088/2053-1591/aa5cd4.

[231] Geltek-Medica, "Electrode Contact Media." [Online]. Available: https://geltek-medica.ru/eng/catalogue/medical/electrode-contact-media/. [Accessed: 07-Oct-2019].

[232] N. Miložič, M. Lubej, U. Novak, P. Žnidaršič-Plazl, and I. Plazl, "Evaluation of Diffusion Coefficient Determination using a Microfluidic Device," in *Chemical and Biochemical Engineering Quarterly*, 2014, vol. 28, no. 2, pp. 215–223, doi: 10.15255/CABEQ.2014.1938.

[233] S. M. Evans, A. L. Litzenberger, A. E. Ellenberger, J. E. Maneval, E. L. Jablonski, and B. M. Vogel, "A microfluidic method to measure small molecule diffusion in hydrogels," *Mater. Sci. Eng. C*, vol. 35, no. 1, pp. 322–334, 2014, doi: 10.1016/j.msec.2013.10.035.

[234] J. de S. Macedo *et al.*, "Kinetic and calorimetric study of the adsorption of dyes on mesoporous activated carbon prepared from coconut coir dust," *J. Colloid Interface Sci.*, vol. 298, no. 2, pp. 515–522, 2006, doi: 10.1016/j.jcis.2006.01.021.

[235] C. Pelekani and V. L. Snoeyink, "Competitive adsorption between atrazine and methylene blue on activated carbon: the importance of pore size distribution," *Carbon N. Y.*, vol. 38, no. 10, pp. 1423–1436, Jan. 2000, doi: 10.1016/S0008-6223(99)00261-4.

[236] D. Brock, W. Lee, D. Segalman, and W. Witkowski, "A Dynamic Model of a Linear Actuator Based on Polymer Hydrogel," *J. Intell. Mater. Syst. Struct.*, vol. 5, no. 6, pp. 764–771, Nov. 1994, doi: 10.1177/1045389X9400500606.

[237] Y. Hirose, G. Giannetti, J. Marquardt, and T. Tanaka, "Migration of Ions and pH Gradients in Gels under Stationary Electric Fields," *J. Phys. Soc. Japan*, vol. 61, no. 11, pp. 4085–4097, Nov. 1992, doi: 10.1143/JPSJ.61.4085.

[238] P. Chansai, A. Sirivat, S. Niamlang, D. Chotpattananont, and K. Viravaidya-Pasuwat, "Controlled transdermal iontophoresis of sulfosalicylic acid from polypyrrole/poly(acrylic acid) hydrogel," *Int. J. Pharm.*, vol. 381, no. 1, pp. 25–33, Oct. 2009, doi: 10.1016/j.ijpharm.2009.07.019.

[239] S. Murdan, "Electro-responsive drug delivery from hydrogels," *J. Control. Release*, vol. 92, no. 1–2, pp. 1–17, Sep. 2003, doi: 10.1016/S0168-3659(03)00303-1.

[240] R. H. Guy, "Current status and future prospects of transdermal drug delivery.," *Pharm. Res.*, vol. 13, no. 12, pp. 1765–9, Dec. 1996.

[241] S. Glass, M. Kühnert, B. Abel, and A. Schulze, "Controlled Electron-Beam Synthesis of Transparent Hydrogels for Drug Delivery Applications," *Polymers (Basel).*, vol. 11, no. 3, p. 501, Mar. 2019, doi: 10.3390/polym11030501.

[242] M. Silindir and A. Y. Özer, "Sterilization Methods and the Comparison of E-Beam Sterilization with Gamma Radiation Sterilization," *FABAD J. Pharm. Sci.*, vol. 34, no. 1, pp. 43–53, 2009.

[243] C. R. Harrell, V. Djonov, C. Fellabaum, and V. Volarevic, "Risks of Using Sterilization by Gamma Radiation: The Other Side of the Coin," *Int. J. Med. Sci.*, vol. 15, no. 3, pp. 274–279, 2018, doi: 10.7150/ijms.22644.

[244] N. A. Peppas and S. L. Wright, "Solute Diffusion in Poly(vinyl alcohol)/Poly(acrylic acid) Interpenetrating Networks," *Macromolecules*, vol. 29, no. 27, pp. 8798–8804, 1996, doi: 10.1021/ma9613392.

Appendix A: Calculation of MB amount in the loading solutions

As stated in the section **2.2.11 Loading of composite membranes and implants with MB**, initial MB concentrations in the loading solutions were adjusted to achieve predetermined molar ratios of MB cations (MB^+) and carboxyl groups (-COOH) in the membrane sample ($n(MB^+)/n(-COOH) = 0.5$, 1, or 1.5) assuming the 100% reactant conversion yield. Initial MB concentrations were calculated by using the previously determined values of wet sample weight m_w, mean mass swelling degree MSD, and mean concentration of carboxyl groups C_{cg}.

At first, the dry sample weight m_d was calculated using the expression:

$$m_{\mathrm{d}} = \frac{100 \cdot m_{\mathrm{w}}}{100 + \mathrm{MSD}(\%)} \tag{A.1}$$

The initial concentration of MB in the loading solution (C_{MB}) was then calculated as:

$$C_{\mathrm{MB}}(\mathrm{g \cdot dm^{-3}}) = \frac{\mathrm{n(MB^+)}}{\mathrm{n(-COOH)}} \cdot m_{\mathrm{d}} \cdot C_{\mathrm{cg}} \cdot \frac{M_{\mathrm{WMB}}}{V_{\mathrm{l}}} \tag{A.2}$$

where M_{WMB} designates the molecular weight of MB and V_l designates the loading solution volume.

Alternatively, MB stock solution of known concentration can be used for the loading of membrane samples. This approach was used to load membrane samples intended for *in vitro* iontophoretic MB release experiments (as described in section **2.2.14 Iontophoretic *in vitro* release of MB from composite PES/PAA membranes**). In such a case, V_l required to achieve the desired molar ratio $n(MB^+)/n(-COOH)$ can be calculated as:

$$V_{\mathrm{l}} = \frac{\mathrm{n(MB^+)}}{\mathrm{n(-COOH)}} \cdot m_{\mathrm{d}} \cdot C_{\mathrm{cg}} \cdot \frac{M_{\mathrm{WMB}}}{C_{\mathrm{MB}}} \tag{A.3}$$

Appendix B: Homogeneity of the chemical composition of UV-PLGA-PAA and G-PLGA-PAAs (III)

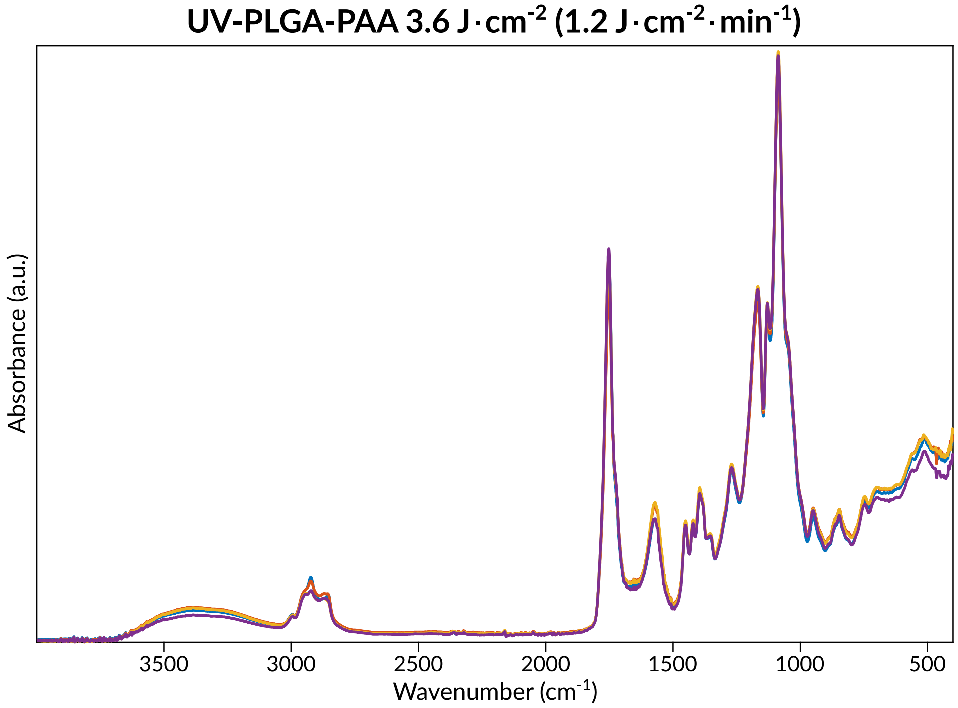

Figure B.1. Representative raw FTIR-ATR spectra recorded at different locations on the surface of the dry UV-PLGA-PAA synthesized using the dose of 3.6 J·cm^{-2} and dose rate of 1.2 J·cm^{-2}·min^{-1}.

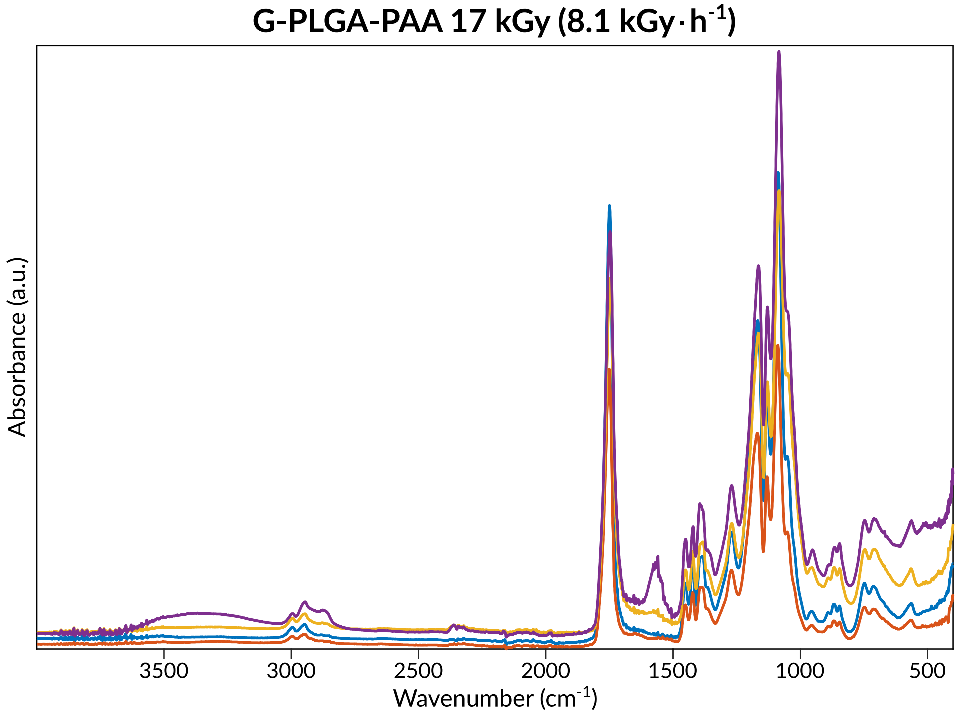

Figure B.2. Representative raw FTIR-ATR spectra recorded at different locations on the surface of the dry G-PLGA-PAA synthesized using the dose of 17 kGy and a dose rate of 8.1 kGy·h^{-1}.

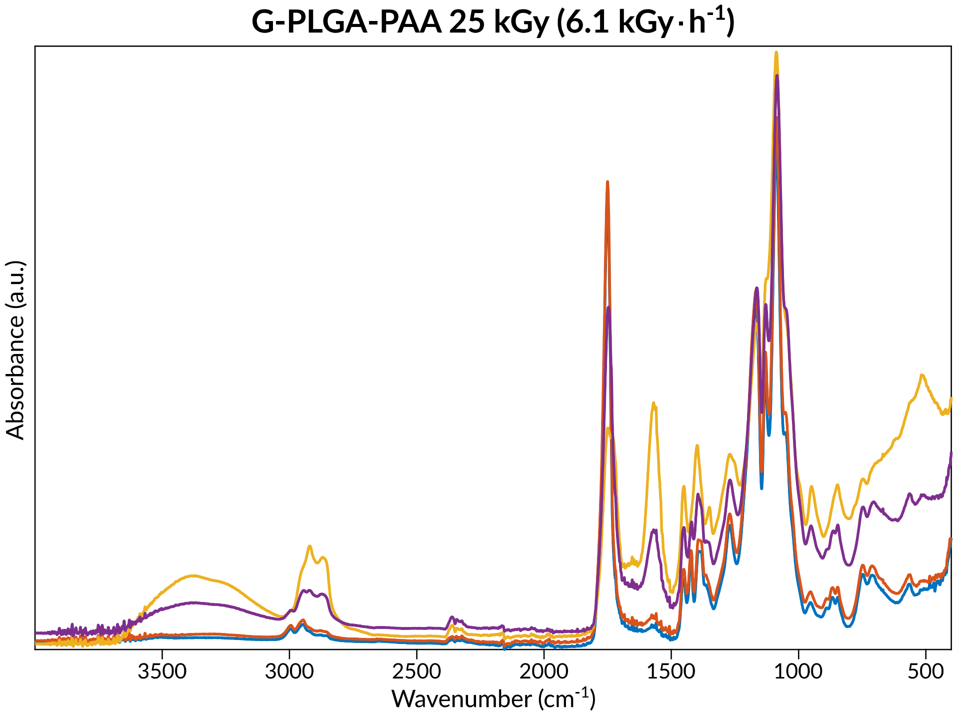

Figure B.3. Representative raw FTIR-ATR spectra recorded at different locations on the surface of the dry G-PLGA-PAA synthesized using the dose of 25 kGy and a dose rate of 6.1 kGy·h^{-1}.

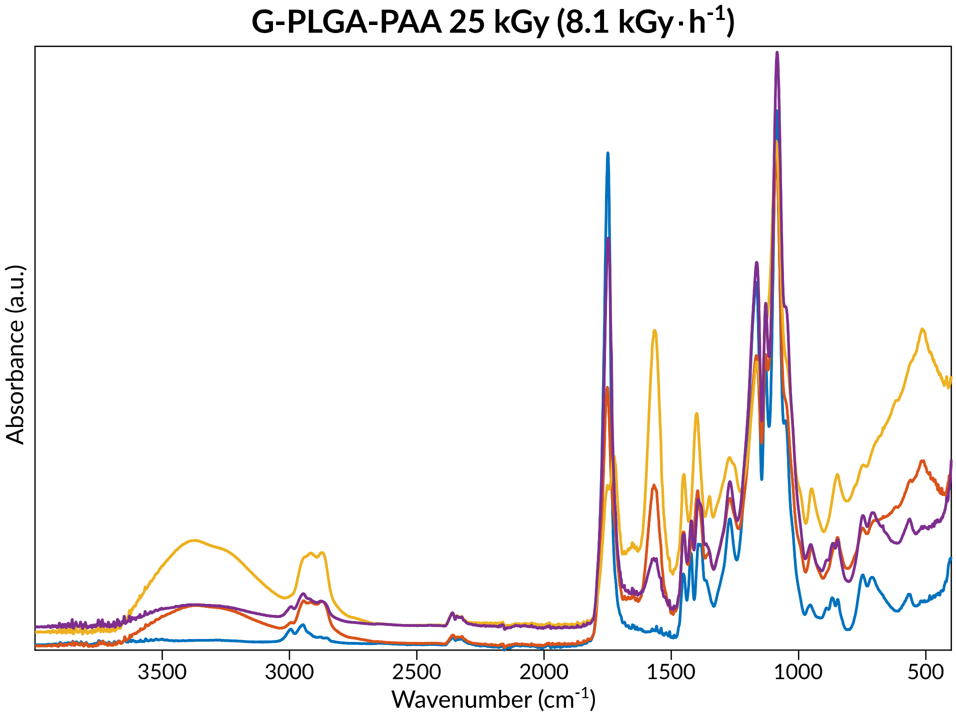

Figure B.4. Representative raw FTIR-ATR spectra recorded at different locations on the surface of the dry G-PLGA-PAA synthesized using the dose of 25 kGy and a dose rate of 8.1 kGy·h^{-1}.

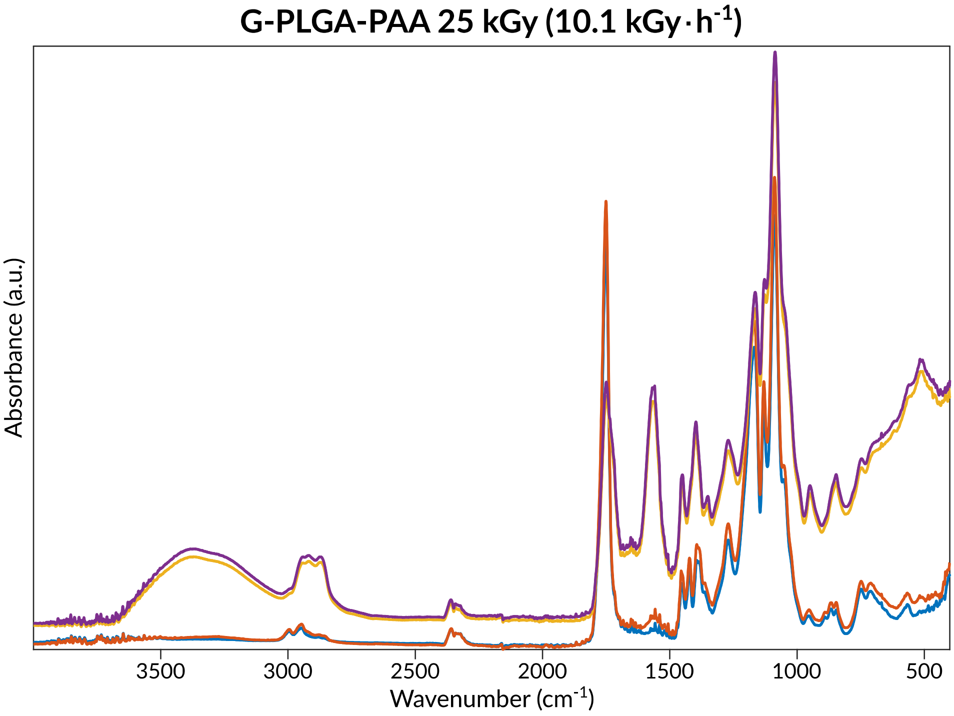

Figure B.5. Representative raw FTIR-ATR spectra recorded at different locations on the surface of the dry G-PLGA-PAA synthesized using the dose of 25 kGy and a dose rate of 10.1 kGy·h^{-1}.

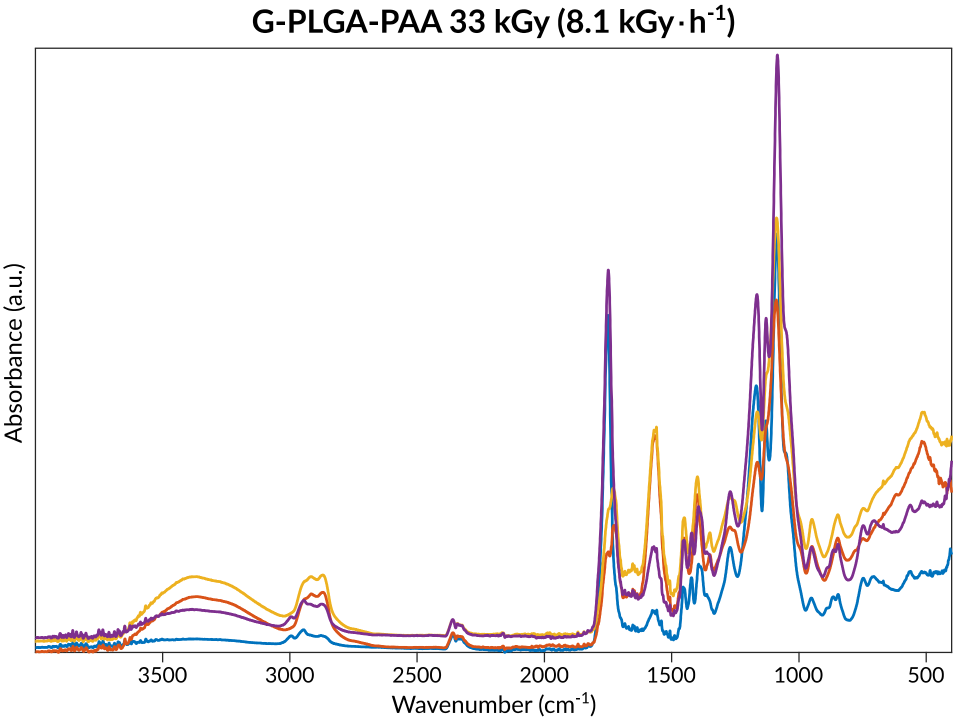

Figure B.6. Representative raw FTIR-ATR spectra recorded at different locations on the surface of the dry G-PLGA-PAA synthesized using the dose of 33 kGy and a dose rate of 10.1 kGy·h^{-1}.

Appendix C: Estimation of the maximum MB amount that can be released via iontophoresis

Calculation of D_a from the **Equation (5.14)** required the data about the maximum MB amount that can be released in PBS (pH = 7.4 and I = 0.154 M) from composite PES/PAA membranes (12PES-5.3AA-5TMPTA) at the end of the *in vitro* iontophoretic release experiment. As it was challenging to measure the maximum amount of iontophoretically released MB experimentally, we made an empirical prediction based on previous experiments of passive MB release in PBS (pH = 8 and I = 0.2 M) conducted for composite PES/PAA membranes (12PES-5.3AA-5TMPTA).

We first assumed that the complete amount of electrostatically bound MB will be released in PBS by iontophoresis in the end (similarly as in the case of passive MB release) if the iontophoresis was continued to fully unload MB from membrane samples and reach the equilibrium state. We then examined the dependence of the average fraction of electrostatically bound MB in the composite PES/PAA membranes on the average MB loading efficiency as illustrated in **Figure C.1** using the data from **Figure 4.22** and **Table 4.2**. As expected, the average fraction of electrostatically bound MB slowly decreased with the rise in average MB loading efficiency for low MB loadings. This finding can be explained by the increasing contribution of MB cations interacting with the surface of the hydrophobic polymer matrix as their concentration rises.

We fitted the data points presented in **Figure C.1** using an empirical power law to predict the fraction of electrostatically bound MB for high MB loading efficiencies. If we designate the MB loading efficiency as LE_{MB} and the fraction of electrostatically bound MB as EB_{MB}, the equation of the fit is given by:

$$EB_{\mathrm{MB}} = K \cdot {LE_{\mathrm{MB}}}^{\beta} \qquad \text{(C.1)}$$

where K designates the scaling factor of the power law and β designates the power-law exponent.

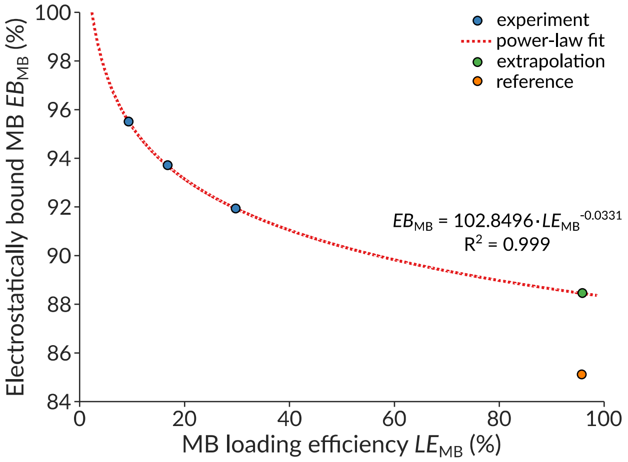

Figure C.1. Dependence of the average fraction of electrostatically bound MB (EB_{MB}) in the composite PES/PAA membranes (12PES-5.3AA-5TMPTA) on the average MB loading efficiency (LE_{MB}) (designated by blue circles). Extrapolated average EB_{MB} for composite PES/PAA membranes used in *in vitro* iontophoretic release experiments (green circle). Reference EB_{MB} value for composite DL-PLCL/PAA implants (orange circle). Empirical power-law fit corresponding to the composite PES/PAA membranes (12PES-5.3AA-5TMPTA) is designated with the red dotted line.

As a reference point for comparison corresponding to high LE_{MB}, we used the average EB_{MB} obtained from the passive MB release experiments carried out for composite DL-PLCL/PAA implants due to the comparable chemical composition and release mechanism. We extrapolated the value of EB_{MB} by extending the power-law fit to the average value of LE_{MB} corresponding to composite PES/PAA membrane samples loaded for iontophoresis experiments (*i.e.* to 95.9% as listed in section **4.8.2 Iontophoretic *in vitro* release of MB from composite PES/PAA membranes**). The extrapolated value of EB_{MB} was 88.5%. The obtained average EB_{MB} was similar to the average fraction of total absorbed MB amount passively released from composite DL-PLCL/PAA implants (85.1%) that were previously loaded with practically the same average LE_{MB} (95.8%). Hence, we can consider the value of 88.4% as a reasonable estimate with an error margin of few percent. Such an error margin will not have a major influence on the calculated value of D_{a}.

The maximum weight of MB that can be released from the composite PES/PAA membrane sample via iontophoresis was estimated as:

$$m_{\mathrm{RMB}} = m_{\mathrm{LMB}} \cdot \frac{LE_{\mathrm{MB}}}{100\%} \cdot \frac{EB_{\mathrm{MB}}}{100\%} \tag{C.2}$$

where m_{RMB} designates the weight of released MB and m_{LMB} designates the weight of MB in the loading solution.

Appendix D: Script for the determination of D_a for the composite DL-PLCL/PAA implants (II)

```
% Full model for monolithic cylinder diffusion with numerical approximation

% apparent diffusion coefficient D [m^2*s^-1]
% measure of boundary layer resistance b
% FR = Mt/Minf = Qt/Qe is the fractional release

% Optimization with gradient descent method applied on b (flag = 1) and D (flag = 2)

clear all
clc
close all

% Implant geometry (cylinder dimensions measured by a caliper)
R = 6.5e-3; % cylinder radius [m]
H = 1.258e-3; % cylinder height [m]
L = H/2; % half of cylinder height (used in the model) [m]

% Measured values for the release kinetics of MB
t = 24*3600*[2,4,7,9,11,14,17,21,24,28]; % time points of MB release [s]
FR_m = [0.242,0.41,0.572,0.69,0.786,0.887,0.971,0.996,1,1]; % measured FR of MB
FR_m_std = [0.003961881,0.011236789,0.017368022,0.02284146,0.020116839,...
   0.018314712,0.007553963,0.001669337,3.24056e-05,0]; % standard deviation
% of 3 experiments with FR measurements for MB

N = 6; % number of initial time points used for fitting
t_f = t(1:N); % time vector for fitting
FR_m_f = FR_m(1:N); % FR vector for fitting
FR_m_std_f =FR_m_std(1:N); % FR standard deviation for fitted points
FR_terms = zeros(N,4); % numerical approximation terms used in the model

% Initial values of variable parameters and steps for change
b = 0; % initial value of intercept corresponding to the boundary layer resistance
bs = 1e-4; % iterative step for b
step_sign_b = 1; % direction of change for b
```

```
D = 2.815e-13; % initial value of the apparent diffusion coefficient [m^2*s^-1]
Ds = 1e-17; % iterative step for D
step_sign_D = 1; % direction of change for D

I = 0; % number of iterations
Imax = 2.5e4; % maximum number of iterations
FR_s = zeros(1,N); % simulated FR obtained by the model
SSE = zeros(1,Imax); % sum of squared errors
test = 1; % control parameter

% Implementation of the simplified gradient descent algorithm

while test
    I = I + 1;

    % Calculation of the simulated FR at all time points
    for n = 1:N
        FR_terms(n,1) = ((D*t_f(n)/(L^2))^0.5)*(2/sqrt(pi) + 4*L/(R*sqrt(pi)));
        FR_terms(n,2) = -(D*t_f(n)/(L^2))*(8*L/(R*pi) + (L/R)^2);
        FR_terms(n,3) = ((D*t_f(n)/(L^2))^1.5)*((2/sqrt(pi))*(L/R)^2 - 1/(6*sqrt(pi))*(L/R)^3);
        FR_terms(n,4) = ((D*t_f(n)/(L^2))^2)*((1/(3*pi))*(L/R)^3 - (1/8)*(L/R)^4);
        FR_s(n) = sum(FR_terms(n,:))+ b;
    end

    SSE(I) = sum((FR_s-FR_m_f).^2);

    if I > 1
        delta = SSE(I)-SSE(I-1);

        if (delta > 0) && (flag == 1)
            step_sign_b = -step_sign_b;
        elseif (delta > 0) && (flag == 2)
            step_sign_D = -step_sign_D;
        end
        if mod(I,2) == 0
            D = D + step_sign_D*Ds;
            flag = 2;
```

```
        else
            b = b + step_sign_b*bs;
            flag = 1;
        end
    end

    if (I >= Imax)
        test = 0;
    end

end

Text_D =['Apparent diffusion coefficient is D = ',num2str(D),' m^2*s^-1'];
disp(Text_D)

Text_b =['Intercept corresponding to the boundary layer resistance is b = ',num2str(b)];
disp(Text_b)
```

Appendix E: Demonstration of iontophoretic MB release from composite PES/PAA membranes (I)

The first demonstration of the iontophoretic MB release from composite PES/PAA membranes was performed using an experimental setup relatively similar to the one illustrated in **Figure 2.4** with some simplifications. The acrylic glass side-by-side diffusion cell was custom-built with the annular cross-section of 10 mm inside diameter and contained two side-chambers of 2 cm^3 volume that can be screwed together. The cell was equipped with two ports (of ~3 mm diameter) for liquid sampling and exchange (one in the middle of each chamber) and two lateral ports (of ~1 mm diameter) for electrode insertion.

A circular sample of approximately 12 mm diameter was initially cut out of the composite PES/PAA membrane (12PES-5.3AA-5TMPTA) piece and equilibrated in PBS (pH = 8 and I = 0.2 M) for 24 h. The prepared sample was then fixed in the middle of the sealed side-by-side cell along with the porous polyester spunbond nonwoven fabric disk of 12 mm diameter. The porous polyester spunbond nonwoven fabric was in direct contact with the membrane to prevent its deformation during the iontophoresis experiment. Immediately after fixing the membrane sample, 1.5 cm^3 aliquot of 1 $g \cdot dm^{-3}$ MB aqueous solution was inserted into each of the side-chambers to initiate loading with MB. The membrane sample was loaded for 24 h in the dark within a sealed cell.

Although it was difficult to exactly measure the MB loading efficiency due to the limitations imposed by the experimental setup, we could roughly estimate the loading efficiency using comparison with other MB loading experiments. By taking into account the initial molar ratio ($n(MB^+)/n(-COOH) \approx 0.27$), loading time, initial MB concentration gradient between the membrane sample and the loading solution, and the presence of the porous polyester spunbond nonwoven fabric, we estimated with good certainty that the loading efficiency was below 10%.

After the membrane sample loading with MB, the residual aqueous solution of MB was removed. The side-chambers were then washed with ethanol and distilled water to clean MB dye residues. Each of the side-chambers was filled with 2 cm^3 of PBS (pH = 8 and I = 0.2 M) and the cylindrical pencil graphite electrodes of 0.5 mm diameter were directly inserted into the lateral ports. To initiate iontophoresis, a continuous electric current of 200 μA was applied between the electrodes connected with the dedicated custom-built current source via alligator clips. The solution within the side-chamber serving as the receptor compartment was stirred at 500 rpm using magnetic stirrer during the experiment. Iontophoretic release of MB was monitored at ambient temperature by sampling 1 cm^3 of the receptor solution every 10 min for 50 min and recording the amount of released MB measured by UV-Vis Spectrometer (Cintra 101, GBC Scientific Equipment Ltd., Australia) at the absorption wavelength of 664 nm. The sampled volume of the receptor solution at each time point during the experiment was immediately replaced with the equivalent volume of fresh PBS (pH = 8 and I = 0.2 M).

Figure E.1 shows the recorded kinetics of *in vitro* iontophoretic MB release during the demonstration experiment. The iontophoretic release kinetics was linear with a positive intercept. The positive intercept is expected as a consequence of finite time required to set up the experiment and initiate the flow of continuous electric current. During this initial stage of the experiment, MB was passively released into the surrounding PBS solution filling the chambers of the side-by-side cell. Linear release kinetics suggests that the applied electric current dominantly drove the release of MB.

The electric current in the experiment was carried mainly by cations in the solution as dictated by the permselectivity of cation-exchange membranes. Assuming ideal permselectivity of the composite PES/PAA membrane and the MB release driven solely by the action of applied continuous electric current, we estimated the intensity of the electric current carried by MB cations from the slope of the linear fit of MB release kinetics. The calculated intensity of electric current carried by MB cations was about 2 μA or 1% of the total electric current. Such a result can be explained by the combined effect of low loading efficiency and the superior properties of competing PBS cations compared to MB cations in terms of electric current transfer such as lower weight and higher ionic mobility.

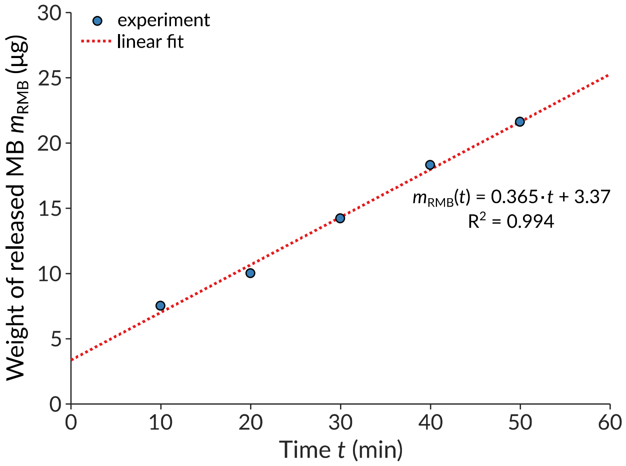

Figure E.1. Iontophoretic *in vitro* release kinetics of MB from composite PES/PAA membrane (12PES-5.3AA-5TMPTA) sample in the demonstration experiment.

Biography

Željko V. Janićijević was born in Ćuprija on 20th of July, 1988. He finished primary school and grammar school in Paraćin, both with honors as the best pupil in the generation. In 2011, he obtained a B.Sc. degree at the University of Belgrade, School of Electrical Engineering, Department of Biomedical and Ecological Engineering, with a GPA of 9.2. He obtained a M.Sc. degree in Biomedical Engineering at the joint international master's program of the University of Luebeck and Luebeck University of Applied Sciences in Germany in 2013. During his studies in Germany, Željko worked on the research projects related to the calibration of pulse oxymetry devices at the Luebeck University of Applied Sciences and the development of microfluidic biosensing platform at the TU Dresden. In 2015, he enrolled in the program of doctoral studies Nuclear, Medical and Ecological Engineering at the University of Belgrade, School of Electrical Engineering.

Since 2014, Željko is employed at the School of Electrical Engineering in the Department of Microelectronics and Technical Physics, where he currently works as a teaching and research assistant. His teaching activities include manifold courses related to materials engineering, sensors, and biophysics. Željko is a multipotentialite with broad research interests encompassing biomaterials, microfluidics, and the development of low-cost electronic devices for research. In his scientific career up to this point, he has published four articles in international peer-reviewed journals and one book chapter. He is a reviewer for the journals Materials & Design and Chemical Industry. Željko currently participates in one national and one H2020-MSCA-RISE project. He is a member of the ETRAN Society and Fab Initiative.

Изјава о ауторству

Име и презиме аутора Жељко Јанићијевић

Број индекса 2015/5010

Изјављујем

да је докторска дисертација под насловом

"Composite reservoirs with crosslinked poly(acrylic acid) hydrogel for controlled drug delivery via nonspecific electrical interactions" (наслов на српском језику: „Композитни резервоари са умреженим хидрогелом поли(акрилне киселине) за контролисану доставу лекова путем неспецифичних електричних интеракција")

- резултат сопственог истраживачког рада;
- да дисертација у целини ни у деловима није била предложена за стицање друге дипломе према студијским програмима других високошколских установа;
- да су резултати коректно наведени и
- да нисам кршио/ла ауторска права и користио/ла интелектуалну својину других лица.

Потпис аутора

У Београду, 04.06.2020.

ЖЈанићијевић

Изјава о истоветности штампане и електронске верзије докторског рада

Име и презиме аутора Жељко Јанићијевић

Број индекса 2015/5010

Студијски програм Нуклеарна, медицинска и еколошка техника

Наслов рада "Composite reservoirs with crosslinked poly(acrylic acid) hydrogel for controlled drug delivery via nonspecific electrical interactions" (наслов на српском језику: „Композитни резервоари са умреженим хидрогелом поли(акрилне киселине) за контролисану доставу лекова путем неспецифичних електричних интеракција")

Ментор доц. др Милош Вујисић

Изјављујем да је штампана верзија мог докторског рада истоветна електронској верзији коју сам предао/ла ради похрањивања у **Дигиталном репозиторијуму Универзитета у Београду.**

Дозвољавам да се објаве моји лични подаци везани за добијање академског назива доктора наука, као што су име и презиме, година и место рођења и датум одбране рада.

Ови лични подаци могу се објавити на мрежним страницама дигиталне библиотеке, у електронском каталогу и у публикацијама Универзитета у Београду.

Потпис аутора

У Београду, 04.06.2020.

ЖЈаничијевић

Изјава о коришћењу

Овлашћујем Универзитетску библиотеку „Светозар Марковић“ да у Дигитални репозиторијум Универзитета у Београду унесе моју докторску дисертацију под насловом:

“Composite reservoirs with crosslinked poly(acrylic acid) hydrogel for controlled drug delivery via nonspecific electrical interactions” (наслов на српском језику: „Композитни резервоари са умреженим хидрогелом поли(акрилне киселине) за контролисану доставу лекова путем неспецифичних електричних интеракција“)

која је моје ауторско дело.

Дисертацију са свим прилозима предао/ла сам у електронском формату погодном за трајно архивирање.

Моју докторску дисертацију похрањену у Дигиталном репозиторијуму Универзитета у Београду и доступну у отвореном приступу могу да користе сви који поштују одредбе садржане у одабраном типу лиценце Креативне заједнице (Creative Commons) за коју сам се одлучио/ла.

1. Ауторство (CC BY)

2. Ауторство – некомерцијално (CC BY-NC)

3. Ауторство – некомерцијално – без прерада (CC BY-NC-ND)

[✓ 4.] Ауторство – некомерцијално – делити под истим условима (CC BY-NC-SA)

5. Ауторство – без прерада (CC BY-ND)

6. Ауторство – делити под истим условима (CC BY-SA)

(Молимо да заокружите само једну од шест понуђених лиценци.
Кратак опис лиценци је саставни део ове изјаве).

Потпис аутора

У Београду, 04.06.2020.

1. **Ауторство**. Дозвољавате умножавање, дистрибуцију и јавно саопштавање дела, и прераде, ако се наведе име аутора на начин одређен од стране аутора или даваоца лиценце, чак и у комерцијалне сврхе. Ово је најслободнија од свих лиценци.

2. **Ауторство – некомерцијално**. Дозвољавате умножавање, дистрибуцију и јавно саопштавање дела, и прераде, ако се наведе име аутора на начин одређен од стране аутора или даваоца лиценце. Ова лиценца не дозвољава комерцијалну употребу дела.

3. **Ауторство – некомерцијално – без прерада**. Дозвољавате умножавање, дистрибуцију и јавно саопштавање дела, без промена, преобликовања или употребе дела у свом делу, ако се наведе име аутора на начин одређен од стране аутора или даваоца лиценце. Ова лиценца не дозвољава комерцијалну употребу дела. У односу на све остале лиценце, овом лиценцом се ограничава највећи обим права коришћења дела.

4. **Ауторство – некомерцијално – делити под истим условима**. Дозвољавате умножавање, дистрибуцију и јавно саопштавање дела, и прераде, ако се наведе име аутора на начин одређен од стране аутора или даваоца лиценце и ако се прерада дистрибуира под истом или сличном лиценцом. Ова лиценца не дозвољава комерцијалну употребу дела и прерада.

5. **Ауторство – без прерада**. Дозвољавате умножавање, дистрибуцију и јавно саопштавање дела, без промена, преобликовања или употребе дела у свом делу, ако се наведе име аутора на начин одређен од стране аутора или даваоца лиценце. Ова лиценца дозвољава комерцијалну употребу дела.

6. **Ауторство – делити под истим условима**. Дозвољавате умножавање, дистрибуцију и јавно саопштавање дела, и прераде, ако се наведе име аутора на начин одређен од стране аутора или даваоца лиценце и ако се прерада дистрибуира под истом или сличном лиценцом. Ова лиценца дозвољава комерцијалну употребу дела и прерада. Слична је софтверским лиценцама, односно лиценцама отвореног кода.